



**Andrea Vanessa Vaca Mora**

**Influence of Polymer Degradation and  
Nanoparticle Addition on the Rheology and  
Flow of Polymer Solutions and Dispersions in  
Porous Media**

**Tese de Doutorado**

Thesis presented to the Programa de Pós-graduação em Engenharia Mecânica, do Departamento de Engenharia Mecânica da PUC-Rio in partial fulfillment of the requirements for the degree of Doutor em Engenharia Mecânica.

Advisor : Prof. Márcio da Silveira Carvalho  
Co-advisor: Dr. Anthony Pierre Jack Hutin

Rio de Janeiro  
May 2024



**Andrea Vanessa Vaca Mora**

**Influence of Polymer Degradation and  
Nanoparticle Addition on the Rheology and  
Flow of Polymer Solutions and Dispersions in  
Porous Media**

Thesis presented to the Programa de Pós-graduação em Engenharia Mecânica da PUC-Rio in partial fulfillment of the requirements for the degree of Doutor em Engenharia Mecânica. Approved by the Examination Committee:

**Prof. Márcio da Silveira Carvalho**

Advisor

Departamento de Engenharia Mecânica – PUC-Rio

**Dr. Anthony Pierre Jack Hutin**

Co-advisor

L'Oréal

**Prof. Aurora Pérez Gramatges**

PUC-Rio

**Dr. Jorge Antonio Avendano Benavides**

PUC-Rio

**Dr. Rogério Mesquita de Carvalho**

PETROBRAS

**Prof. Ronald Alfonso Mercado Ojeda**

UIS

Rio de Janeiro, May 17th, 2024

All rights reserved.

**Andrea Vanessa Vaca Mora**

Biotechnology Engineering at Universidad de las Fuerzas Armadas (ESPE), Quito, Ecuador.

Bibliographic data

Vaca Mora, Andrea Vanessa

Influence of Polymer Degradation and Nanoparticle Addition on the Rheology and Flow of Polymer Solutions and Dispersions in Porous Media / Andrea Vanessa Vaca Mora; advisor: Márcio da Silveira Carvalho, Anthony Pierre Jack Hutin. – 2024.

118 f: il. color. ; 30 cm

Tese (doutorado) - Pontifícia Universidade Católica do Rio de Janeiro, Departamento de Engenharia Mecânica, 2024.

Inclui bibliografia

1. Engenharia Mecânica – Teses. 2. Nanopartículas. 3. Solução de polímero. 4. Degradação mecânica. 5. Reometria. 6. Microfluídica. I. Carvalho, Márcio. II. Hutin, Anthony Pierre Jack. III. Pontifícia Universidade Católica do Rio de Janeiro. Departamento de Engenharia Mecânica. IV. Título.

CDD: 621

To Aracely, my mother, Mario, my father,  
and my brothers, Mario Andrés and Josue.

## Acknowledgments

To Prof. Marcio Carvalho, my advisor, for his trust and guidance. His intellect and kindness have fostered a valuable and welcoming atmosphere in this journey.

To Dr. Anthony Hutin, for his invaluable guidance and support throughout my thesis. His advice has been essential to my academic success.

To Dr. Jorge Avendaño, his patience, insight, and attentive ears during my academic journey have been invaluable.

To my LMMP colleagues, thank you for your priceless contributions and unwavering dedication. Your collaborative spirit was fundamental to the success of my thesis.

To my dear doctoral colleagues, who have supported me since the day I arrived in Brazil, I extend my heartfelt gratitude. Together, we faced challenges, celebrated small achievements, and shared laughter in the midst of fatigue in that "gray room". Thank you for being part of my academic journey.

To the wonderful connections I have made during my academic journey in Brazil, whom I now consider my family, thank you for enriching my life in countless ways.

To Dr. Alexis Debut, Head of the Nanomaterials Characterization Laboratory at CENCINAT, thank you for your invaluable contribution to my PhD thesis. The crucial TEM images you provided significantly enriched my research. Additionally, I appreciate Ms. Karla Vizuetes expertise in sample preparation for TEM observations.

To my family, for their unwavering belief in me and their steadfast support, even during the challenging times when distance weighed heavily on our hearts. Each one of them has played a fundamental role in helping me turn my dreams into reality.

To CNPq and PUC-Rio, for the aids granted, without which this work does not could have been accomplished.

This study was financed in part by the Coordenação de Aperfeiçoamento de Pessoal de Nível Superior - Brasil (CAPES) - Finance Code 001.

## Abstract

Vaca Mora, Andrea Vanessa; Carvalho, Márcio (Advisor); Hutin, Anthony Pierre Jack (Co-Advisor). **Influence of Polymer Degradation and Nanoparticle Addition on the Rheology and Flow of Polymer Solutions and Dispersions in Porous Media**. Rio de Janeiro, 2024. 118p. Tese de Doutorado – Departamento de Engenharia Mecânica, Pontifícia Universidade Católica do Rio de Janeiro.

Partially hydrolyzed polyacrylamide (HPAM) is widely employed in enhanced oil recovery (EOR) process. However, its effectiveness is hindered by degradation of polymer molecules during flow through injection lines, valves and reservoir. This degradation leads to a decrease in average molecular weight and subsequently reduces the solution's viscosity and viscoelastic properties, impacting its effectiveness on displacing oil. Our research characterized the degree of mechanical degradation of HPAM solutions using shear and extensional rheology. We induced degradation by flowing the solutions through a valve with varying constriction and flow rates and through a microfluidic porous medium model. Our findings reveal that the addition of silica ( $\text{SiO}_2$ ) nanoparticles has a negligible effect on the shear and extensional viscosities of fresh solutions and minimizes the mechanical degradation of HPAM solutions. The rheological properties of HPAM solutions with  $\text{SiO}_2$  nanoparticles are not significantly affected by mechanical degradation, suggesting that incorporating nanoparticles could enhance the efficiency of polymer injection in EOR processes by stabilizing HPAM solutions. In addition, our study explored oil displacement flow using both fresh and degraded HPAM polymer solutions in microfluidic devices used as models of porous media. The findings suggest that fresh HPAM is more efficient in displacing oil than degraded HPAM. Furthermore, the addition of silica nanoparticles into degraded NPs-HPAM solutions resulted in a 9-13% increase in oil recovery, highlighting the enormous potential of nanoparticles in enhancing EOR processes.

## Keywords

Nanoparticles; Polymer solution; Mechanical degradation; Extensional rheometry; Rotational rheometry; Microfluidics.

## Resumo

Vaca Mora, Andrea Vanessa; Carvalho, Márcio; Hutin, Anthony Pierre Jack. **Influência da degradação de polímeros e da adição de nanopartículas na reologia e no fluxo de soluções e dispersões de polímeros em meios porosos**. Rio de Janeiro, 2024. 118p. Tese de Doutorado – Departamento de Engenharia Mecânica, Pontifícia Universidade Católica do Rio de Janeiro.

A poliacrilamida parcialmente hidrolisada (HPAM) é amplamente empregada no processo de recuperação avançada de petróleo (EOR). No entanto, sua eficácia é prejudicada pela degradação das moléculas do polímero durante o fluxo através das linhas de injeção, válvulas e reservatório. Essa degradação leva a uma diminuição do peso molecular médio e, conseqüentemente, reduz a viscosidade e as propriedades viscoelásticas da solução, afetando sua eficácia no deslocamento do petróleo. Para abordar essas questões, nossa pesquisa caracterizou o grau de degradação mecânica das soluções de HPAM usando reologia de cisalhamento e extensional. Induzimos a degradação fazendo as soluções fluírem por uma válvula com constrição e diferentes vazões através de um modelo microfluídico de um meio poroso. Os resultados revelam que a adição de nanopartículas de sílica ( $\text{SiO}_2$ ) tem um efeito insignificante sobre as viscosidades de cisalhamento e extensional de soluções frescas e minimiza a degradação mecânica das soluções de HPAM. As propriedades reológicas das soluções de HPAM com nanopartículas de  $\text{SiO}_2$  não são significativamente afetadas pela degradação mecânica, o que sugere que a incorporação de nanopartículas poderia aumentar a eficiência da injeção de polímeros em processos de EOR por meio da estabilização das soluções de HPAM. Além disso, nosso estudo explorou escoamento de deslocamento de óleo usando soluções de polímero HPAM frescas e degradadas em dispositivos microfluídicos usados como modelos de meios porosos. Os resultados sugerem que o HPAM fresco é mais eficiente na produção de óleo do que o HPAM degradado. Além disso, a adição de nanopartículas de sílica em soluções degradadas de NPs-HPAM resultou em um aumento de 9-13% na recuperação de petróleo, destacando o enorme potencial das nanopartículas no aprimoramento dos processos de EOR.

### Palavras-chave

Nanopartículas; Solução de polímero; Degradação mecânica; Reometria; Microfluídica.

## Table of contents

<b>1</b>	<b>Introduction</b>	<b>14</b>
1.1	Enhanced Oil Recovery Strategies	15
1.2	Historical perspectives on polymer flooding	17
1.3	Polymer of common use in EOR: types and properties	20
1.4	Polymer Rheological Behavior	24
1.5	Polymer Flooding Mechanisms in EOR	33
1.6	Polymer solution flow in porous media	36
1.7	Mechanical Degradation in Polymer Flooding for EOR	39
1.8	Effects of Addition of SiO <sub>2</sub> Nanoparticles on HPAM	41
1.9	Oil displacement experiment in microfluidics devices	46
1.10	Summary of Key Findings in the Literature	50
1.11	Gaps and Opportunities for Future Research	51
1.12	Objectives	52
1.13	Outline	53
<b>2</b>	<b>Materials and methods</b>	<b>54</b>
2.1	Polymer solutions	54
2.2	Silica Nanoparticles	55
2.3	Solutions/Dispersion Preparation	56
2.4	Mechanical Degradation	57
2.5	Rheological Characterization	58
2.6	EOR analysis by Microfluidics	64
<b>3</b>	<b>Rheological Properties of Fresh and Degraded Polymer solution/dispersion</b>	<b>70</b>
3.1	Shear Viscosity of Fresh and Degraded Polymer Solutions	70
3.2	Apparent Extensional Viscosity of Fresh and Degraded Polymer Solutions	75
3.3	The Effect of SiO <sub>2</sub> Nanoparticles on Mechanical Degradation of HPAM Solutions	78
<b>4</b>	<b>Flow for Fresh and Degraded Polymer Solutions and NPs-HPAM Dispersions through porous media micromodel</b>	<b>82</b>
4.1	Mechanical degradation in the flow through a microfluidic porous media model	82
4.2	Oil displacement by the injection of fresh polymer solutions	87
4.3	Oil displacement by injection of degraded HPAM solutions	90
4.4	Oil displacement with NPs-HPAM dispersion	94
<b>5</b>	<b>Conclusion and future work</b>	<b>99</b>
<b>6</b>	<b>Bibliography</b>	<b>101</b>

## List of figures

Figure 1.1	Polymer flooding scheme adapted from (2).	14
Figure 1.2	Oil reservoir production: primary, secondary, and tertiary phases, adapted from (1).	16
Figure 1.3	Enhanced Oil Recovery: a review of Thermal and Non-thermal approaches, adapted from (30).	17
Figure 1.4	Classification of polymers by structure, adapted from (56).	21
Figure 1.5	The condensed structural formula of the HPAM polymer (between dotted lines) and a schematic diagram. In the diagram, blue spheres indicate the chemical skeleton while red negative charges denote the carboxylic groups (73).	23
Figure 1.6	Schematic illustration of polymer chains, which are long chains of repeating units. The chains are depicted as blue spheres and are shown at different concentration regimes, adapted from (77).	24
Figure 1.7	Illustration of shear stress in a flow between two parallel plates. (79).	25
Figure 1.8	Viscosity Behavior of Newtonian and Non-Newtonian Fluids from (80).	26
Figure 1.9	Shear viscosity curve of polymer solutions (84).	27
Figure 1.10	Constitutive models of viscoelastic theory: (a) Maxwell model and (b) Kelvin model. $G$ represents the extension modulus, and $\eta$ indicates the viscosity adapted from (94).	29
Figure 1.11	Uniaxial extension flow with a constant extension rate along the $x_1$ axis.	29
Figure 1.12	Uniaxial extension flow with a constant extension rate along the $x_1$ axis. The polymer chains are depicted as blue spheres.	30
Figure 1.13	The schematic diagram depicts the process of uniaxial extension, where a cylindrical object is stretched in a single direction.	31
Figure 1.14	Improvement of displacement front stability in oil reservoirs by adding HPAM: (a) Waterflooding and (b) Polymer flooding (105).	34
Figure 1.15	After water (a), glycerin (without elasticity) (b), and HPAM flooding (c), residual oil is found in the dead ends (79).	35
Figure 1.16	(a) In a post-conventional water flooding scenario, the oil remains as isolated drops. (b) Introducing a viscoelastic polymer solution creates an oil thread that serves as a pathway for the oil to flow upstream. This ultimately leads to the formation of an oil bank downstream (68).	36
Figure 1.17	Influence of shear rate on the viscoelastic behavior of HPAM solution in (a) shear flow, such as in rotational rheometer (b) extensional flow, such as in porous media adapted from (3, 125)	37
Figure 1.18	Schematic diagram of the experimental set-up and the contraction flow into the capillary adapted from (8).	40
Figure 1.19	Schematic diagram for preparing (a) Polymer Grafted Nanoparticle and (b) Polymer Nanofluid Suspension (158, 159).	41
Figure 1.20	Schematic diagram to illustrate the three-dimensional network interactions between $SiO_2$ NPs and HPAM polymer solutions (158).	42

Figure 1.21	Simulating Reservoir-Scale Polymer Flooding Processes using Microfluidics: An Illustrative Diagram adapted from (23).	46
Figure 1.22	Impact of capillary number on residual oil saturation following injection of water, glycerol, and PEO solutions (172).	47
Figure 1.23	A series of images in bright field mode demonstrates the sporadic nature of emulsion flow through porous media. The images illustrate the formation of distinct water flow paths as drops pass through pore throats. The first time sequence (a) shows emulsion drops obstructing pore throats (1) and (2), while the second sequence (b) portrays emulsion drops that can pass through pore throats (1) and (2). A red arrow indicates the flow path in each sequence (173).	48
Figure 1.24	Investigation of the effect of silica nanoparticles on oil recovery factor. The nanofluid solution represented by the yellow curve had an ultimate recovery of 84%, while the Xanthan Gum solution with silica NPs, represented by the green curve had an ultimate recovery of 88% (24).	49
Figure 2.1	Molecular structure of a partially hydrolyzed polyacrylamide (73).	54
Figure 2.2	Experimental setup used to mechanically degrade the polymer solutions by flowing them through a needle valve.	57
Figure 2.3	Discovery Series Hybrid Rheometer DHR-3.	59
Figure 2.4	HAAKE CaBER 1 instrument.	60
Figure 2.5	Picture of the CaBER geometry containing a fluid sample at rest $t = t_s$ and undergoing filament thinning for $t > 0$ .	61
Figure 2.6	Micromodel device (189).	66
Figure 2.7	Pore structure (white) of the 2D Physical Rock micromodel device.	66
Figure 2.8	Scheme for the experimental setup for microfluidic application.	67
Figure 2.9	Diagram of the experimental setup for microfluidic application.	68
Figure 3.1	Steady-state shear viscosity as a function of shear rate of fresh and degraded HPAM solutions for different flow conditions and polymer concentrations.	73
Figure 3.2	Size exclusion chromatogram of fresh and degraded 4,000 ppm HPAM solutions. Solutions were degraded at $10\text{ mL}/\text{min}$ and $0.25\text{ mm}$ orifice diameter.	74
Figure 3.3	Evolution of the filament diameter of the fresh and degraded 4,000 ppm HPAM solutions at different flow rates through a $0.25\text{ mm}$ needle valve.	76
Figure 3.4	Apparent extensional viscosity of the fresh and degraded 4,000 ppm HPAM solutions at different flow rates through a $0.25\text{ mm}$ needle valve.	77
Figure 3.5	Steady-state shear viscosity of fresh and degraded HPAM solutions, with and without $\text{SiO}_2$ nanoparticles. Solutions were degraded at $10\text{ mL}/\text{min}$ and $0.25\text{ mm}$ orifice diameter.	79
Figure 3.6	Apparent extensional viscosity of fresh and degraded HPAM solutions, with and without $\text{SiO}_2$ nanoparticles. Solutions were degraded at $10\text{ mL}/\text{min}$ and $0.25\text{ mm}$ orifice diameter.	80
Figure 3.7	Transmission electron microscopy (TEM) images.	81

Figure 4.1	Shear viscosity curves of low molecular weight HPAM solutions at 4,000 <i>ppm</i> , fresh and degraded at different flow rates. Solid lines represent the Williamson model.	83
Figure 4.2	Apparent extensional viscosity curves of HPAM solutions at 4,000 <i>ppm</i> , fresh and degraded at different flow rates. The curves were fitted with Equation 2-6(186).	85
Figure 4.3	Pore space occupation by the polymer (blue) and oil (transparent) at the end of the injection process at different flow rates.	88
Figure 4.4	Residual oil saturation as a function of capillary number for fresh HPAM solutions.	89
Figure 4.5	Steady-state shear viscosity of fresh and degraded HPAM solutions	91
Figure 4.6	Apparent extensional viscosity of fresh and degraded HPAM solutions	92
Figure 4.7	Evolution of the oil recovery obtained with both the fresh (A) and degraded HPAM solutions(B) (left). Pore occupation at five pore volumes injected (right). The pore occupation by the fluids is represented in blue.	93
Figure 4.8	Steady-state shear viscosity of fresh and NPs-HPAM degraded solutions. The NPs-HPAM dispersion was degraded at 10 <i>mL/min</i> and 0.25 <i>mm</i> orifice diameter through a valve.	94
Figure 4.9	Apparent extensional viscosity of fresh and NPs-HPAM degraded solutions. The NPs-HPAM dispersion was degraded at 10 <i>mL/min</i> and 0.25 <i>mm</i> orifice diameter through a valve.	95
Figure 4.10	Comparison of oil displacement versus pore volume injected (left) and pore occupation at five pore volumes injected (right) using fresh HPAM (A) and NPs-HPAM degraded at 10 <i>mL/min</i> (B). The pore occupation by the fluids is represented in blue.	96
Figure 4.11	Performance of degraded HPAM solution and NPs-HPAM dispersion in the oil recovery process.	97

## List of tables

Table 1.1	Overview of types of polymer used in petroleum industry. (65).	22
Table 1.2	Polymers modeling where $\eta$ : Viscosity; $K$ : Consistency index; $\dot{\gamma}$ : Shear rate; $n$ : Flow behavior index; $\eta_{\infty}$ :Infinite-shear viscosity; $\eta_0$ :Zero shear viscosity; $a$ : Transition parameter and $\sigma_y$ : Yield stress are fitting factors.	28
Table 1.3	Constitutive models and their equations.	33
Table 1.4	Overview of the results obtained from flooding tests conducted on polymer solutions with the addition of nanoparticles, aimed at studying their effects on oil recovery.	45
Table 2.1	Properties of the polymer solution used in this research.	55
Table 2.2	Properties of AEROSIL® 200(176).	55
Table 2.3	Test conditions for different plate diameters and concentrations	62
Table 3.1	Mechanical degradation in shear $\Delta_s$ of HPAM solutions at different concentrations and flow rates for a constriction diameter of 0.25mm.	75
Table 3.2	Mechanical degradation in shear $\Delta_s$ of HPAM solutions at different concentrations and flow rates for a constriction diameter of 0.15mm	75
Table 3.3	Mechanical degradation in extension of 4,000 <i>ppm</i> HPAM solutions at different flow rates through the needle valve for a constriction diameter of 0.25mm.	77
Table 3.4	Relaxation times of the fresh and degraded HPAM solutions, with and without nanoparticles. Samples were degraded at flow rate of 10 <i>mL/min</i> and needle valve for a constriction diameter of 0.25 <i>mm</i> .	79
Table 3.5	Mechanical degradation in shear and extension for the solutions with and without nanoparticles. Samples were degraded at flow rate of 10 <i>mL/min</i> and needle valve for a constriction diameter of 0.25 <i>mm</i> .	80
Table 4.1	Mechanical degradation in shear $\Delta_s$ of 4,000 <i>ppm</i> HPAM solutions at different flow rates through the micromodel.	84
Table 4.2	Mechanical degradation in extension of 4,000 <i>ppm</i> HPAM solutions at different flow rates through the microfluidic device.	86
Table 4.3	Capillary number and viscosity of injected polymer solutions at different flow rates.	87
Table 4.4	Viscosity ratio and capillary number on residual oil recovery in microfluidic systems.	90

*If you know you're on the right track, if you  
have this inner knowledge, then nobody can  
turn you off... no matter what they say.*

**Barbara McClintock**, *Nobel Prize.*

# 1 Introduction

Enhanced Oil Recovery (EOR) is a critical process in oil production with the goal of maximizing the volume of produced oil. Chemical EOR methods have been developed and tested, with polymer solution flooding emerging as one of the most promising alternatives, as shown in Figure 1.1. This technique involves injecting polymer solutions into the reservoir to increase the viscosity of the displacing fluid, and consequently reduce the mobility ratio, and reduce the residual oil saturation. Polymer flooding is highly efficient in enhancing oil displacement, making it one of the favored EOR methods due to its potential to recover high volumes of oil (1).

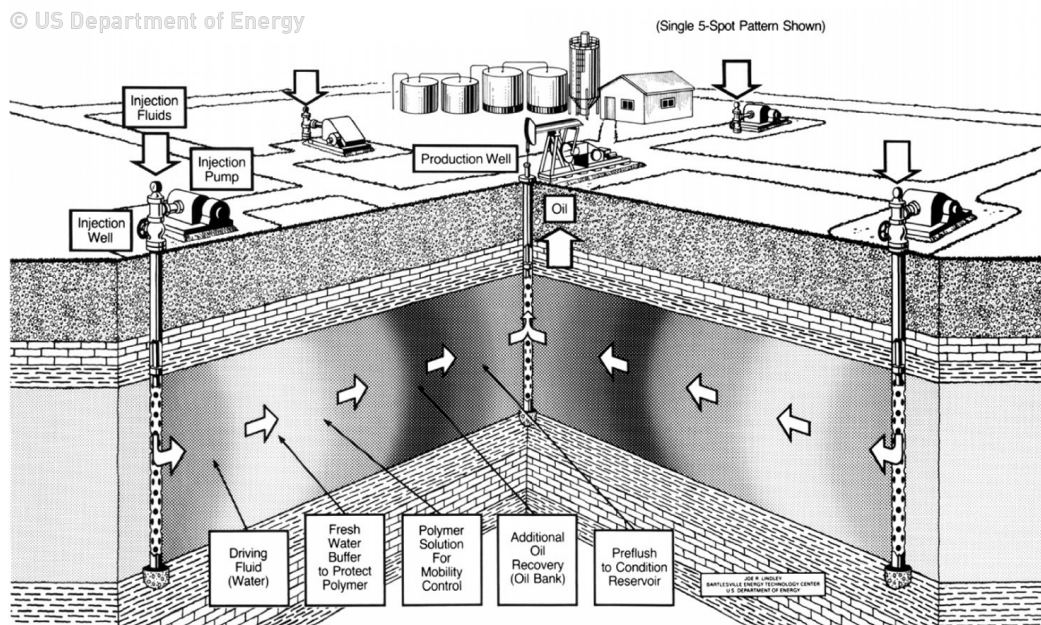


Figure 1.1: Polymer flooding scheme adapted from (2).

The polymer hydrolyzed polyacrylamide (HPAM) is a key focus in EOR studies due to its unique non-Newtonian behavior, shear thinning, and viscoelastic properties that make it suitable for EOR applications (3, 4, 5). HPAM is effective for offering long-term stability and relatively low adsorption (6, 7). However, HPAM has some limitations, such as its susceptibility to chemical and mechanical degradation and poor stability under various conditions (8, 9). To address these limitations and improve the performance of HPAM in EOR, researchers have explored the incorporation of nanoparticles into HPAM solutions (10, 11, 12).

Recent studies (13, 14, 15) have shown that nanoparticles (NPs), particularly silica nanoparticles, have significant potential to enhance the efficiency of HPAM in EOR. The addition of silica nanoparticles to HPAM solutions can improve their stability and increase oil recovery rates under various conditions (13, 16, 17, 18). Silica nanoparticles are highly stable, have a large surface area, and can interact with the HPAM molecules through hydrogen bonding and electrostatic interactions. The surface chemistry of nanoparticles is also an important factor that can impact their interaction with HPAM, thus influencing the overall performance of oil displacement processes (19).

To ensure effectiveness and optimize the conditions for using such solutions, conducting a thorough analysis of the flow behavior in porous media is essential. Traditionally, core flooding tests have been used for this purpose, but they can be time-consuming and expensive, requiring significant resources and expertise (20).

Microfluidic models have emerged as a promising alternative to core flooding tests in recent years. These models replicate some of the features of the pore structures of reservoir rocks at a much smaller scale, allowing for detailed visualization and analysis of fluid flow and displacement processes. Microfluidic devices offer several advantages over traditional core flooding tests, including reduced sample size, faster experimentation times, and the ability to visualize dynamic processes with high spatial resolution (21, 22).

Microfluidic models have become increasingly valuable in studying the performance of nanoparticles in EOR processes, including their interaction with HPAM and their impact on flow behavior in porous media (23, 24, 25, 26). Researchers can determine optimal conditions for using chemical solutions in EOR processes, leading to increased oil recovery rates and improved economic viability of oil production.

## 1.1

### Enhanced Oil Recovery Strategies

Oil reservoir production can be divided into three phases as sketched in Figure 1.2. The primary phase has the shortest lifespan and produces only 5-15% of hydrocarbons (27). During this phase, oil flows freely from the reservoir due to natural pressure or well-stimulation. The secondary phase involves injecting water or gas into the reservoir to maintain pressure. This phase results in increased hydrocarbon recovery, but in cases where the rock is more compact, or the oil is heavier, recovery is limited (20-40%)(1). The tertiary phase involves using enhanced oil recovery techniques. The average global recovery during this phase is about 40%, and further research is being

conducted to recover the remaining 65-70% (1, 28, 29).

Notably, the application of EOR techniques has undergone a significant change in recent times. The conventional chronological sequence of production has been modified, and EOR techniques are now being employed earlier in the production process. This shift is indicative of an attempt to enhance efficiency and optimize production (30).

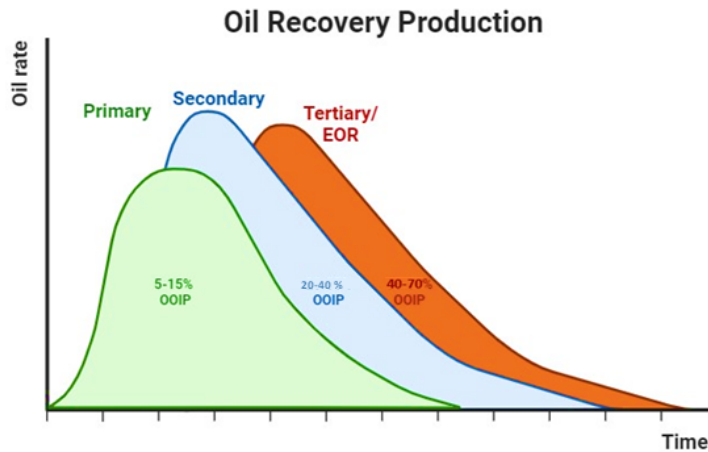


Figure 1.2: Oil reservoir production: primary, secondary, and tertiary phases, adapted from (1).

EOR strategies are broadly classified into thermal and non-thermal approaches, as presented in Figure 1.3. The thermal EOR methods involve heating the reservoir to reduce oil viscosity and facilitate its flow; while effective in specific situations, it presents challenges for deep reservoirs, thin pay zones, and those with underlying aquifers due to heat loss (31).

The non-thermal methods for EOR involve injecting different substances into the reservoir to change the conditions and improve the displacement of oil. Some of these techniques include gas injection, where gases like carbon dioxide or nitrogen are injected into the reservoir to enhance oil displacement; chemical flooding, which involves injecting chemicals such as surfactants, polymers, or alkaline solutions to modify the reservoir's properties and improve oil recovery; and microbial flooding (32, 33). These methods have become popular due to their cost-effectiveness and lower environmental impact compared to thermal methods. The oil industry is showing a growing interest in these techniques, which are closely tied to oil prices, prompting a reevaluation of oil extraction strategies (34).

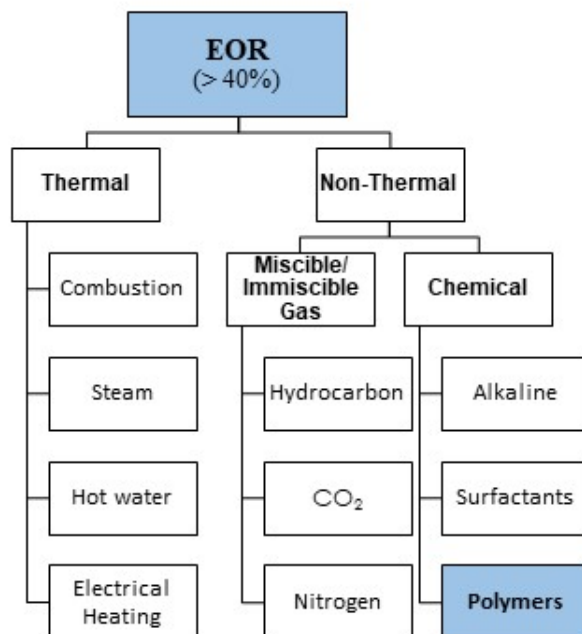


Figure 1.3: Enhanced Oil Recovery: a review of Thermal and Non-thermal approaches, adapted from (30).

## 1.2

### Historical perspectives on polymer flooding

In 1960, the Daqing field saw the first laboratory studies on the use of polymers to enhance oil recovery. These studies aimed to understand how effective polymers could be in achieving this goal. Later, in 1972, the first polymer flooding pilot was conducted in the same field. This pilot involved injecting polymers into the reservoir to evaluate their impact on oil production (35, 36).

In 1978, Chang (37) conducted a comprehensive evaluation of polymer flooding technology that included both historical context and new laboratory discoveries. Through this research, Chang identified key financial and operational factors that impact the economics of polymer flooding. Additional expenses, such as drilling, well interventions, and completion costs, varied depending on the reservoir depth and years of operation. According to Chang's report, polyacrylamide polymers cost \$US 1.35/1b, while Xanthan Gum was priced at \$US 2.50/1b. Chang's review found that although polymer flooding was relatively inexpensive, its use in commercial applications was still limited due to various factors. Chang emphasized the simplicity and cost-effectiveness of the polymer injection process and stressed the importance of converting waterfloods to polymer floods early on. He also underscored the significance of post-flood evaluation.

In 1983, Manning et al. (38) conducted a survey on polymer floods. They discovered 273 projects in different stages of development, ranging from abandoned to contemplated, with many being pilot projects. Their findings were consistent with previous surveys, except for the reported oil recovery rate of 3.74 barrels of polymer injection. This indicates that the polymer flooding technology had shown promising results in enhancing oil recovery at that time.

A review conducted by Needham and Doe in 1987 (39) analyzed 27 field cases across the United States, France, and Germany regarding the technology of polymer flood. The study discovered that polyacrylamide polymers were the go-to choice for polymer flooding, while biopolymers were only used in three projects. The researchers also delved into the use of aluminum citrate as a crosslinker in some projects. Based on the Dykstra-Parson (DP) method, the study summarized polymer flood applications and concluded that it may not be economically feasible in cases with viscous oils with adverse mobility ratios ( $M \geq 100$ ) and highly heterogeneous reservoirs ( $DP > 0.8$ ). However, the authors reported successful economic and technical outcomes of polymer flooding in secondary and tertiary applications in sandstone and carbonate reservoirs.

Du and Guan (2004) (40), based on 40 years of experience, provided a comprehensive overview of the key factors impacting the effectiveness of polymer flooding. They identified the mobility ratio, reservoir permeability, DP coefficients, economic and technical successes, reservoir temperatures, and injectivity issues as crucial factors influencing the outcome of polymer flood projects.

In 2011, Gao (41) reviewed five cases of polymer floods in oil reservoirs with viscosities ranging from 80 to 2,000 cP. The study demonstrated that these floods are technically and economically viable and highlighted the importance of factors such as brininess, degradation, and adsorption on polymer viscosity. Gao's observations indicate that low productivity poses a significant challenge that demands attention in the context of field applications.

Mogollón and Lokhandwala (2013) (42) summarized three polymer floods in highly viscous reservoirs ( $>150$  cP) and assessed the viability of polymer flooding in such reservoirs. They confirmed its technical and economic feasibility and emphasized the effect of the polymer injection rates on the project's financial aspects.

In 2014, Saleh, Wei, and Bai (43) performed a detailed statistical examination of 481 polymer floods. Based on field data, they suggested updated screening criteria for polymer flooding. Their analysis showed that polymer flooding can be applied to low-permeability reservoirs, high reservoir temper-

atures, and high oil viscosity reservoirs, expanding its applicability to a wider range of reservoirs.

Renouf (2014) (44) conducted a study on 32 polymer floods in Western Canada, focusing primarily on heavy oil fields. The research revealed that polymer floods can recover additional oil from reservoirs. The percentage of oil recovery ranged from 0.5% to 14%, which is an improvement. However, the study also found that injectivity reduction is a common problem associated with polymer floods.

In 2014, Standnes and Skjevraak (45) completed a thorough analysis of 72 polymer flooding projects, spanning from 1964 to 2014, including 6 offshore and 66 onshore. The review revealed that HPAM polymers were the most commonly used (92%), with a few instances of biopolymers and one project utilizing hydrophobic associative polymer. Of the projects studied, approximately 40 were successful, while 6 were deemed discouraging. The study found that secondary-mode polymer injection resulted in higher success rates than tertiary injections. There were no significant differences between successful and discouraging projects regarding polymer concentration, resistance factors, polymer retention, well spacing, reservoir temperature, and oil viscosity.

Sheng, Leonhardt, and Azri (2015) (46) analyzed 733 polymer floods globally and found that the average incremental cost of polymer flooding was \$US 4.35 per barrel. They also proposed new screening criteria for polymer flooding to expand its applicability to low-permeability and high-oil-viscosity reservoirs.

Zhang et al. (2016) (47) carried out a survey on 55 polymer floods in China. Based on their field applications, they recommended revised screening criteria for polymer flooding. They suggested that polymer injection should be applied in reservoirs where the oil's viscosity is less than 285 cP.

By December of 2017, the Daqing oil field successfully extracted 1.6 billion barrels (0.219 billion tons) of oil. Polymers have proven to be particularly effective in certain reservoirs, such as Thinly-bedded Clastic Layers (TCLs) with low-permeability layers, resulting in an impressive 4% incremental oil recovery factor (IORF) of the original oil in place (OOIP). Daqing continues to explore new methods to improve oil recovery in post-polymer-flooding reservoirs, including field tests with high-concentration, high-molecular-weight (HCHMW) polymers, making it the largest polymer application to date (48, 49, 50).

The research and surveys conducted over the years have provided valuable insights into the effectiveness of polymer flooding in oil reservoirs. These studies have highlighted the impact of factors such as polymer types, reservoir

characteristics, injection rates, and environmental considerations on the success of polymer flooding projects. The use of polyacrylamide polymers has been predominant, with biopolymers being utilized in fewer cases. Additionally, updated screening criteria for polymer flooding have expanded its applicability to low-permeability reservoirs and those with high oil viscosity. Despite some challenges, such as injectivity reduction and the impact of factors like water salinity and polymer degradation on project outcomes, polymer flooding remains a technically and economically viable enhanced oil recovery method, particularly in reservoirs with favorable characteristics.

### 1.3

#### **Polymer of common use in EOR: types and properties**

The polymer flooding method involves injecting an aqueous solution that contains polymers into the oil reservoir. These polymers consist of monomers, that are bonded together by covalent bonds. Depending on the repeating units of the monomers, different types of polymer structures can be formed, including linear, branched, or three-dimensional networks, as shown in Figure 1.4. Polymers are known for their high molecular weight, typically ranging from thousands to millions of Daltons, and their polydispersity, which is measured by the polydispersity index (PDI). A lower PDI, found in monodisperse polymers with a narrower molecular weight distribution, enhances mechanical strength and modulus due to uniform chain lengths. On the other hand, polydisperse polymers with higher PDIs show a broader distribution of molecular weights, resulting in increased brittleness due to the presence of shorter chains that act as defects. This correlation between polydispersity and mechanical properties extends to other physical attributes such as optical, electrical, and thermal properties, emphasizing the importance of understanding and managing polydispersity to customize polymer properties for various applications.(51, 52, 53, 54, 55).

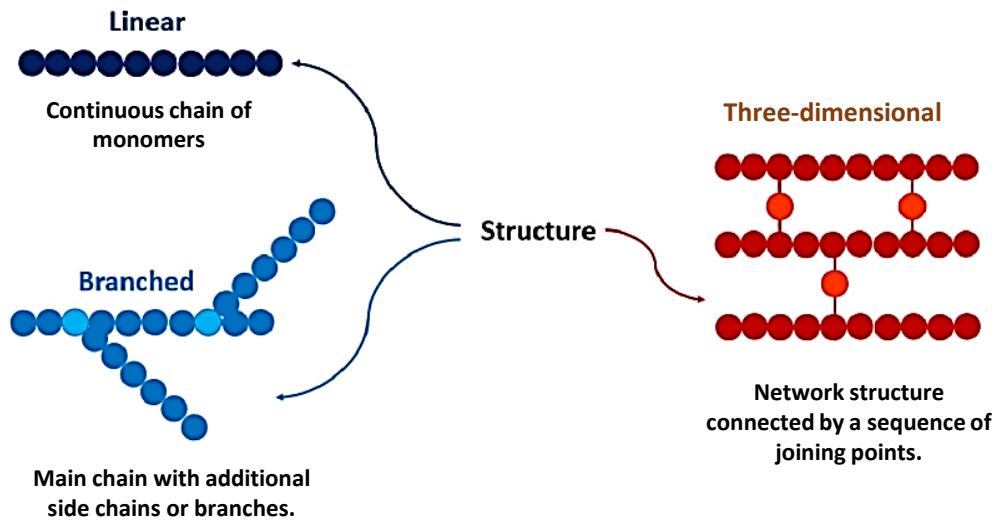


Figure 1.4: Classification of polymers by structure, adapted from (56).

Polymers play a crucial role in the petroleum industry, where they are used for various purposes. These polymers can be divided into two main categories: biopolymers and synthetic polymers. Biopolymers, like Xanthan gum, are naturally occurring, while synthetic polymers, such as HPAM, are artificially produced. Xanthan gum and HPAM are two widely used polymers in the oil industry. They are used for various applications, such as increasing the viscosity of drilling fluids, reducing friction, and improving oil recovery rates. A comprehensive overview of the various types of polymers used in the petroleum industry is provided in Table 1.1.

Product Name	Monomeric Unit	Molecular Weight [Da]	Form	Price (USD)	Properties	References
<b>Biopolymer</b>						
Xanthan gum	D-mannose, D-glucose, pyruvic acid, D-glucuronic acid	$2 \times 10^6$ to $2 \times 10^7$	Powder	12/kg	Thickening, cross-linking	Garcia et al. (57)
Scleroglucan	D-glucose	$1.3 \times 10^5$ to $6 \times 10^6$	Powder	50/kg	Thickening	Bakhshi et al. (58)
Welan gum	D-glucose, D-glucuronic acid, L-mannose, L-rhamnose	$6.6 \times 10^6$	Powder	1.5/kg	Cross-linking, thickening	Ai et al. (59)
Cellulose	D-glucose	$2 \times 10^6$	Powder	4/kg	Thickening, filtration, adsorption	Gupta et al. (60)
Guar gum	D-mannose	$10^6$ to $2 \times 10^6$	Powder	2/kg	Thickening, cross-linking	Rellegadla et al. (61)
Sesbania gum	D-galactose, D-mannose, D-galactose	$5 \times 10^5$	Powder	1.75/kg	Thickening, cross-linking, adsorption	Tang et al. (62)
Chitin/chitosan	D-glucosamine, N-acetyl-D-glucosamine	$2 \times 10^3$ to $10^6$	Powder	220/kg	Adsorption	Abraham et al. (63)
<b>Synthetic polymer</b>						
HPAM	Acrylamide and acrylate	$25 \times 10^6$	Powder	4/kg	Thickening, viscoelasticity	Li et al. (64)
KYPAM	AM/AHPE	$25 \times 10^6$	Powder	6/kg	Cross-linking	Li et al. (64)

Table 1.1: Overview of types of polymer used in petroleum industry. (65).

HPAM is a synthetic linear polymer that is more commonly used in EOR due to its low cost and ability to be produced on a large scale, as mentioned in several studies (66, 67, 68, 5). However, the utilization of high molecular weight HPAM in porous media can give rise to challenges. Specifically, the injection of this polymer into formations with low permeability may pose a significant difficulty due to the large hydrodynamic volume of the polymer (69). Compared to other polymers, HPAM displays properties of both elastic and viscous materials with the highest viscosity and viscoelastic properties, which makes it an ideal choice for EOR applications (70, 71). The high viscosity of HPAM is a result of the long chain molecules and the negative charges present along the polymer chains. Due to these negative charges, the polymer chains repel each other, causing them to stretch and increase in viscosity (Figure 1.5). According to Lee (72), it has been reported that HPAM can attain the desired level of viscosity even at low concentrations.

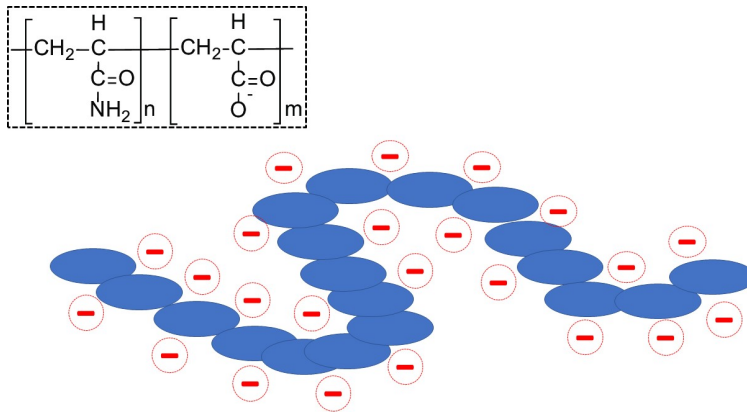


Figure 1.5: The condensed structural formula of the HPAM polymer (between dotted lines) and a schematic diagram. In the diagram, blue spheres indicate the chemical skeleton while red negative charges denote the carboxylic groups (73).

The concentration of polymer in a solution affects its state, which can range from dilute to semi-dilute or concentrated and depends on the degree of chain entanglement (Figure 1.6). A dilute solution is characterized by well-separated polymer chains that do not interact significantly with each other. The concentration of the polymer is low, resulting in a low viscosity. Dilute solutions are often studied to understand the intrinsic properties of polymer chains, such as their conformation, dynamics, and interactions with the solvent. They serve as a starting point before moving on to more complex systems like semidilute or concentrated solutions.

Semidilute solutions are the intermediate stage between dilute and concentrated solutions. In semidilute polymer solutions, the concentration of

chains is high enough that they start interacting with each other, leading to entanglements and increased viscosity. Both intra-chain and inter-chain interactions determine the behavior of polymer chains in semidilute solutions.

Concentrated solutions are characterized by densely packed polymer chains that exhibit significant interactions, such as overlap and entanglement. The high concentration of polymer chains results in collective behavior and various intermolecular interactions. Physical crosslinks may also form. Therefore, the properties of concentrated solutions are influenced by the structure of the polymer network, intermolecular interactions, and chain entanglements. The interactions between polymer chains significantly impact the solution's macroscopic properties, leading to unique behaviors that differ from those observed in dilute or semidilute solutions (74, 75, 76).

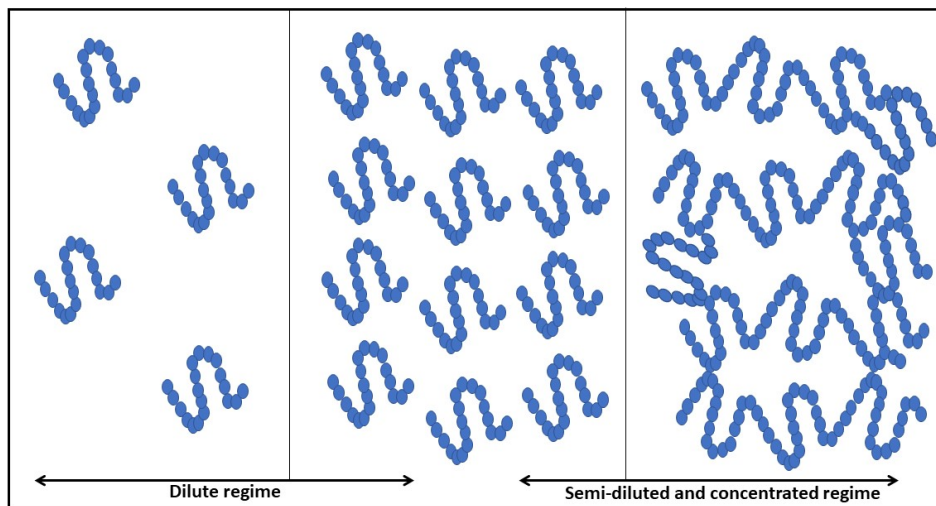


Figure 1.6: Schematic illustration of polymer chains, which are long chains of repeating units. The chains are depicted as blue spheres and are shown at different concentration regimes, adapted from (77).

## 1.4 Polymer Rheological Behavior

Rheology is a subfield of physics concerned with investigating the behavior of materials under the influence of external forces. It encompasses the study of how materials deform and flow in response to these forces and has applications in various fields, including materials science, engineering, and geophysics. Essentially, rheology seeks to understand how materials respond to mechanical stress and how they can be manipulated or optimized for various applications (78).

The viscosity is a fundamental property of fluids, which characterizes their resistance to flow. It can be visualized by imagining a fluid in a confined space between two parallel plates, with one plate stationary and the other in motion.

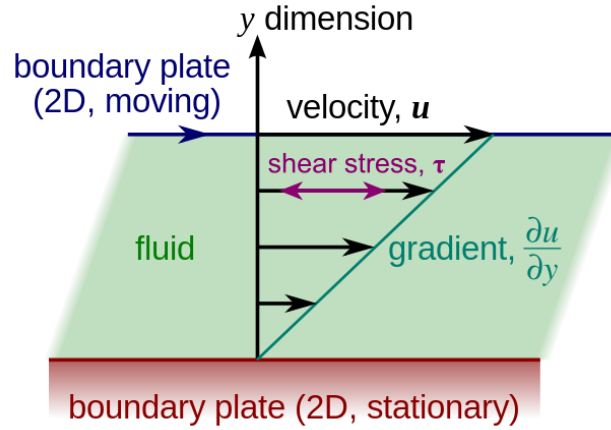


Figure 1.7: Illustration of shear stress in a flow between two parallel plates. (79).

In this scenario, the velocity of fluid particles is highest near the moving plate and gradually decreases as we move toward the stationary plate (78). The rate of change of velocity with the distance between the plates is called the shear rate  $\dot{\gamma}$ , defined in Equation 1-1, while the force exerted on the moving plate per unit area is called the shear stress defined in Equation 1-2. The ratio of shear stress to shear rate defines viscosity  $\eta$  and is shown in Equation 1-3.

$$\dot{\gamma} = \frac{du}{dy} \quad (1-1)$$

$$\tau = F/A \quad (1-2)$$

$$\eta = \frac{\tau}{\dot{\gamma}} \quad (1-3)$$

There are two categories of fluids based on their viscosity behavior and kinematic history: Newtonian and non-Newtonian fluids (Figure 1.8). Newtonian fluids have a constant viscosity, whereas non-Newtonian fluids exhibit viscosity that changes with the shear rate. This results in a non-linear correlation between shear stress and shear rate. Non-Newtonian fluids display pseudoplastic or dilatant behavior, where the former refers to a decrease in viscosity as the shear rate increases, and the latter refers to an increase in viscosity with an increasing shear rate (80, 81).

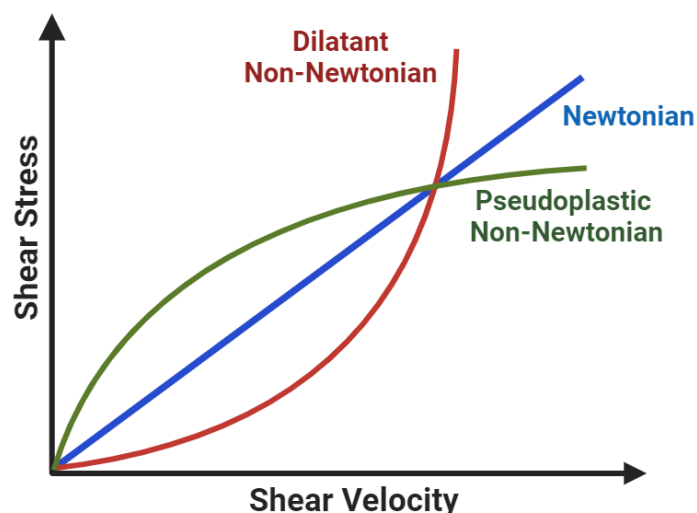


Figure 1.8: Viscosity Behavior of Newtonian and Non-Newtonian Fluids from (80).

Non-Newtonian behavior comes from unique characteristics of the liquid like high average molecular weight ( $M_w$ ), broad molecular weight distribution (MWD), and the ability to change the configuration of polymer coils in response to flow (82). The behavior of non-Newtonian fluids differs significantly from Newtonian fluids that comply with Newton's law of viscosity. This characteristic has a significant impact on how polymer solutions behave under different types of flow, such as porous media that involve both shear and extensional kinematics (83).

#### 1.4.1 Shear Viscosity of polymer solutions

To evaluate the viscosity of polymer solutions, a rheometer that applies a simple shear flow to the solution is commonly utilized (78). The shear viscosity curve of polymer solutions in the semi-dilute regime is commonly represented by Figure 1.9 within a moderate concentration range.

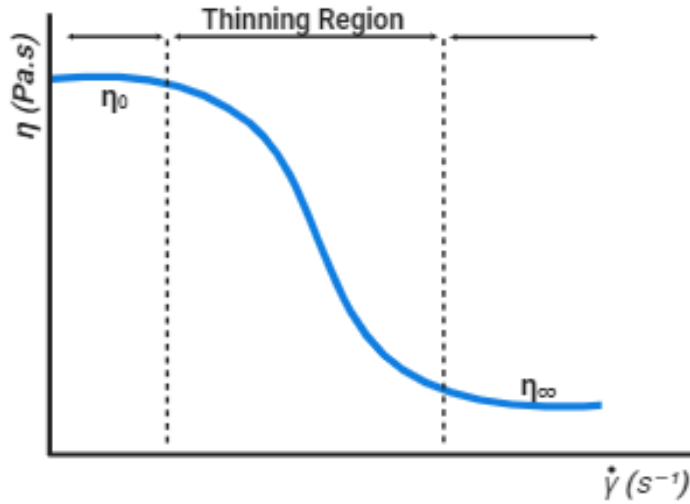


Figure 1.9: Shear viscosity curve of polymer solutions (84).

In an ideal scenario, if shear measurements were conducted over an extensive and sufficient range of shear rates, three regions could be identified over the viscosity curve. The first region is the upper Newtonian plateau or the zero-shear viscosity ( $\eta_0$ ). At low shear rates, the viscosity of polymer solutions is determined solely by their concentration and the size of polymer molecules. The internal bonds between polymer coils remain unchanged, resulting in Newtonian behavior dominating viscosity. As shear rates rise, polymer coils separate and align with the flow direction. This alignment disrupts the Newtonian behavior, reducing the friction between polymer coils, which is manifested as a non-Newtonian shear thinning regime where viscosity decreases with increasing shear. The third region commences when the shear rate is increased even further where the shear is sufficiently high to break all internal bonds between polymer coils, resulting in the lowest possible viscosity of the tested polymer solution. Another Newtonian plateau is observed at this range, called infinite-shear viscosity ( $\eta_\infty$ ) (85, 86, 87).

Numerous models have been proposed to describe the relationship between viscosity and shear rate in simple shear flow (Table 1.2). These models are used to describe the shear thinning behavior and provide insights into the rheological properties of polymer solutions, such as their flow behavior index and consistency index.

Name	Viscosity equation
Power-Law (88)	$\eta = K\dot{\gamma}^{n-1}$
Carreau-Yasuda (89)	$\eta = \eta_{\infty} + (\eta_0 - \eta_{\infty}) (1 + (\lambda\dot{\gamma})^a)^{\frac{n-1}{a}}$
Herschel-Bulkley (90)	$\eta = \sigma_y \dot{\gamma}^{-1} + K\dot{\gamma}^{n-1}$

Table 1.2: Polymers modeling where  $\eta$  : Viscosity;  $K$  : Consistency index;  $\dot{\gamma}$  : Shear rate;  $n$  : Flow behavior index;  $\eta_{\infty}$  : Infinite-shear viscosity;  $\eta_0$  : Zero shear viscosity;  $a$ : Transition parameter and  $\sigma_y$ : Yield stress are fitting factors.

### 1.4.2

#### Viscoelasticity and Extensional behavior of polymer solutions

A viscoelastic fluid is a material that displays a combination of elastic and viscous characteristics (91, 92). In order to comprehend viscoelastic behavior, it is imperative to have a clear understanding of the properties exhibited by both elastic and viscous substances. When an ideally elastic substance experiences slight deformation, it will naturally return to its original state once the stress is removed. Hook's law states that achieving complete energy recovery in a material's deformation during a shear process is possible without consequential loss (93). Shear stress ( $\tau$ ), shear or rigidity modulus ( $G$ ), and strain (deformation) ( $\dot{\gamma}$ ) are related as follows:

$$\tau = G\gamma \quad (1-4)$$

In contrast, an ideally viscous material completely dissipates the energy during deformation. Once the load is removed, the material does not revert to its original shape but stays deformed just as it was at the peak of the loading phase. Newton's law explains this characteristic:

$$\tau = \eta\dot{\gamma} \quad (1-5)$$

where  $\eta$  is the viscosity of the material.

The basic mechanical models of viscoelasticity are the Kelvin and the Maxwell models. The Kelvin model integrates both elastic and viscous behavior by combining a spring (representing the elastic component) and a dashpot (representing the viscous component) in parallel (Figure 1.10b). The Maxwell model, on the other hand, represents viscoelastic behavior as a spring and dashpot connected in series (Figure 1.10a).

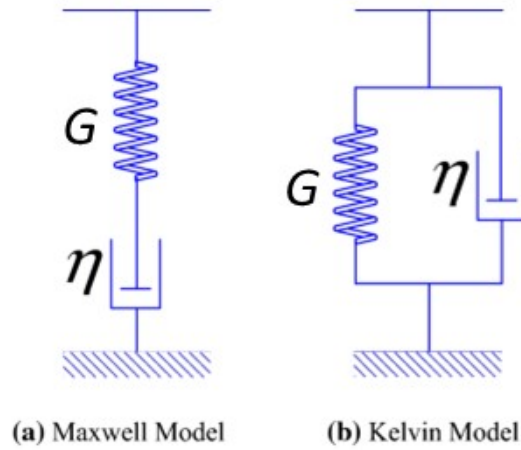


Figure 1.10: Constitutive models of viscoelastic theory: (a) Maxwell model and (b) Kelvin model.  $G$  represents the extension modulus, and  $\eta$  indicates the viscosity adapted from (94).

Extensional flows are characterized by persistent deformation of a material element. It is classified according to the direction of the extension (95). Uniaxial extension is sketched in Figure 1.11. The velocity components for uniaxial extension flow with constant extension rate  $\dot{\epsilon}$ , in Cartesian coordinates, are given by:

$$v_1 = \dot{\epsilon}x_1, v_2 = -\frac{1}{2}\dot{\epsilon}x_2, v_3 = -\frac{1}{2}\dot{\epsilon}x_3. \quad (1-6)$$

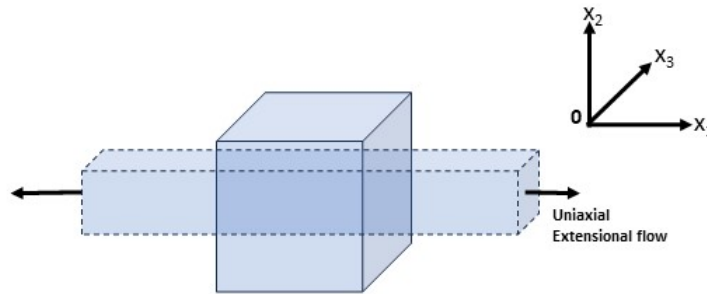


Figure 1.11: Uniaxial extensional flow with a constant extension rate along the  $x_1$  axis.

These equations describe how the fluid's velocity components change in a uniaxial extensional flow, where the fluid is stretched in one direction (along the  $x_1$  axis) and contracts in the other two perpendicular directions (along the  $x_2$  and  $x_3$  axes) due to the extensional fluid rate ( $\dot{\epsilon}$ ). As a result, two fluid particles that are initially a distance  $L_0$  apart in the  $x_1$  direction are a distance  $L$  apart after time  $t$ , where  $L$  is given by the equation:

$$L = L_0 \exp(\dot{\epsilon}t) \quad (1-7)$$

As depicted in Figure 1.12, molecules become aligned and stretched along the  $x_1$  direction within this flow field. Notably, in a purely extensional deformation, the fluid element undergoes only extension with no rotation or shearing (93). The uniaxial extension is of particular interest since it allows for the investigation of the unique behavior of materials under steady extensional flow conditions. Therefore, most extensional rheometers are designed to generate uniaxial extensional flow to study the rheological properties of materials in this specific flow regime (96, 97, 98).

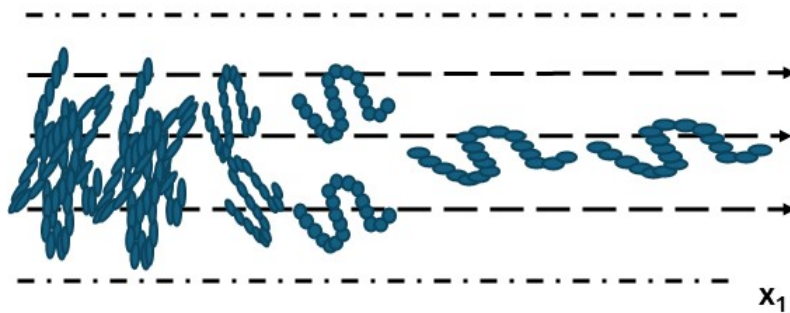


Figure 1.12: Uniaxial extensional flow with a constant extension rate along the  $x_1$  axis. The polymer chains are depicted as blue spheres.

In order to understand the rheological behavior of materials in uniaxial extensional flow, a material element of a specific shape is often analyzed for deformation. As depicted in Figure 1.13, a cylindrical rod-shaped element is commonly used for this purpose. The element with an initial diameter  $D_0$  and initial length  $L_0$  is stretched homogeneously at a constant extensional rate along the axial direction  $z$ , and the radius of the element decreases uniformly along the length.

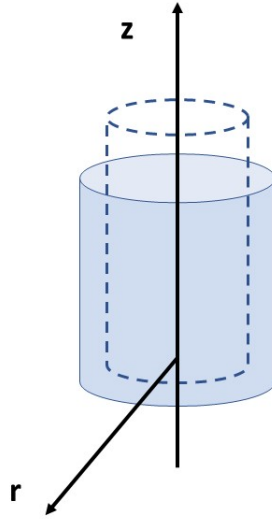


Figure 1.13: The schematic diagram depicts the process of uniaxial extension, where a cylindrical object is stretched in a single direction.

The strain in the  $z$  direction is given by:

$$\varepsilon = \frac{\Delta z}{z} \quad (1-8)$$

and the deformation rate is

$$\dot{\varepsilon} = \frac{\varepsilon}{\Delta t} = \frac{1}{\Delta t} \frac{\Delta z}{z} = \frac{1}{z} \frac{\Delta z}{\Delta t} = \frac{v_z}{z} \quad (1-9)$$

where  $v_z$  is the velocity component in the axial direction,  $z$  is the axial position, and  $\Delta z$  and  $\Delta t$  are the changes in position and time, respectively. Hence  $v_z = \dot{\varepsilon}z$ .

For an incompressible fluid, for the continuity equation

$$\frac{\partial v_z}{\partial z} = -\frac{1}{2} \frac{\partial}{\partial r} (r v_r) = \dot{\varepsilon} \quad (1-10)$$

from which the radial velocity is found to be  $v_r = -2\dot{\varepsilon} \frac{r}{2}$ . The other component  $v_\theta$  is zero. For this flow field, streamlines are given by  $r^2 z = \text{constant}$ .

By integrating the Equation of the velocity component in the axial direction, it has been found that the length of the specimen,  $L_t$ , increases exponentially from its initial length,  $L_0$ , as given by Equation (1-7). Furthermore, from the Equation of the radial velocity, the filament diameter,  $D_t$ , at any time  $t$  decreases from its initial value,  $D_0$ .

$$D(t) = D_0 \exp\left(-\frac{\dot{\varepsilon}t}{2}\right). \quad (1-11)$$

Within this equation, the variable  $\varepsilon$  signifies the Hencky strain, defined as:

$$\varepsilon = 2\ln\left(\frac{D(t)}{D_0}\right). \quad (1-12)$$

In constant extensional flow, the Hencky strain can be expressed as  $\dot{\varepsilon}t$ , where  $\dot{\varepsilon}$  is the effective extensional rate.

Consider a scenario where uniaxial extension begins at  $t = 0$ , and the fluid is initially stress-free. During this situation, the fluid opposes the extensional motion, and this resistance to extensional deformation is known as extensional viscosity  $\eta_e$ . This term is similar to the widely recognized shear viscosity, which represents resistance to shear motion.

When discussing extensional viscosity, we're referring to the relationship between the applied extensional stress (denoted as  $\sigma_{zz}$ ) and the extensional strain rate ( $\dot{\varepsilon}$ ). It's important to keep in mind that the total stress in the axial direction ( $\sigma_{zz}$ ) includes an unknown pressure component (p), which must be subtracted to determine the extensional viscosity accurately. Do this, we can take the difference between the normal stress in the r direction ( $\sigma_{rr}$ ) and the total stress in the z-direction ( $\sigma_{zz}$ ). This difference is equivalent to the difference between the stresses associated with deformation in the two directions ( $\tau_{zz} - \tau_{rr}$ ). Thus, we can define  $\eta_E$  as such:

$$\eta_e = \frac{\tau_{zz} - \tau_{rr}}{\dot{\varepsilon}} \quad (1-13)$$

A comprehensive understanding of the behavior of viscoelastic fluids under uniaxial extension requires careful consideration of the relationship between extensional viscosity and fundamental factors. In this context, the relaxation time ( $\lambda$ ) is of particular interest as it plays a significant role in determining extensional viscosity, reflecting the time taken by the polymer to return to its original shape after undergoing deformation in porous media. Recent studies have shown that the extensional relaxation time provides accurate results, particularly in scenarios where shear forces are not predominant (99, 100, 4, 101, 102, 103).

The extensional relaxation time provides valuable insights into how materials respond to applied stresses and deformations over time, allowing for a distinction between elastic and viscous behavior. This concept is crucial

in estimating the response of viscoelastic fluids to extensional deformation, particularly in complex flow conditions encountered in porous media and enhanced oil recovery processes. Therefore, the method used to calculate the relaxation time can significantly impact the ability to predict the behavior of viscoelastic materials (104).

The upper convected Maxwell model (UCM) is commonly used to estimate the extensional relaxation time of polymers. This model fits well with the elastic regime of filament-diameter vs. time data, providing valuable insights into the extensional behavior of polymers. The mathematical solutions presented in Table 1.3 allow fits to raw diameter data and calculated viscosity data, which is particularly beneficial as the extensional viscosity versus strain fit is sensitive to different aspects of the data compared to just the diameter fit (100, 4, 101).

Constitutive Model	Viscosity equation	Mathematical solution
Newtonian Model	$\tau = \eta\dot{\epsilon}$	$R_{\text{mid}}(t) = 0.071 \left(\frac{\sigma}{\eta_s}\right) (t_c - t)$
Power Law Fluids	$\tau = K\dot{\epsilon}^n$	$R_{\text{mid}}(t) = \phi_{\text{est}} \frac{\sigma}{K} (t_c - t)^n$
Upper Convected Maxwell (UCM)	$\tau + \lambda \frac{D\tau}{Dt} = \eta\dot{\epsilon}$	$R_{\text{mid}}(t) = R_0 (GR_0/\sigma)^{\exp(-1/3\xi)}$

Table 1.3: Constitutive models and their equations.

In addition, the extensional relaxation time is important in flow of polymer solutions through porous media due to the intense extensional flow caused by significant changes in the flow cross-section as the liquid flows through the pore throats. This environment leads to substantial polymer deformation, further emphasizing the importance of understanding and measuring the extensional viscosity and relaxation time for accurate predictions of fluid behavior under such conditions. Overall, the extensional properties are a crucial factor in the behavior of viscoelastic fluids under uniaxial extension and require careful consideration in research and practical applications.

## 1.5 Polymer Flooding Mechanisms in EOR

The success of polymer flooding in EOR can be attributed to different mechanisms (39): reducing the water/oil mobility ratio, reducing the residual oil saturation, and improving conformance. The mobility ratio ( $M$ ), Equation 1-14, is defined as the ratio of the mobility of the displacing fluid (water) to that of the displaced fluid (oil). The addition of polymer to water increases

water viscosity, reducing the viscosity contrast between oil and water, therefore leading to a lower mobility ratio which improves sweep efficiency.

$$M = \frac{\mu_o k_w}{\mu_w k_o}, \quad (1-14)$$

$\mu_w$  and  $\mu_o$  are the viscosity of water and oil, and  $k_w$  and  $k_o$  are the relative permeabilities of water and oil, respectively.

Reducing the water/oil mobility ratio enhances fractional oil flow ( $f_o$ ), as defined by the Buckley–Leverett theory, and presented in Equation 1-15. This improvement results in a more rapid oil production and delayed water breakthrough. Early initiation of polymer flooding is often beneficial for fields with high mobility ratios.

$$f_o = \frac{1}{1 + M}. \quad (1-15)$$

Conformance control involves managing reservoir heterogeneity to improve flooding process sweep efficiency. Its effectiveness, however, depends on various factors, including oil and reservoir properties, polymer type and concentration, and specific flooding conditions.

Figure 1.14 (105) illustrates the enhanced displacement front stability in polymer flooding compared to waterflooding, contributing to increased sweep efficiency and crude oil recovery. A comprehensive understanding of these mechanisms is crucial for designing effective polymer flooding strategies in EOR applications (106, 107).

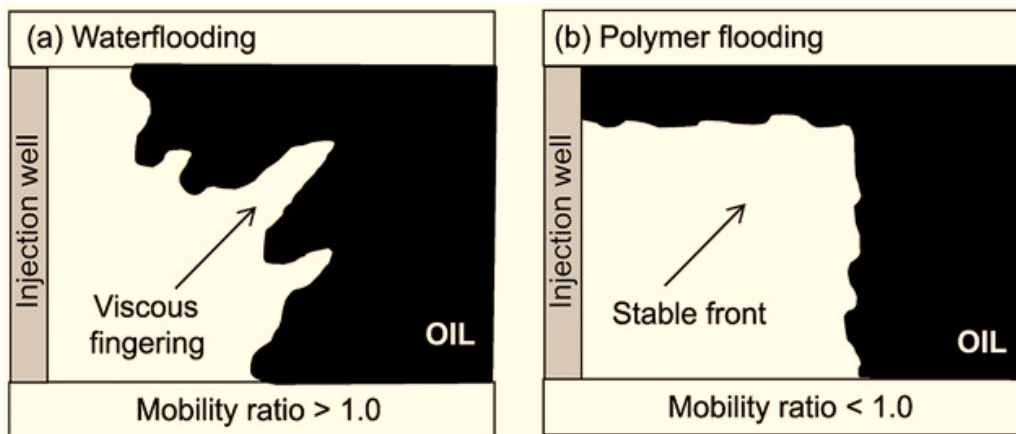


Figure 1.14: Improvement of displacement front stability in oil reservoirs by adding HPAM: (a) Waterflooding and (b) Polymer flooding (105).

The literature suggests different ways in which viscoelastic polymer solutions can minimize residual oil saturation. These mechanisms include:

**Pulling Mechanism:** The polymer solution pulls out oil trapped in pore dead ends. Following water flooding, where residual oil is fragmented into

individual drops, the injection of viscoelastic polymer solutions pulls these drops together to form oil threads, as shown in Figure 1.15. These threads facilitate the movement of oil towards the downstream residual oil, leading to the creation of an oil bank that can be more effectively recovered (68, 108, 109, 110).

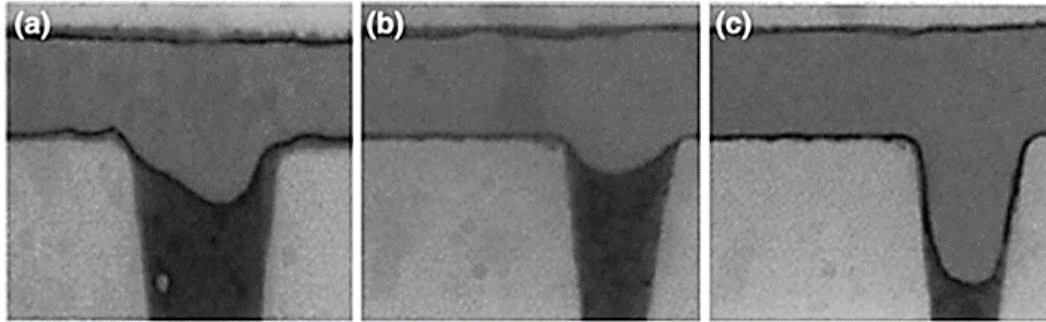


Figure 1.15: After water (a), glycerin (without elasticity) (b), and HPAM flooding (c), residual oil is found in the dead ends (79).

**Stripping Mechanism:** The higher shear stress along the pore walls in the polymer solution strips continuous oil films in oil-wet cores more effectively than waterflooding (111). This stripping mechanism has been found to have a positive impact on oil recovery, as reported by several studies (112, 113, 114, 115). The stripping effect also changes the wettability of the rock surface from oil-wet to more water-wet, which further increases oil recovery.

**Oil-Thread Flow Mechanism:** After waterflooding, residual oil exists as isolated droplets that are difficult to extract, as shown in Figure 1.16 (a). Fortunately, polymer solutions can be used to capture these droplets and form elongated columns of oil, known as "oil threads," which transport the oil downstream, as shown in Figure 1.16 (b). The viscoelastic properties of the polymer solution play a critical role in maintaining the cylindrical shape of these oil threads, preventing them from breaking apart (79, 108). While interfacial tension between the oil and polymer solution could potentially destabilize these oil columns and break them into droplets, the elasticity of polymer solutions can resist this deformation. As a result, the oil column may become thinner and break up into smaller ganglia, leading to lower residual oil saturation, or it may be broken into longer-length oil ganglia that are more easily mobilized (116).

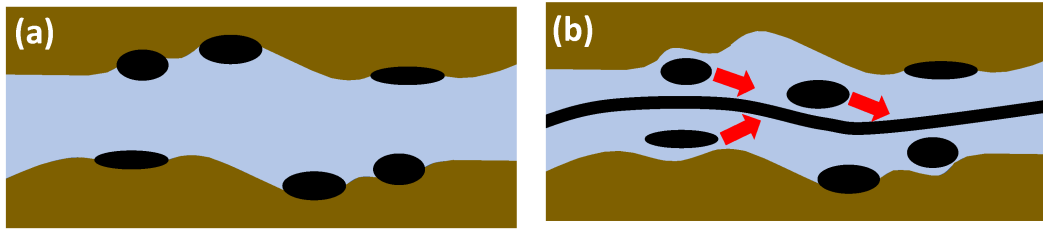


Figure 1.16: (a) In a post-conventional water flooding scenario, the oil remains as isolated drops. (b) Introducing a viscoelastic polymer solution creates an oil thread that serves as a pathway for the oil to flow upstream. This ultimately leads to the formation of an oil bank downstream (68).

**Thickening Deformation Effect:** The apparent viscosity of polymer solutions increases in high-permeability zones, which redirects the solution into low-permeability zones and improves sweep efficiency (117, 118, 119). Recent research indicates that the extra pressure associated with the flow of viscoelastic polymer solution through porous media is not only associated with the high extensional viscosity but also to a flow instability and leads to chaotic flow, a phenomena known as elastic turbulence. This interpretation is supported by several studies (120, 121) which demonstrate the potential of viscoelasticity, specifically elastic turbulence, to enhance oil recovery.

## 1.6

### Polymer solution flow in porous media

Polymer solutions exhibit unique behavior when flowing through porous media due to the complex kinematics of the pore scale flow. The flow in the pore space is complex, with regions dominated by shear and regions dominated by extensional deformation. The flow response of polymer solutions through porous media is strongly dependent on how the solution behaves when submitted to different deformation kinematics. The characteristics of porous media, such as porosity and permeability, are essential to understanding the difference between the flow behavior of HPAM polymers in shear flow and in flow through porous media.

Figure 1.17 illustrates the typical mechanical response of HPAM polymer solutions in flow through porous media, with regions of shear (a) and extensional (b) deformation. The complex flow behavior through porous media is represented by the apparent viscosity ( $\eta_{app}$ ) described by Darcy's law (Equation 1-16), which results from the polymer solution's response to both shear and extensional deformation rates. At a very low deformation rate (flow rate), the viscosity is constant, which represents the Newtonian plateau of the flow curve. As the flow rate increases, the shear viscosity falls (shear thinning be-

havior). At an even higher flow rate, the deformation rate associated with the extensional flow becomes high enough that the extensional thickening behavior of the polymer solution becomes relevant, leading to an increase in the apparent viscosity. At a very high flow rate, the polymer molecules break, reducing the average molecular weight of the solution and, consequently, the apparent viscosity of the flow (122, 123, 124, 3).

$$\eta_{app} = \frac{kA}{q} \frac{\Delta P}{L} \quad (1-16)$$

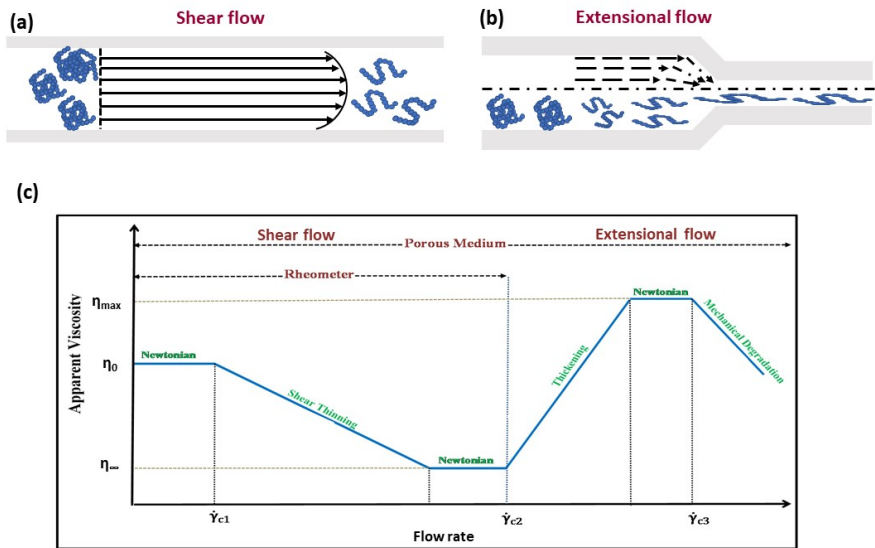


Figure 1.17: Influence of shear rate on the viscoelastic behavior of HPAM solution in (a) shear flow, such as in rotational rheometer (b) extensional flow, such as in porous media adapted from (3, 125)

The behavior of HPAM in porous media has been studied extensively, and it has been found that its viscoelastic properties are responsible for its thickening behavior. This behavior is characterized by increased viscosity as the flow rate rises. This behavior is not observed in a rheometer or the flow through a tube because these flows are only subjected to shear deformation, whereas, in porous media, the flow is subjected to both shear and extensional deformation (126, 127, 128, 129, 87).

Three theories in the literature explain the thickening behavior of HPAM solutions in the flow through porous media: (a) the coil–stretch theory, (b) the transient network theory, and (c) the presence of elastic flow instabilities.

The coil–stretch transition theory asserts that the increase in the apparent viscosity occurs due to extensional viscosity that develops when polymer molecules extend from a coiled state to a stretched state in response to an elongational flow field. The transition occurs when the rate of elongational flow exceeds a critical value that is related to the relaxation time of the

polymer molecule. Beyond this rate, the molecules no longer have enough time to recoil to their original conformation between successive stretching events, leading to a stretched state. This stretching of individual molecules causes an increase in viscosity and resistance to flow and is a critical factor in dilatant behavior but only accounts for the behavior of individual molecules in solution (130, 131, 132).

Transient network theory suggests that flow resistance in semi-dilute polymers increases due to molecular interactions and entanglement formation at high flow velocities. This behavior is particularly observable in elongational flow systems, where the polymer chains can stretch and become entangled, forming a transient network that affects the viscosity of the solution. This leads to non-Newtonian flow behaviors, such as increased resistance to flow or enhanced elongational viscosity, which highlight the role of transient entanglement networks in extensional rheology. The transient network theory suggests multiple polymer chains entangle and form temporary networks within the solution. These networks are transient because they are not permanent chemical bonds but physical entanglements that can form and reform during the flow. The presence of these networks can significantly alter the macroscopic rheological properties of the polymer solution, leading to enhanced viscoelastic behavior and more significant thickening effects (133, 134).

Recent studies have provided insights into the thickening behavior observed during polymer transport in porous media. This phenomenon is attributed to elastic instabilities resulting from polymer-induced stresses. These instabilities generate chaotic flow fields, similar to those seen in inertial turbulence, and are influenced by the rheology of the polymer solution and the flow field's geometry. Kawale et al. (135) conducted experiments with microfluidics and observed two elastic instabilities when an HPAM solution flowed through porous media in the presence of salt. The first instability occurred during a shear-thinning regime, resulting in the formation of stationary dead zones around obstacles. Increasing the flow rate led to the second elastic instability, causing the dead zones to become unstable, accompanied by strong temporal fluctuations in pressure drop and flow field. The authors attributed the onset of shear-thickening to the second type of elastic instability. Browne and Datta used direct flow visualization in a 3D porous medium and showed that shear thickening is due to the onset of elastic instability, resulting in strong spatiotemporal fluctuations. They argued that the viscous dissipation caused by flow fluctuations leads to the anomalous increase in the apparent viscosity (136, 137, 138, 139, 140, 141, 142).

Understanding the thickening behavior of HPAM solutions is crucial

for EOR applications. This is because HPAM injection can improve front stability during polymer flooding, alleviating viscous fingering. This improved front stability is attributed to the viscoelasticity of HPAM, including its thickening behavior. However, problems such as high-pressure buildup due to shear thickening behavior can affect injectivity under certain reservoir conditions. Additionally, retention and mechanical degradation, associated with polymer viscoelasticity, may affect injectivity under certain reservoir conditions (143, 144, 145).

## 1.7

### **Mechanical Degradation in Polymer Flooding for EOR**

The deformation thickening effect observed in the flow of polymer solutions through porous media is beneficial for oil displacement. However, the intensity of viscoelastic forces is limited due to mechanical degradation of polymer molecules (3). Mechanical degradation occurs across various flow regions during the injection process of a polymer solution into an oil reservoir. Polymer molecules undergo high deformation rates while passing through pumps, flow lines, constrictions, valves, and the reservoir. The deformation rate experienced as the polymer solution flows through the reservoir rock ranges from 50,000 to 100,000  $\text{s}^{-1}$  in regions close to the injection wells. These intense deformation rates cause macromolecule chains of the polymer to break, resulting in a reduction in molecular weight distribution and, consequently, in solution viscosity and viscoelastic forces. Ultimately, mechanical degradation diminishes the mobility control potential of polymer solutions (8, 146, 147, 148, 127).

According to a study carried out by Al Hashmi et al. (8), the degradation of HPAM in an aqueous solvent was analyzed using a capillary rheometer. Figure 1.18 illustrates the experimental setup used. The aim of the researchers was to determine the extent of mechanical degradation by measuring the loss in viscosity of the solution effluent.

The researchers found that the total degradation of HPAM remained below 20% up to a shear rate of 15,000  $\text{s}^{-1}$ . However, beyond this value, the extent of degradation increased as the shear rate increased further. This suggests that the mechanical degradation of HPAM is a non-linear process, and it accelerates at high shear rates.

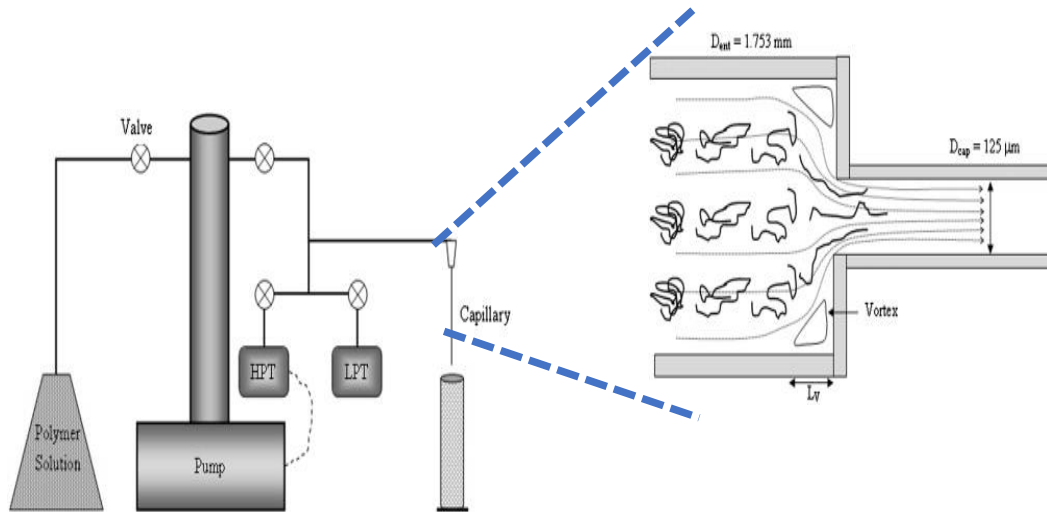


Figure 1.18: Schematic diagram of the experimental set-up and the contraction flow into the capillary adapted from (8).

Al-Shakry et al. (149) conducted a comprehensive study to investigate how mechanical degradation affects the flow properties of polymers in porous media and changes their rheology. The study involved subjecting polymer solutions to different degrees of pre-shearing and pre-filtering, which resulted in a significant reduction in the viscosity of the polymer solutions. These findings suggest that mechanical degradation, especially in HPAM polymer solutions, can have a significant impact on their viscosity and viscoelastic properties.

A similar study by Jouenne et al. (150) analyzed the behavior of HPAM polymer solutions when injected at high flow rates into a porous medium. The study explored various physicochemical parameters, such as salinity, polymer concentration, molecular weight, and degradation state, and their effects on the mobility reduction of these solutions. The authors also investigated the correlation between mobility reduction and the polymer's elasticity, which was measured using ex-situ methods like the screen-factor measurement and a newly developed extensional viscometer. The authors argue that traditional small-strain viscoelastic measurements may not adequately characterize the elastic behavior of polymer solutions under the large strain conditions experienced within a porous medium, such as during enhanced oil recovery operations.

In certain field applications, polymer solutions have demonstrated a 64% viscosity reduction in the flow from injector to producer wells (151). One possible approach to mitigate the effect of mechanical degradation in

enhanced oil recovery involves increasing the initial polymer concentration (152). Between 1990 and 2002, oilfield polymer injection projects mainly used HPAM concentrations of 1,000 to 1,300 ppm, whereas, for the period 2002-2016, concentrations were between 2,000 and 2,500 ppm (153). Concentrations in excess of 3,500 ppm are now commonplace in the industry (50). Some core flooding experiments designed to study the displacement of highly viscous crude oils (1,000 or 8,400 cp oils) used polyacrylamide concentrations ranging from 500 to 10,000 ppm (154). Nonetheless, this approach carries several drawbacks, such as high cost (155) and the risk of reservoir strata blockage, if concentrations are excessively high (156).

## 1.8

### Effects of Addition of SiO<sub>2</sub> Nanoparticles on HPAM

In the context of EOR, nanotechnology has recently been explored to enhance the efficiency of polymer solutions during flooding operations (10). Figure 1.19 shows the two approaches that have been considered: one involves incorporating nanoparticles into the polymer structure during its synthesis process, known as Polymer Grafted Nanoparticle (PGN). The second approach disperses particles in a previously prepared polymer solution, referred to as Polymer Nanofluid Suspension (PNS) (157). While both approaches show significant potential, PGN involves greater complexity in development, potentially compromising its applicability.

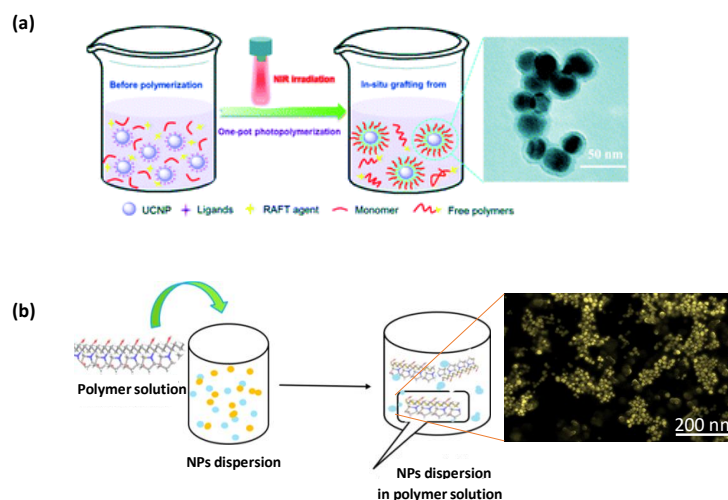


Figure 1.19: Schematic diagram for preparing (a) Polymer Grafted Nanoparticle and (b) Polymer Nanofluid Suspension (158, 159).

Research efforts have predominantly focused on PNS due to its higher

application feasibility, being tested in various polymeric solutions, leading to a substantial improvement in stability and performance (160, 161, 162, 11). Among various inorganic nanoparticles,  $SiO_2$  nanoparticles are widely used due to their high surface area, affinity between -OH (nanoparticle) and COO- (HPAM) groups, and cost-effective production (163).

The stability and rheological response of the solution depend on the conformation of the polymeric chains on the nanoparticle surface. According to Hu et al. (158), it is suggested that a three-dimensional network may be formed due to hydrogen bonds between carbonyl groups in low molecular weight polymers and silanol groups on the surface of  $SiO_2$  nanoparticles, as indicated in Figure 1.20.

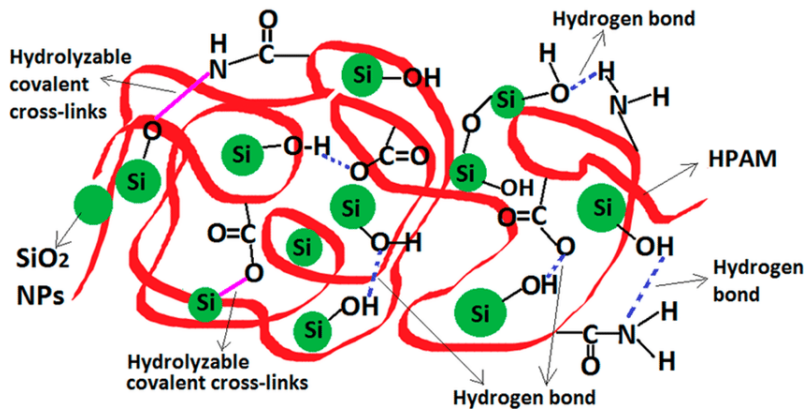


Figure 1.20: Schematic diagram to illustrate the three-dimensional network interactions between  $SiO_2$  NPs and HPAM polymer solutions (158).

Molecular dynamic simulations have been employed to study aggregation phenomenon of nanoparticles and polyacrylamide in polymer blends. Wei et al. (131) deduced hydrogen bonding interactions and van der Waals forces between polar functional groups in polymer molecular chains and silanol groups on the surface of  $SiO_2$  NPs from the binding energies in a reduced model of monomer polymer molecules. The results suggest significant interactions between nanoparticles and polymers, forming a more stable NPs-HPAM network.

Several studies have investigated the effect of adding  $SiO_2$  NPs to HPAM polymer solutions for EOR, demonstrating a significant improvement in the percentage of oil recovery (Table 1.4). Viscosity is one of the properties that improves with the addition of  $SiO_2$  NPs. Maghzi et al. (26) observed a 10% increase in the volume of oil displaced with the addition of only 0.1 wt.% of nanoparticles compared to the injection of a polymer solution without nanoparticles. These results suggest that the presence of  $SiO_2$  NPs in HPAM polymer can enhance its rheological properties, potentially leading to better oil recovery efficiency.

Further, the addition of  $SiO_2$  NPs to HPAM polymer can enhance its stability under elevated temperatures and in high salinity environments. Experimental evidence indicates that incorporating nanoparticles into HPAM solutions prevents the destruction of the polymer network structure and preserves its extended conformation even after prolonged exposure to elevated temperatures (164, 165). Despite previous investigations into  $SiO_2$  NPs dispersions in HPAM across diverse studies, the specific impact of mechanical degradation in NPs-HPAM systems remains unexplored. Particularly, the effect of  $SiO_2$  NPs addition on the rheological behavior of HPAM solutions subjected to mechanical degradation remains unknown.

Authors	Date	Dispersion medium	Porous media	Main findings	Extra oil recovery
Corredor et al.(12)	2019	Propanol DI water	Sandstone	Adding 0.2% SiO <sub>2</sub> -OTES NPs to HPAM solution increased oil recovery from 71.4% to 75.7% OOIP.	4.3 %
Zhang et al.(19)	2017	DI water	Sandstone	The HPAM/SiO <sub>2</sub> modified suspension improves flooding performance and increases oil recovery factor compared to other HPAM-based suspensions. It is effective at concentrations of 0.5-2.0 wt%.	10.54 %
Agi et al.(18)	2020	DI water	Sandstone	RH-SiO <sub>2</sub> NPs of 0.1wt% inhibited the precipitation and thermal degradation of HPAM	24 %
Cheraghian et al.(166)	2016	Brine	Sandstone	Nanosilica polymer solution showed an increase in oil recovery compared to polymer solution after one pore volume fluid injection.	8.3 %
Aliabadian et al.(167)	2019	DI water	-	NPs maintained HPAM network structure at sufficient concentration.	-
Kumar et al.(168)	2020	Brine	Sandstone	Adding 0.5 wt% NPs protected the polymer chains from damage caused by mechanical, chemical, and thermal stresses.	39 %

Authors	Date	Dispersion medium	Porous media	Main findings	Extra oil recovery
Rezai et al.(16)	2016	DI water	Sandstone	0.1 wt% clay NPs enhance polymer solution resistance to salinity and temperature, improving stability and performance.	33 %
Liu et al.(169)	2021	Ethanol	Sandstone	The polymer with 1.5 wt% NPs had excellent viscoelastic properties.	7.82 %
Maghzi et al.(26)	2013	DI water	Glass micromodel	Adding 0.1wt% silica NPs can enhance the solution's pseudoplasticity.	10 %
Maurya et al.(11)	2016	DI Water Brine	-	Silica NPs improve suspension's salt tolerance and thermal degradation, and increasing their concentration strengthens network structure and improves viscosity.	-
Santamaria et al.(170)	2021	DI water	Sandstone Micromodel	The incorporation of SiO <sub>2</sub> NPs increases the viscoelasticity of the polymer.	>30 %

Table 1.4: Overview of the results obtained from flooding tests conducted on polymer solutions with the addition of nanoparticles, aimed at studying their effects on oil recovery.

## 1.9

## Oil displacement experiment in microfluidics devices

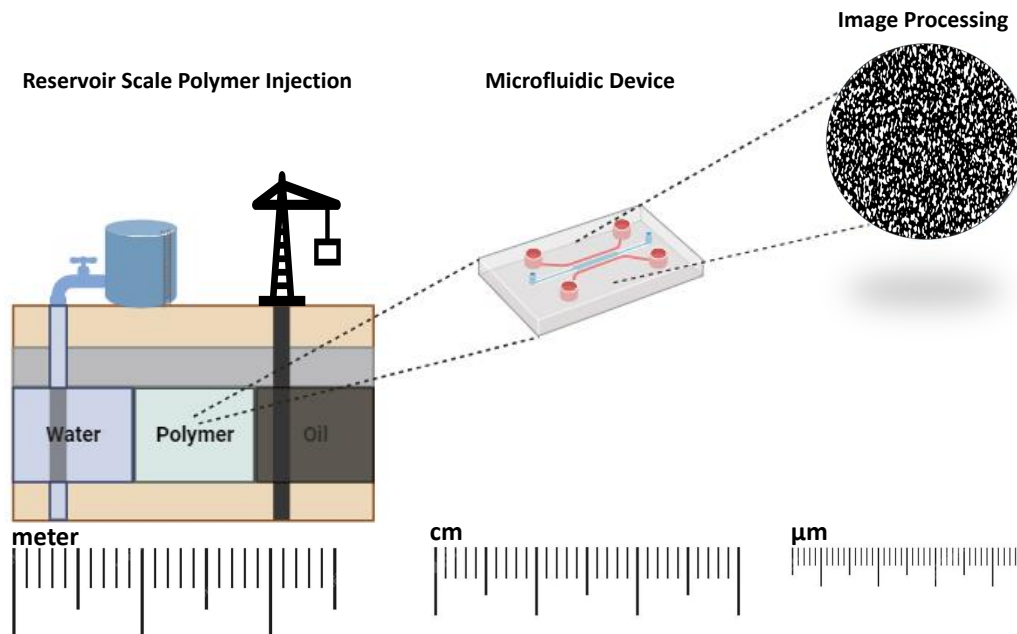


Figure 1.21: Simulating Reservoir-Scale Polymer Flooding Processes using Microfluidics: An Illustrative Diagram adapted from (23).

Microfluidic devices have promising applications in petroleum engineering, particularly in the design of EOR operations. By enabling the visualization and analysis of fluid interactions at the microscale or pore-scale level, these devices offer precise control over fluids and can mimic the porosity and permeability of reservoir rocks (Figure 1.21). Consequently, microfluidics can help us understand the behavior of fluids within reservoir rocks. This understanding is crucial for optimizing EOR strategies and developing more efficient techniques. Moreover, experiments performed using microfluidic devices require a very small amount of fluids and are run at much shorter time, making microfluidics ideal for fluid and process conditions optimization.

The use of microfluidic chips allows for the visualization and mimicry of microscale processes involved in EOR, such as wettability alteration, interfacial tension reduction, and fluid diversion. Nilson et al.(171) conducted a series of microfluidic experiments to evaluate the potential of various fluids with different rheological properties to enhance oil recovery. To simulate a two-dimensional slice from a sandstone core, they used microfluidic devices, which provided a realistic insight into fluid behavior in porous media. The initial experiments revealed that a water-surfactant solution increased oil recovery by approximately 15% compared to water alone, with the same flow rates.

However, FLOPAAM<sup>TM</sup>, a viscoelastic and shear-thinning polymer solution, proved to be more effective at displacing oil than water or the surfactant solution, increasing oil recovery at all flow rates studied. Furthermore, the thickening nanoparticle solutions, at a shear rate of approximately  $10 \text{ s}^{-1}$ , exhibited remarkable potential for oil recovery. The microfluidic sandstone platform proved to be a quick and cost-effective method to evaluate the performance of fluids with different rheological properties on oil recovery. By accurately reproducing a two-dimensional slice from a sandstone core, the microfluidic devices allowed for a realistic examination of fluid behavior in porous media.

Lima et al.(172) conducted experiments to investigate the impact of viscoelastic forces on oil displacement and mobilization of oil ganglia in a microfluidic model of a porous medium. The oil in the micromodel pore space was displaced by three different water phases: pure water, a glycerol solution with higher viscosity than pure water, and a viscoelastic polymer solution with the same shear viscosity as the glycerol solution. Their findings revealed that at lower flow rates, the glycerol solution and viscoelastic polymer solution exhibited similar flow behavior when it came to displacing oil within the porous medium. However, at higher capillary and Weissenberg numbers, the viscoelastic extensional flow generated additional pressure, mobilizing trapped oil ganglia in the narrow capillaries of the porous medium. This resulted in decreased residual oil saturation, with smaller oil ganglia remaining in the porous medium after the injection of the polymer solution compared to those left by pure water or glycerol solution.

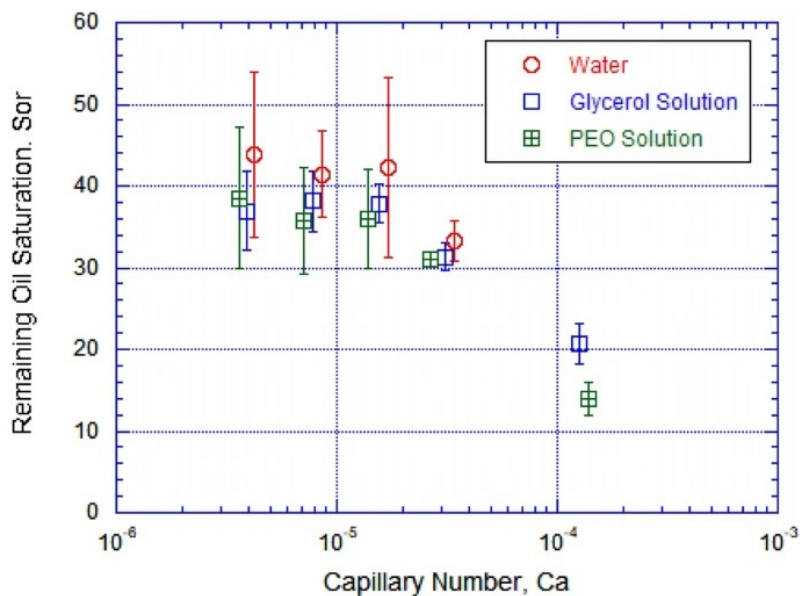


Figure 1.22: Impact of capillary number on residual oil saturation following injection of water, glycerol, and PEO solutions (172).

Microfluidics are also used to study other EOR methods beside polymer solution injection. As an example, De Amorin et al. (173) recently conducted a study on the use of oil-in-water emulsions to enhance oil recovery. The study delved into the microscale flow behavior of the emulsions and their impact on the overall liquid flow in a 2D PDMS/glass porous media micromodel, as shown in Figure 1.23. The research focused on the size of the emulsion drops, the distribution of pores, and the capillary numbers. The results indicated that the pressure difference across the pores could push the drops through and reduce the number of trapped drops, leading to a weaker reduction in water mobility. In contrast, a low capillary number resulted in more trapped drops, leading to a significant increase in mobility reduction. The size distribution of the emulsion drops played a crucial role in this phenomenon. The study concludes that optimizing the capillary numbers and the size distribution of the emulsion drops based on the pore throat size distribution of a given reservoir can achieve the desired reduction in water mobility and improve oil recovery rates.

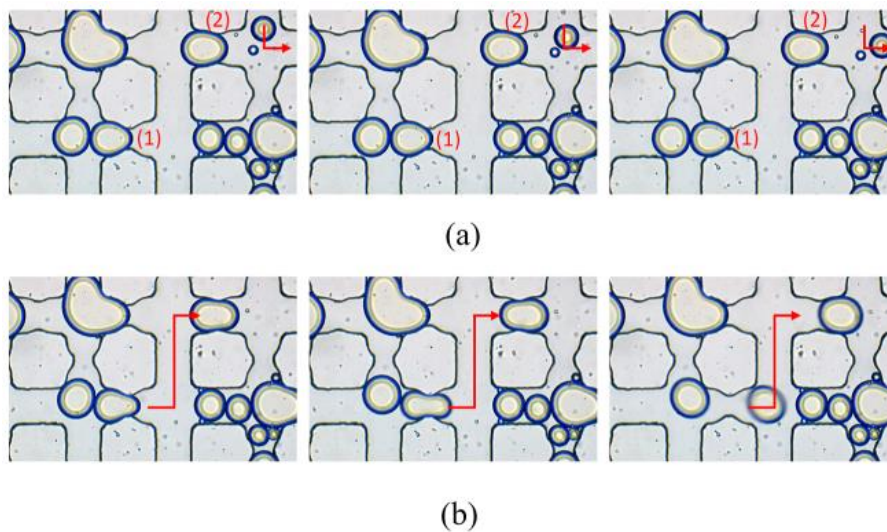


Figure 1.23: A series of images in bright field mode demonstrates the sporadic nature of emulsion flow through porous media. The images illustrate the formation of distinct water flow paths as drops pass through pore throats. The first time sequence (a) shows emulsion drops obstructing pore throats (1) and (2), while the second sequence (b) portrays emulsion drops that can pass through pore throats (1) and (2). A red arrow indicates the flow path in each sequence (173).

Researchers are currently studying microfluidics-based "rock-on-chip" systems to gain a better understanding of oil-nanoparticles-rock interactions at a microscopic level. A recent study by Rueda et al. (24) examined how

nanoparticles could potentially improve the efficiency of polymer flooding in water-wet micromodels. The study found that adding silica nanoparticles to biopolymer solutions significantly improved oil displacement efficiency and reduced residual oil saturation compared to using biopolymers alone. These results suggest that incorporating nanoparticles into oil recovery processes can enhance their overall efficiency and effectiveness. The improved performance was attributed to a more homogeneous dispersion of nanoparticles in the solution and a reduction in polymer adsorption on the rock surface, which resulted in improved sweep efficiency and recovery factor.

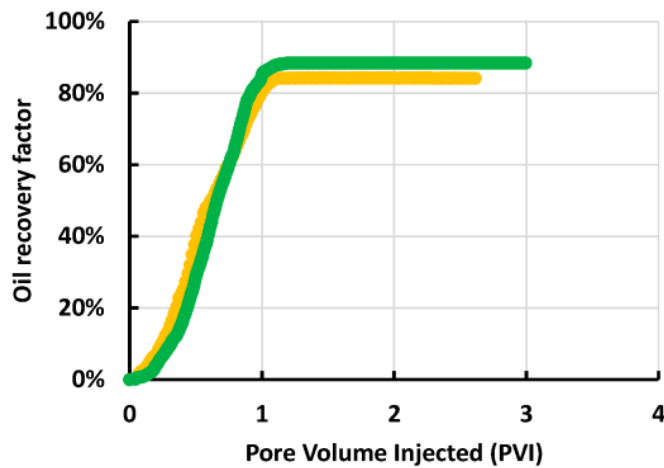


Figure 1.24: Investigation of the effect of silica nanoparticles on oil recovery factor. The nanofluid solution represented by the yellow curve had an ultimate recovery of 84%, while the Xanthan Gum solution with silica NPs, represented by the green curve had an ultimate recovery of 88% (24).

Kumar et al. (174) investigate the use of surfactant-assisted functional silica nanofluids in low-salinity seawater for enhanced oil recovery using a microfluidic chip that simulates a reservoir. The nanofluids were prepared by dispersing functionalized silica nanoparticles in low-salinity seawater containing surfactants. It was observed that the injection of fluid containing low-salinity water, surfactant, and nanoparticles resulted in higher oil recovery compared to using only low-salinity water or surfactant alone. The increase in oil recovery is attributed to the ability of surfactants and nanoparticles to interact at the solid-liquid-liquid interphase, creating a conducive environment for oil recovery.

## 1.10

### Summary of Key Findings in the Literature

The study on EOR has revealed crucial insights into improving hydrocarbon recovery. The production process involves three phases- primary, secondary, and tertiary, with the tertiary phase employing EOR techniques to recover the remaining 65% of hydrocarbons. EOR strategies are classified into thermal and non-thermal approaches, among which non-thermal methods are gaining popularity due to their lower environmental impact and cost-effectiveness. Polymer flooding is an important chemical method that utilizes polymers, such as HPAM, to improve recovery through mechanisms like reduced water/oil mobility ratio and reducing residual oil saturation. Several studies have explored the complex flow behavior of HPAM in porous media, revealing its non-Newtonian behavior and thickening properties. The use of SiO<sub>2</sub> nanoparticles has shown promise in enhancing the efficiency of HPAM in EOR by improving its stability and increasing oil recovery under various conditions. Furthermore, microfluidic devices have emerged as a promising tool for simulating and understanding oil displacement processes at the pore scale, providing insights into phenomena like wettability alteration, phase behavior, and the impact of additives such as nanoparticles on EOR efficiency.

## 1.11

### Gaps and Opportunities for Future Research

This research delves into nanoparticles and their interaction with polymer solutions, aiming to enhance oil recovery. A key aspect of the study is examining the impact of mechanical degradation on polymer solutions within porous media, which provides valuable insight into the rheology and flow of these solutions. This understanding is vital for optimizing the polymer flooding process and achieving efficient oil recovery.

Recently, researchers have explored the use of nanotechnology to improve the efficiency of polymer solutions during flooding operations. The addition of nanoparticles to polymer solutions in oilfield operations has been shown to improve their performance substantially. Silica nanoparticles are one of the most studied systems, and researchers have studied the direct mixing of silica nanoparticles into polymer solutions.

Previous research typically only investigated the addition of  $\text{SiO}_2$  nanoparticles to polymeric solutions and their impact on HPAM stability at elevated temperatures and in high-salinity environments. However, the specific impact of mechanical degradation on NPs-HPAM systems remains unexplored.

In particular, the effect of adding  $\text{SiO}_2$  nanoparticles on the rheological behavior of HPAM solutions subjected to mechanical degradation is unknown. In this work, we quantify the mechanical degradation by rheological characterization of the solutions before and after flowing them through a needle valve at different flow force conditions. We explore the addition of  $\text{SiO}_2$  nanoparticles to minimize the mechanical degradation of polymer solutions by measuring the shear and extensional viscosity of fresh and mechanically degraded NPs-HPAM dispersions.

Moreover, we explore oil displacement strategies using microfluidic devices as a model of a porous medium into which we injected fresh and degraded HPAM solutions with and without  $\text{SiO}_2$  nanoparticles. Taking advantage of the unique capabilities of microfluidic devices, this research aims to provide a comprehensive understanding of how rheological parameters affect the performance of polymer solutions in oil displacement in porous media.

## 1.12

### Objectives

1. The proposed research involves conducting rheological studies on dispersions of nanoparticles in hydrolyzed polyacrylamide polymer solutions (NPs-HPAM) subjected to mechanical degradation. The aim is to determine the effectiveness of nanoparticles in mitigating the degradation effects on the dispersion's rheological properties.
2. The study also intends to investigate the process of oil displacement through the injection of HPAM polymer solutions and mechanically degraded NPs-HPAM dispersions. The efficiency of displacement and the impact of nanoparticles on the process is analyzed. The research aims to provide valuable insights into the potential application of nanoparticles to enhance the efficiency of oil recovery processes.

### 1.13

#### Outline

The thesis is made up of six chapters that provide a comprehensive analysis of the research conducted. Chapter 1 provides a succinct overview of the research problems, along with a comprehensive analysis of prior work that pertains to the problem at hand and its objectives. Chapter 2 provides a detailed explanation of the materials and methodologies used to conduct the experiments. In Chapter 3, the rheological properties of fresh and degraded polymer solution/dispersion are displayed and analyzed. Chapter 4 presents the results of oil displacement by fresh and degraded polymer solutions/dispersion, providing key insights into the research findings. Finally, Chapter 5 concludes the thesis by summarizing the research findings and providing a discussion on the future work to be conducted.

## 2

### Materials and methods

This chapter discusses the materials and methodologies used in our study to investigate the rheological behavior of low and high molecular weight partially hydrolyzed polyacrylamide (HPAM) and their dispersions with silica nanoparticles (NPs-HPAM). The success of any scientific experiment relies on the careful selection of materials and precise implementation of experimental procedures. Therefore, we provide a comprehensive overview of the materials used, including HPAM polymers and silica nanoparticles  $SiO_2$ , and describe in detail the preparation processes that we utilized to ensure reliable results. We also outline the experimental setups that we employed for mechanical degradation and rheological analysis, emphasizing their significance in understanding the complex interplay of these materials under various conditions.

#### 2.1

##### Polymer solutions

In our research, we conducted experiments using the FLOPAAM<sup>™</sup> 3130s as commercial oilfield polymer solution, from SNF. A detailed list of the properties of this polymer can be found in Table 2.1. HPAM is classified as a polyelectrolyte due to the negatively charged carboxylate groups that are present in its molecular structure (Figure 2.1).

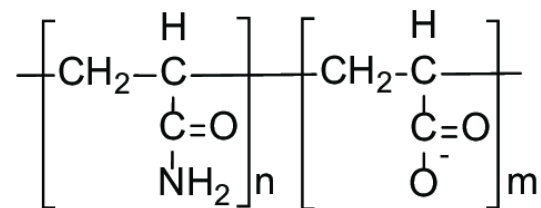


Figure 2.1: Molecular structure of a partially hydrolyzed polyacrylamide (73).

According to research by Sorbie (66), the degree of hydrolysis does not affect the thickening capacity of HPAM; instead, the molecular weight of the polymer contributes to the high viscosity solution by increasing the hydrodynamic volume of the polymer chain. For EOR purposes, HPAM polymers typically have molecular weights ranging from 2 to  $20 \times 10^6 \text{g/mol}$  (146).

Name	Commercial Name	Molecular Weight (MDa)	Hydrolysis degree (%)
HPAM	Flopaam 3130s	2	25-30

Table 2.1: Properties of the polymer solution used in this research.

## 2.2

### Silica Nanoparticles

In this study, we utilized fumed silica nanoparticles that were provided by Evonik (previously known as Degussa Industries). AEROSIL<sup>®</sup> 200, with an average primary particle size of 12 nm, was used as a hydrophilic fumed silica filler. Its chemical formula is  $SiO_2$  and appears as a white powder.

These nanoparticles possess an amorphous structure and are almost spherical in shape. During the production process, high temperatures cause the fumed silica nanoparticles to fuse into aggregates that create branched fractal structures. This process is irreversible, and the branched fractal structures can be considered the primary structure of fumed silica nanoparticles (175). The physicochemical properties of fumed silica nanoparticles are listed in Table 2.2.

Specific surface area	175-225 $m^2/g$
Specific weight	2.2 $g/cm^3$
Heat Capacity $C_p$ at 50 °C	0.85 $J.g^{-1}.k^{-1}$
Heat of wetting of water	$-150 \times 10^7 J.m^{-2}$
pH value in 4% dispersion	3.7-4.5

Table 2.2: Properties of AEROSIL<sup>®</sup> 200(176).

## 2.3

### Solutions/Dispersion Preparation

#### 2.3.1

##### Preparation of polymer solutions

A stock solution of 12,000 *ppm* was prepared by adding the polymer to Milli-Q<sup>®</sup> water (18.2 *MΩ.cm* at 25 °C). The water is stirred at 700 *rpm* using a magnetic stirrer to create a vortex, and the polymer solution is left in agitation for 12 hours (177). The other two polymer concentrations explored, e.g. 1,000 *ppm* and 4,000 *ppm*, were prepared by diluting the stock solution with Milli-Q<sup>®</sup> water.

#### 2.3.2

##### Preparation of NPs-HPAM Dispersion

The SiO<sub>2</sub> nanoparticles HPAM (NPs-HPAM) dispersions were prepared in two steps. First, the hydrophilic fumed silica SiO<sub>2</sub> nanoparticles (AEROSIL<sup>®</sup> 200, Evonik) (Tab. 2.2) were dispersed in Milli-Q<sup>®</sup> using the ultrasound homogenizer Q700 model (Qsonica) for 40 minutes at 30 % of amplitude with the following parameters: output frequency 20 *kHz* and maximum power 700 *W*. The intensity-weighted mean hydrodynamic size ( $Z_{av}$ ) of the dispersion, measured by dynamic light scattering (DLS) method using a Zetasizer Nano-ZS90 (Malvern), was approximately 150±50 *nm* (178). In the second step, the polymer was added to the dispersion that was obtained using the same protocol mentioned above for preparing polymer solutions. It was ensured that the addition occurred after the sonication process to prevent degradation in the fresh solution.

## 2.4 Mechanical Degradation

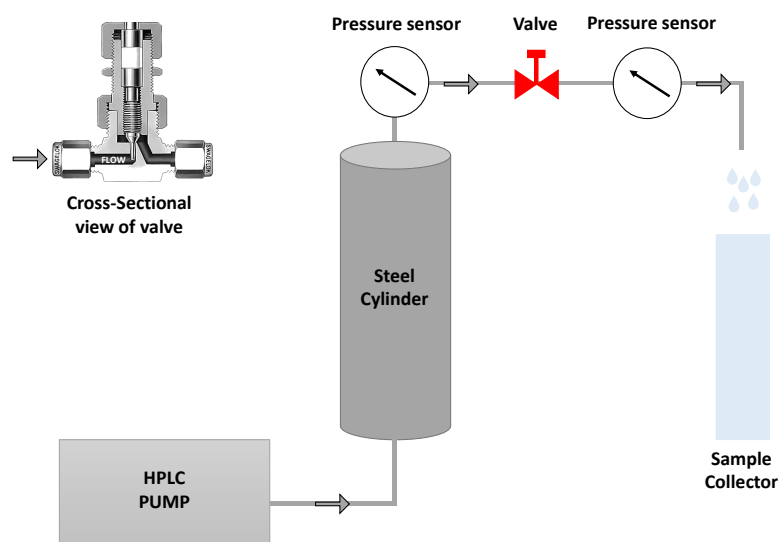


Figure 2.2: Experimental setup used to mechanically degrade the polymer solutions by flowing them through a needle valve.

The mechanical degradation of polymer solutions was achieved by flowing the liquid through a metering needle valve at different flow conditions. Figure 2.2 presents a sketch of the experimental setup. The polymer solution was stored in a stainless steel piston cylinder (with a capacity of 300 mL). The piston moves at a constant speed, controlled by the flow rate set at a high-precision HPLC pump. The polymer solution flows through a metering needle valve (from Swagelok). The valve used in this experiment has a stem with a long, tapered, needle-shaped plunger that fits into the valve seat, as shown in the insert of Fig. 2.2. As the polymer solution passes through the valve, it experiences both shear and extensional deformation, which may lead to the breakup of the polymer molecules. The deformation rate of the flow through the valve was controlled by the injection flow rate and the valve configuration. The flow rate was set at 2, 5, 7, and 10 mL/min. By turning the handle attached to the plunger, the size of the orifice can be controlled. The valve constriction diameters used in this experiment were 0.15 and 0.25 mm. We estimated the shear rate experienced by the liquid as it flows through the valve orifice using Poiseuille equation. The range of shear rate achieved with the setup was from 20,000 to 600,000 s<sup>-1</sup>, above the critical shear rate at which HPAM solution show mechanical degradation (8).

## 2.5 Rheological Characterization

To obtain a comprehensive understanding of the changes in the properties of the HPAM polymer solutions and NPs-HPAM dispersion caused by mechanical degradation, it is imperative to investigate their response to both shear and extensional viscosity. Shear viscosity was measured in a rotational rheometer, while an extensional rheometer was used to measure the extensional viscosity by stretching the fluid. These rheological assessments were conducted at a constant temperature of  $23^{\circ}\text{C}$  to maintain consistency, with temperature control achieved through careful regulation of the room environment. By examining the changes in both shear and extensional viscosity, we can gain a better understanding of how the mechanical degradation has affected the polymer solution and NPs-HPAM dispersion.

### 2.5.1 Shear Viscosity

The steady-state shear viscosity curve of HPAM and NPs-HPAM dispersions was measured using a Discovery hybrid rheometer (DHR 3, TA Instrument), with a cone-plate geometry (diameter 40 mm, angle  $2^{\circ}$ ) as presented in Figure 2.3. The gap was preset to the standard 0.057 mm. To obtain steady-state shear viscosity values, we employed the following protocol: for shear rates between  $0.1$  and  $10\text{ s}^{-1}$ , multiple measurements were conducted with an acquisition time of  $30\text{ s}$  until three consecutive measurements showed a deviation of less than 1.5%. For higher shear rates, namely above  $100\text{ s}^{-1}$ , each measurement was obtained with a peak hold for  $120\text{ s}$  or until a steady state was reached. This detailed procedure resulted in accurate and reliable rheological data for the HPAM polymer solutions and NPs-HPAM dispersion, which can be used for further analysis and research purposes.



Figure 2.3: Discovery Series Hybrid Rheometer DHR-3.

The degree of mechanical degradation was evaluated by comparing the flow curves of each sample before and after mechanical degradation (8, 179). The Williamson model provided the best fit to the measured flow curve for the range of shear rate explored (180). The model is represented by:

$$\eta(\dot{\gamma}) = \frac{\eta_0}{1 + (k\dot{\gamma})^n}. \quad (2-1)$$

$\eta_0$  is the zero-shear viscosity,  $k$  is the consistency index, and  $n$  denotes the power law index.

The variation of the zero-shear viscosity was used to quantify the mechanical degradation in shear  $\Delta_s$ , which is defined as:

$$\Delta_s = \left( 1 - \frac{\eta_0^{[Deg]}}{\eta_0} \right), \quad (2-2)$$

where  $\eta_0$  and  $\eta_0^{[Deg]}$  are the zero-shear viscosity of the fresh and degraded solution, respectively.  $\Delta_s \approx 0$  represents the situation at which the solution does not show any change on its shear rheological properties after flowing through the needle valve.

## 2.5.2

### Extensional Rheology

This section provides a detailed overview of the methodologies used to determine the apparent extensional viscosity of the fluids using the Capillary Breakup Extensional Rheometer (CaBER 1).

#### 2.5.2.1

##### Capillary Breakup Extensional Rheometer

To determine the apparent extensional viscosity of HPAM polymer solutions and NPs-HPAM dispersion, we used the Capillary Breakup Extensional

Rheometer, or CaBER 1 (Thermo Haake), shown in Figure 2.4. This device creates an unstable fluid filament between two cylindrical plates of a predetermined diameter in a capillary rupture test. A certain volume of liquid is placed filling the gap between two rods. The rods are then quickly separated over a specific distance, generating uniaxial tensile stress that is applied to the sample (181). To obtain accurate measurements, we adjusted the strike time to extend the fluid before capillary forces caused it to break up. The strike time had to be quick enough to measure the breakup. The evolution of the filament's midpoint diameter, known as  $D_{mid}$ , over time is measured using a sensitive laser micrometer. The apparent extensional viscosity is evaluated based on the variation of diameter with time. CaBER 1 is an essential tool for characterizing the behavior of fluid materials under uniaxial extensional stress, especially in understanding the extensional response of polymer solutions. Its ability to measure the extensional viscosity of fluids is crucial in developing a comprehensive understanding of their properties and behavior.



Figure 2.4: HAAKE CaBER 1 instrument.

Extensional rheometers are governed by a series of natural length and time parameters that play a crucial role in controlling the dynamics of the filament thinning and rupture process. To better understand the method, it is necessary to understand the role of each of these parameters individually.

The aspect ratio of the initial sample is defined as  $\Lambda_0 = h/D_0$  where  $h$  is the initial gap and  $D_0$  is the rod diameter (Figure 2.5) and according to numerical simulations conducted by Harlen et al. (182) and Yao et al.(183), the optimal aspect ratio usually falls between 0.5 and 1. This helps to minimize the impact of the initial reverse squeeze flow when the plates are first separated at low aspect ratios  $\Lambda(t) \ll 1$ , as well as the sagging and bulging of the cylindrical sample at high aspect ratios. The final aspect ratio,  $\Lambda_f = f/D_0$ , where  $f$  is the final height, that is achieved when the plates are separated, determines the total Hencky strain that is applied (184).

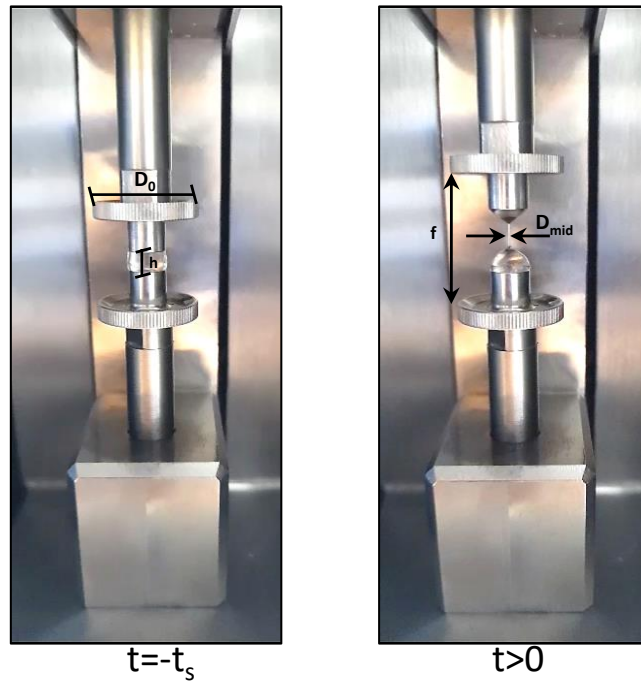


Figure 2.5: Picture of the CaBER geometry containing a fluid sample at rest  $t=-t_s$  and undergoing filament thinning for  $t > 0$ .

We tested three different rod diameters during the experiment while keeping the final gap setting between 10 to 20 *mm*, based on the defined initial and final aspect ratio limits and recommendations mentioned in the operation manual. The diameter of the plate plays a crucial role in determining the sensitivity of the measurement to the extensional rate. As per the equation  $\dot{\epsilon} = 2V/D_0$ , which represents the relationship between the extensional strain rate  $\dot{\epsilon}$ , velocity  $V$ , and diameter  $D_0$ , a smaller plate diameter results in a higher extensional strain rate, making the measurement more sensitive to the extensional rate. Table 2.3 below presents the operational parameters for each geometry, which is critical for understanding the influencing factors behind the obtained results.

Table 2.3: Test conditions for different plate diameters and concentrations

Diameter (mm)	Conc. (ppm)	Initial Gap (mm)	Final Height (mm)	Initial Aspect Ratio	Final Aspect Ratio
4	12,000	2	9.92	1.00	4.96
6	4,000	3	9.88	1.00	3.29
8	1,000	2	9.57	0.50	2.39

In order to obtain precise measurements of fluid breakup, we adjust the strike time  $t_s$  or step strain deformation rate. The strike time is adjusted for two key reasons. Firstly, the stretch rate must be fast enough to complete the stretching of the fluid before capillary forces cause it to break up, ensuring accurate measurements. When dealing with materials with lower viscosity, a faster strike time is recommended to avoid any errors. Secondly, the stretch rate can have a significant impact on the breakup kinetics of complex non-Newtonian materials, akin to the dependence of non-Newtonian materials on extensional rate (181). In our experiments, we assume that the plate separation occurs instantaneously, but in reality, it takes a finite amount of time, which is denoted by  $\delta_t0$  and typically greater than or equal to 50 *ms* (184). Due to inertia in the plate and drive subsystem, the strike time must be greater than or equal to  $\delta_t0$ . To gain a better understanding of material responses, we used different strike times during our experiments.

### 2.5.2.2

#### Apparent Extensional Viscosity

In the preceding sections, we thoroughly described the CaBER equipment and the primary parameters needed to obtain diameter data over time. This critical data plays a significant role in shaping the extensional rheological behavior of studied fluids. We tested different values for the parameters, such as rod diameter, aspect ratios, and strike times.

Looking ahead, we delve into the methodology of generating the apparent extensional viscosity, which is a crucial property that characterizes the flow behavior of polymer solutions. Additionally, we examine the detailed steps of data processing required to obtain the appropriate model parameters. This fundamental step is necessary to understand the complex behaviors exhibited by HPAM polymer solutions and NPs-HPAM dispersions under extensional stress, forming the foundation of our experimental approach. Through a detailed analysis of the data collected from monitoring diameter evolution with time, we have made significant strides on the evaluation of extensional properties of polymer solutions. Specifically, our investigations have led us to

identify two key properties that characterize the fluid behavior: the extensional relaxation time  $\lambda$  and the apparent extensional viscosity function  $\eta_E$ . To determine the relaxation time of a solution, we utilized the Upper Convected Maxwell Model, a widely used constitutive model that describes the behavior of viscoelastic fluids. This involved fitting the exponential decay of the transient filament diameter on the CaBER. The equations that define this model have been outlined in Olsson et al. (185). By utilizing this approach, we were able to obtain a comprehensive understanding of the behavior of viscoelastic fluids and the various factors that influence their flow properties.

$$D_{mid}(t) = D_0 \left( \frac{GD_0}{4\sigma} \right)^{1/3} \exp\left(-\frac{t}{3\lambda}\right) \quad (2-3)$$

where

$D_{mid}$ : Midpoint diameter at time  $t$ ,

$D_0$ : Initial plate diameter,

$G$ : Elastic Modulus,

$\sigma$ : Surface tension.

Surface tension,  $\sigma = 0.069\text{N/m}$ , is a critical parameter to evaluate extensional viscosity using CaBER. We utilized the Tracker Standard Drop Tensiometer from Teclis Scientific to measure surface tension.

The apparent extensional viscosity is calculated with the following relationship:

$$\eta_e = \frac{-\sigma}{(dD_{mid}/dt)} \quad (2-4)$$

As the diameter of the filament decreases, the process of numerically differentiating the experimental data for diameter ( $D$ ) becomes more challenging and prone to increased noise. To overcome this issue and improve the accuracy of the data, a fitting method was employed using an empirical equation proposed by Oliveira et al.(186) specifically designed to minimize noise in diameter data.

$$D(t) = \left( D_1 + \frac{k_1}{t + t_1} \right) \exp\left(-\frac{t}{3\lambda}\right) - V_2(t - t_2) \quad (2-5)$$

with  $D_1$ ,  $t_1$ ,  $k_1$ ,  $V_2$ , and  $t_2$  as fitting parameters. We evaluate the derivative of the fitted evolution of the diameter instead of the raw data.

The apparent extensional viscosity was calculated as a function of the Hencky strain, defined as  $\varepsilon$ ,

$$\varepsilon = 2\ln\left(\frac{D_{mid}(t)}{D_0}\right) \quad (2-6)$$

The mechanical degradation of the polymer solutions were quantified in terms of their extensional behavior by two parameters: the reduction of

the high strain apparent extensional viscosity  $\Delta_{e\eta}$  and the reduction of the relaxation time  $\Delta_{e\lambda}$ , which are defined as:

$$\Delta_{e\eta} = \left(1 - \frac{\eta_{e\infty}^{[Deg]}}{\eta_{e\infty}}\right), \quad (2-7)$$

$$\Delta_{e\lambda} = \left(1 - \frac{\lambda_{\infty}^{[Deg]}}{\lambda_{\infty}}\right), \quad (2-8)$$

where  $\eta_{e\infty}$ ,  $\eta_{e\infty}^{[Deg]}$ ,  $\lambda_{\infty}$  and  $\lambda_{\infty}^{[Deg]}$  are the high Hencky strain extensional viscosity and the relaxation time of the fresh and degraded solution, respectively.  $\Delta_{e\eta} \approx 0$  and  $\Delta_{e\lambda} \approx 0$  represent the situation at which the solution does not show any change on its extensional rheological properties after flowing through the needle valve

### 2.5.3

#### Supplementary Characterization Techniques

##### 2.5.3.1

#### Size-Exclusion Chromatography (SEC-UV)

SEC-UV was used to show the break up of polymer molecules as they flow through the constriction. Chromatograms were obtained with the fresh and degraded polymer solutions. The chromatographic analysis was conducted using an Agilent 1260 Infinity II chromatographer, equipped with a PSS SUPREMA Ultrahigh column (300 x 8 mm; 10  $\mu$ m) and a UV detector (at 205 nm). Throughout the experiment, the column temperature was maintained at 30°C. The chromatograms were recorded and processed using the Agilent OpenLab software (version 2.5)(187).

##### 2.5.3.2

#### Transmission electron microscopy

The morphology of the degraded NPs-HPAM dispersion was visualized using a Transmission Electron Microscope (TEM, FEI Tecnai G2 spirit Twin). Approximately 5  $\mu$ l of the dispersion was placed on a formvar/carbon-coated TEM grid. The sample was stained with 0.1% phosphotungstic acid (PTA) for 1 second to enhance the contrast between the nanoparticles and the polymer molecules (188).

## 2.6

#### EOR analysis by Microfluidics

Our research aimed to obtain a comprehensive understanding of the rheological behavior of the HPAM polymer solutions and NPs-HPAM dispersions

and also the impact of these properties in the flow through porous media. The analysis of the flow through porous media was conducted in a series of experiments using a porous medium micromodel. Our first objective was to investigate the mechanical degradation of HPAM at the microscale, which allowed us to understand better the mechanisms of degradation and the factors influencing this process. Our second objective was to explore the potential benefits of incorporating nanoparticles into HPAM solutions with the goal of mitigating mechanical degradation. By flooding these fluids through the micromodel, we were able to study the impact of NPs on the properties of HPAM and its overall performance in polymer flooding.

### 2.6.1

#### Microfluidic device

As part of our experiment, we used the porous medium micromodel depicted in Figure 2.6; it features a 20 *mm* long and 10 *mm* wide water-wet porous matrix with an etch depth of 20  $\mu\text{m}$ . Upstream and downstream of the porous matrix, there are inflow and outflow channels with flow distribution chambers of 500  $\mu\text{m}$  width. According to the supplier's specifications, the matrix has a 57% porosity, a pore volume of 2.3  $\mu\text{L}$ , and a permeability of 2.5 *D*. The device has a pattern that resembles the structure of a slice of a sandstone rock as shown in Figure 2.7. These structures were randomly distributed, resulting in throats and channels. The mean pore size of the physical rock network is the average size of the pores in the medium, which measures 142.63  $\mu\text{m}$ . However, there is a significant amount of variation in pore size within the medium (SD=60.19  $\mu\text{m}$ ) (174). It is important to note that the micromodel is a 2D device, and the height of 20  $\mu\text{m}$  is the smallest dimension in most pore throats.

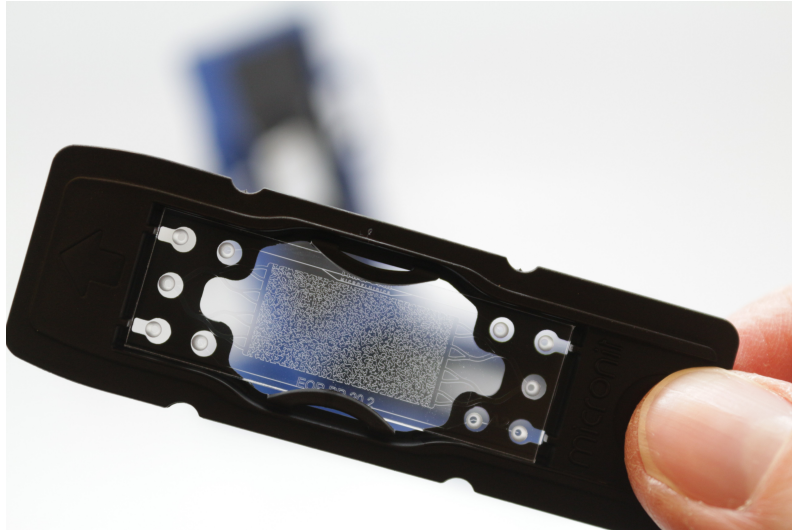


Figure 2.6: Micromodel device (189).

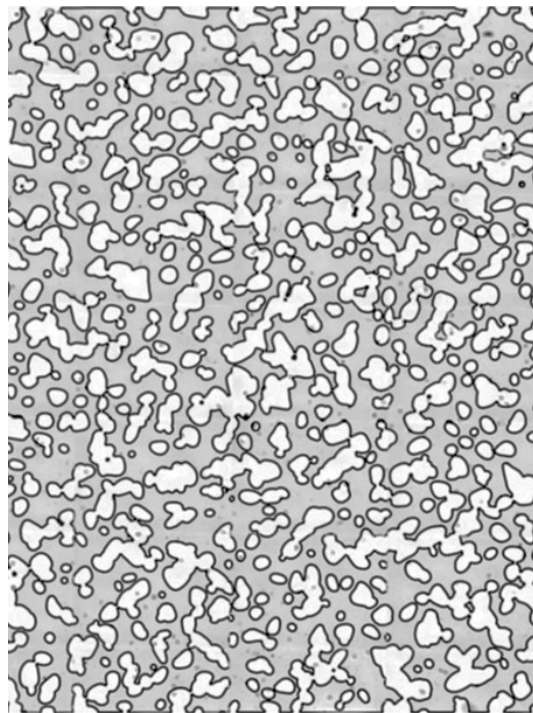


Figure 2.7: Pore structure (white) of the 2D Physical Rock micromodel device.

## 2.6.2 Experimental setup and procedures

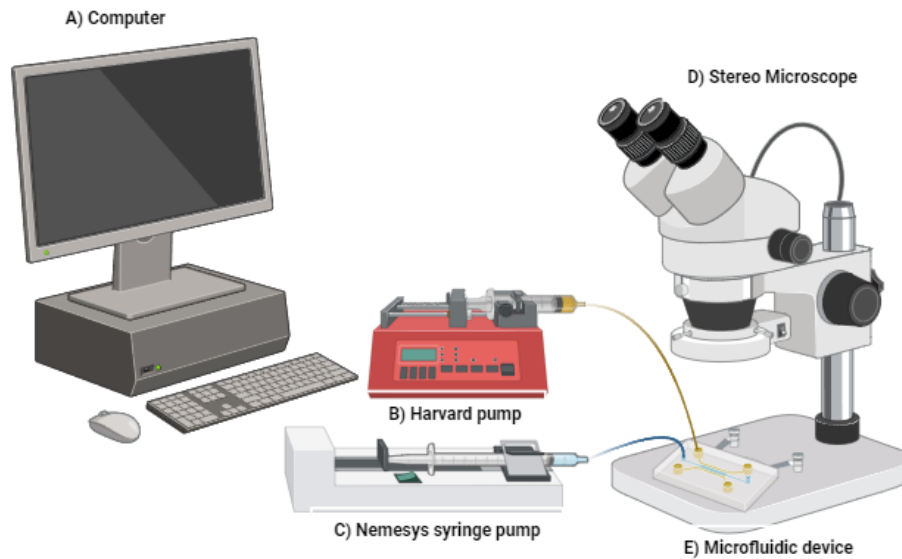


Figure 2.8: Scheme for the experimental setup for microfluidic application.

The fluid injection system (Figure 2.8) consists of a syringe pump (Harvard Apparatus) used to saturate the porous medium micromodel. The injection of HPAM and NPs-HPAM was performed using a Nemesys syringe pump (Cetoni GmbH). The syringes of the system are made of metal, which can withstand high pressures. In addition, two two-way microfluidic valves (IDEX) were used to connect the saturation syringe to the porous medium micromodel and the pressure sensor to the porous medium micromodel. A device that can be added to the Nemesys pump was used to measure the pressure. This external pressure sensor is placed between the Nemesys pump and the micromodel (Figure 2.9). This sensor has a flat ceramic diaphragm that can withstand different pressure ranges. We used the 1450 psi sensor for the degradation experiments and the 70 psi sensor for the HPAM and NPs-HPAM injection oil displacement experiments. The outlet was open to the atmosphere, and the inlet pressure was measured during the test. Nemesys pump control and pressure data management were collected using CETONI Elements software. The porous media micromodel was placed on the stage of an SMZ45T stereomicroscope (Nikon) for viewing. An MC170 HD digital camera was used to record the polymer flooding during the experiment, as shown in Figure 2.8.

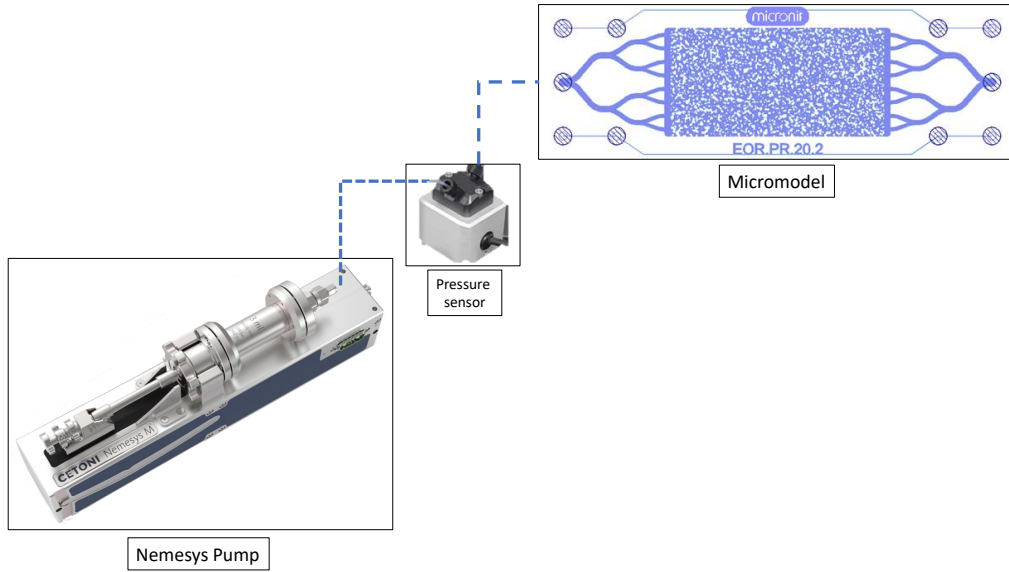


Figure 2.9: Diagram of the experimental setup for microfluidic application.

The absolute permeability of the micromodel ( $k$ ) was evaluated from the measured values of the pressure drop across the porous medium ( $\Delta P = (P_1 - P_2)$ ) during the flow of Milli-Q<sup>®</sup> water at different flow rates ( $q$ ). This measurement scheme is based on Darcy's law equation 2-9

$$q = -\frac{kA}{\mu} \frac{(P_1 - P_2)}{L} \quad (2-9)$$

- $q$  is the volumetric flow rate of the fluid,
- $k$  is the absolute permeability,
- $A$  is the cross-sectional area of the porous media,
- $\frac{(P_1 - P_2)}{L}$  is the pressure gradient,
- $\mu$  is the fluid viscosity.

The micromodel was flooded with the aqueous phase at a constant flow rate of  $0.1 \mu\text{L}/\text{min}$  until complete saturation of the pore space. From this point, the injection flow rates were increased from 25 to  $200 \mu\text{L}/\text{min}$ , and at steady state, the pressure at the inlet and outlet of the porous media was recorded. Steady-state was considered to have been reached after at least 30 min of injection when the pressure showed no variation with time. The absolute permeability of the micromodel was calculated from the average of three independent experiments. In addition, the absolute permeability measurement was considered as an important measure to control polymer adsorption in the porous medium micromodel.

### 2.6.2.1

#### Polymer degradation experiments

Polymer degradation experiments were performed at  $23^{\circ}\text{C}$  with a concentration of 4,000 ppm. Different injection rates (5,25,150  $\mu\text{L}/\text{min}$ ) were tested. At least one milliliter of each sample was collected to analyze shear and extensional rheological behavior. The values reported of degradation indexes are the average of the three experiments, with the standard deviation as the error bar.

### 2.6.2.2

#### Two-phase flow experiments: Oil displacement by HPAM and NPs-HPAM injection

Oil displacement by injection of HPAM solutions and NPs-HPAM dispersions experiments were performed at three different capillary numbers and at a temperature of  $23^{\circ}\text{C}$ . To increase the residual oil saturation in the porous medium, a high-viscosity 500PS® (AGECOM) mineral oil was used.

Oil displacement experiments were carried out with the following injected systems:

1. System 1: Fresh HPAM.
2. System 2: HPAM degraded solution by flowing through the valve.
3. System 3: NPs-HPAM degraded dispersion by flowing through the valve.

After oil displacement by each system, a complete image of the micro-model was acquired to observe the phase distribution and quantify remaining oil saturation and quantify oil recovery. Image J was used as the image processing software. The images are processed by color thresholding based on saturation and brightness before converting them to 8-bit images. The oil saturation for each image is then evaluated based on the ratio of the colored area (oil remaining in the network) to the total area of interest (fully saturated network) as a function of the number of pixels. By using a calibration rule, the number of pixels is translated to a volume value (190). The chips are reused in this study. Therefore, they go through a thorough cleaning procedure after each test. It includes flooding the chip first with Milli-Q® water to remove excess viscous material, then a mixture of a 1 vol-% concentrated Hellmanex III liquid cleaning solution, Milli-Q® water, and  $\text{CO}_2$ . Finally, the chips are dried at  $75^{\circ}\text{C}$  in an oven to ensure the cleanliness of the chips for the next tests.

### 3

## Rheological Properties of Fresh and Degraded Polymer solution/dispersion

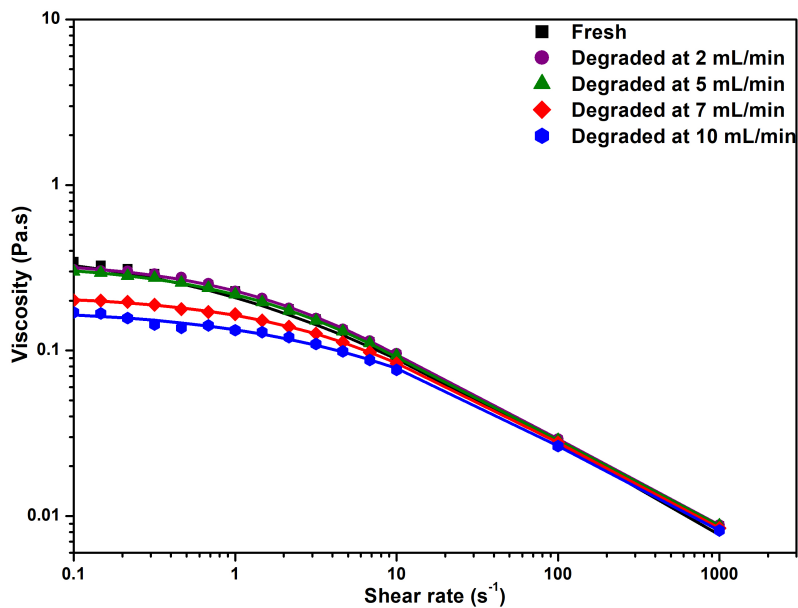
This chapter presents the rheological behavior of HPAM solutions in response to mechanical degradation. We investigated how different factors, including polymer concentrations, constriction diameter, flow rates, and nanoparticle additions, can influence the rheological response.

### 3.1

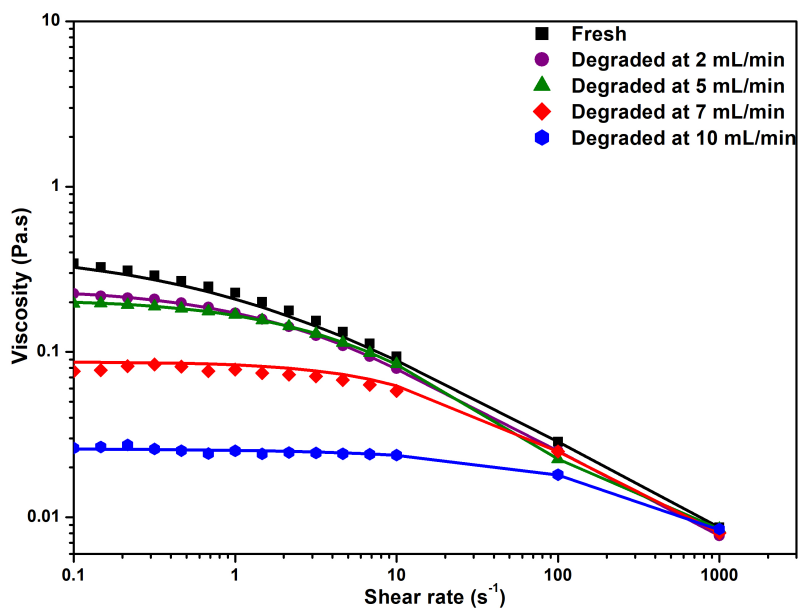
#### Shear Viscosity of Fresh and Degraded Polymer Solutions

We characterized the mechanical degradation of HPAM solutions at different concentrations, e.g. 1,000 *ppm*, 4,000 *ppm* and 12,000 *ppm*, and different flow conditions, by analyzing the variation on their shear viscosity before and after flowing through a needle valve. As discussed before, the deformation rate at which the solution experienced as it flows through the needle valve was varied by imposing three values of flow rate and two values of orifice diameter of the valve.

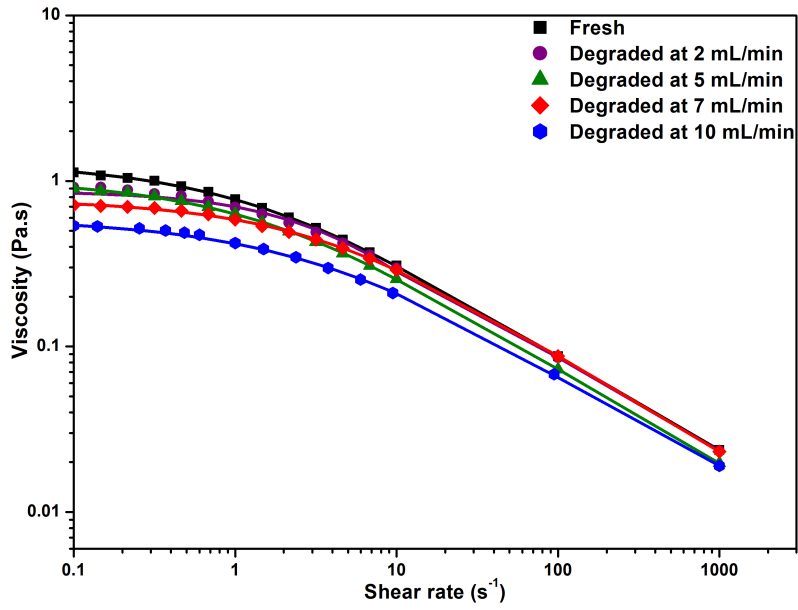
Figure 3.1 (a) and 3.1 (b) present the steady-state shear viscosity in the dilute regime (concentration of 1,000 *ppm*) for the fresh and degraded solutions at different flow rates for orifice diameter equal to 0.25*mm* and 0.15*mm*, respectively. The data reveals that all solutions exhibit strong shear-thinning behavior. The continuous line in the plots represent the Williamson model fit. The viscosity at low shear rate falls as the flow rate through the valve rises and orifice diameter decreases, as expected. Stronger degree of mechanical degradation occurs at higher deformation rate. At high enough shear rate, the viscosity of the degraded solutions approaches that of the fresh solutions.



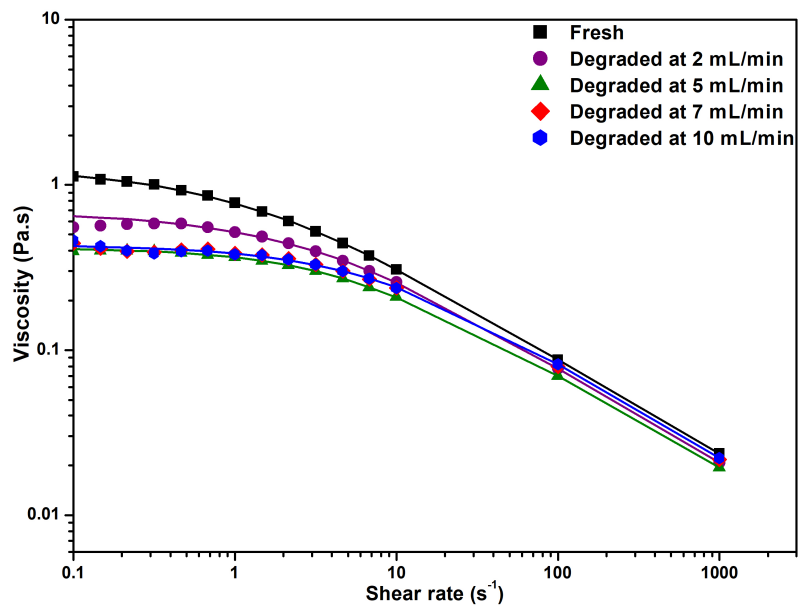
(a) 1,000 ppm (0.25 mm)



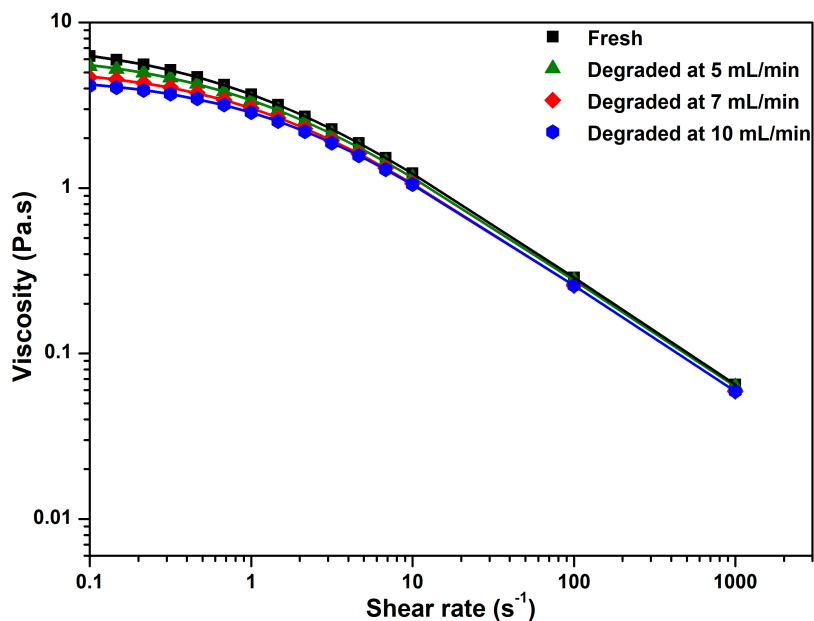
(b) 1,000 ppm (0.15 mm)



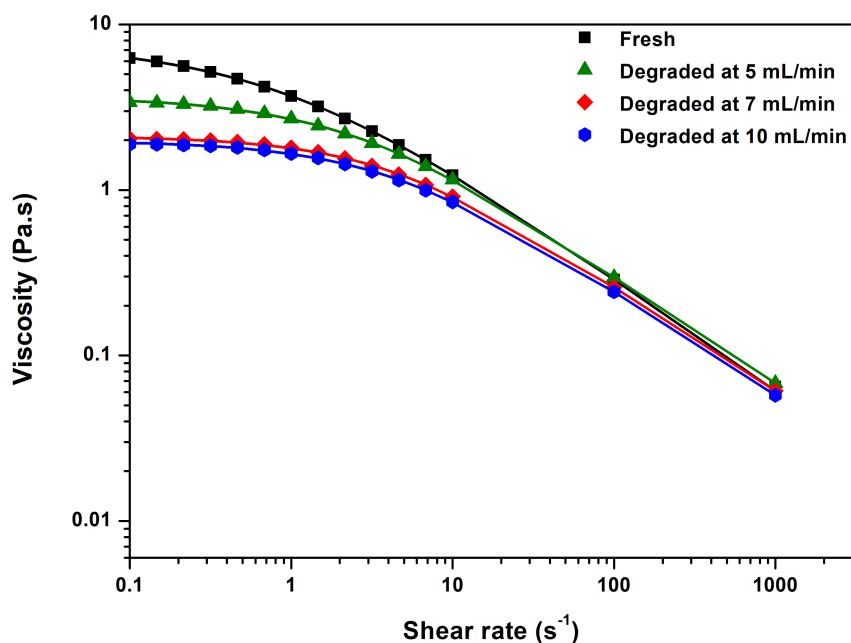
(c) 4,000 ppm (0.25 mm)



(d) 4,000 ppm (0.15 mm)



(e) 12,000 ppm (0.25 mm)



(f) 12,000 ppm (0.15 mm)

Figure 3.1: Steady-state shear viscosity as a function of shear rate of fresh and degraded HPAM solutions for different flow conditions and polymer concentrations.

The shear viscosity of the fresh and degraded 4,000 and 12,000 *ppm* solutions are presented in Figures. 3.1 (c) to 3.1 (f), for both orifice diameters. As expected, the viscosity increases with polymer concentration. The overall behavior is similar to the results presented before for the lowest concentration solutions; higher deformation rates in the flow through the valve, associated with higher flow rates and smaller orifice diameter, led to a higher degree of degradation.

The reduction of the low-shear viscosity of the degraded polymer solutions is caused by the break up of the polymer chains as the solution flows the valve. This is clear by comparing the size-exclusion chromatogram of the fresh and degraded solution. Figure 3.2 presents these results for the 4,000 *ppm* solution, degraded by the flow through the orifice diameter of 0.25*mm* at  $q = 10\text{mL min}$ . In the degraded solution, the peak at the lowest retention time, associated with the largest molecules, is reduced, and a new peak, at a higher retention time, is formed. This suggests the possibility of the breakdown of long polymer molecules into smaller units.

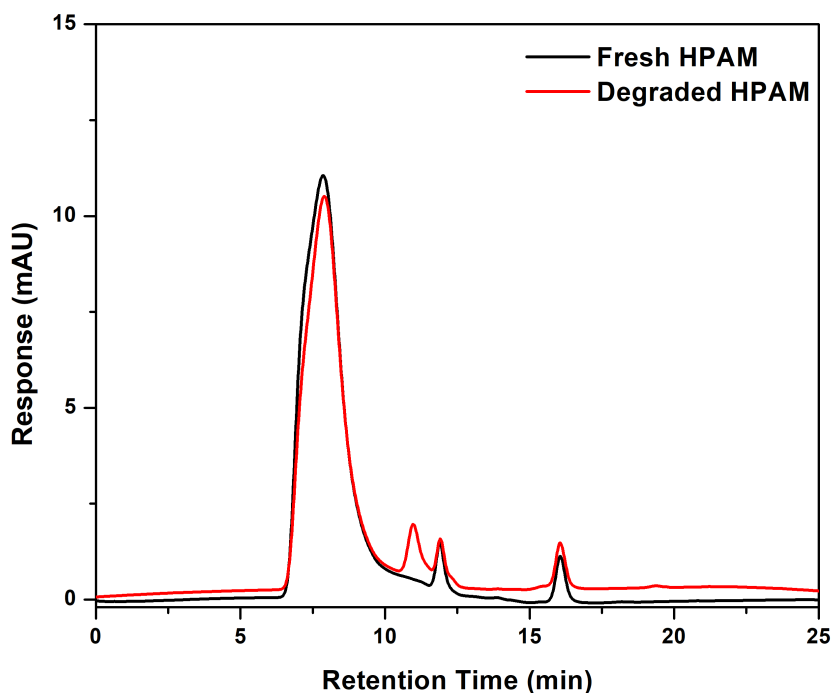


Figure 3.2: Size exclusion chromatogram of fresh and degraded 4,000 *ppm* HPAM solutions. Solutions were degraded at  $10\text{mL/min}$  and 0.25*mm* orifice diameter.

The intensity of the mechanical degradation in shear  $\Delta_s$  can be computed from the zero-shear viscosity parameter  $\eta_0$  obtained from fitting the data of

the fresh and degraded solutions to the Williamson model. The results are presented in Table 3.1 and Table 3.2 for orifice diameters of 0.25mm and 0.15mm, respectively.

Flow rate	Shear Rate	1,000 ppm	4,000 ppm	12,000 ppm
<i>mL/min</i>	<i>1/s</i>	$\Delta_s$ [%]		
2	$2.17 \times 10^4$	7±1	23±4	-
5	$5.43 \times 10^4$	24±6	28±6	20±2
7	$7.61 \times 10^4$	44±9	33±7	27±2
10	$1.09 \times 10^5$	55±11	64±16	49±13

Table 3.1: Mechanical degradation in shear  $\Delta_s$  of HPAM solutions at different concentrations and flow rates for a constriction diameter of 0.25mm.

Flow rate	Shear Rate	1,000 ppm	4,000 ppm	12,000 ppm
<i>mL/min</i>	<i>1/s</i>	$\Delta_s$ [%]		
2	$1.01 \times 10^5$	35 ± 6	51 ± 5	-
5	$2.52 \times 10^5$	51 ± 14	64 ± 10	46 ± 15
7	$3.52 \times 10^5$	79 ± 7	67 ± 4	61 ± 10
10	$5.03 \times 10^5$	89 ± 18	67 ± 5	68 ± 10

Table 3.2: Mechanical degradation in shear  $\Delta_s$  of HPAM solutions at different concentrations and flow rates for a constriction diameter of 0.15mm

The results show that, in general, the lowest degree of degradation is observed at the highest polymer concentration, which supports previous results in the literature (191). Moreover, the sensitivity of the degree of degradation to the shear rate is higher at the lowest concentration. These behaviors can be explained by the fact that polymer molecules at high concentration entangle, which creates physical cross-links between the chains and stronger chain interactions (192, 193), making it more difficult for external stresses to disrupt the polymer structure (194).

We proceed with the analysis only with the concentration of 4,000 ppm, which is within the range of concentration in polymer injection projects, between 1,000 and 5,000 ppm.

### 3.2 Apparent Extensional Viscosity of Fresh and Degraded Polymer Solutions

As discussed before, in the CaBER rheometer, the apparent extensional viscosity is evaluated from the time evolution of a filament diameter. In general, longer filament breakup times are associated with stronger viscoelastic stresses and consequently high extensional viscosity. The midpoint filament diameter data for both fresh and degraded 4,000 ppm polymer solutions at different flow

rates and  $0.25\text{mm}$  orifice diameter are shown in Figure 3.3. Markers represent the experimental data and the continuous curves are the fit using Equation (2-5). The plot illustrates a rapid initial viscous-dominated phase, followed by an intermediate time scale where the diameter time-evolution follows a nearly exponential decay. During this stage, surface tension drives flow that leads to the filament breakup, while the fluid's elasticity strives to prevent this process (100, 195). The fresh polymer solution has a longer breakup time,  $t_b \approx 0.42\text{s}$  compared to the degraded solutions, indicating greater resistance to capillary breakup. The flow resistance is caused by the stretching of the polymer chains. In the degraded solutions, the polymer molecules were broken as then flow through the valve, leading to weaker extensional resistance force. The solution that was degraded at the highest flow rate,  $10\text{mL}/\text{min}$ , has the shortest breakup time, e.g.  $t_b \approx 0.29\text{s}$ .

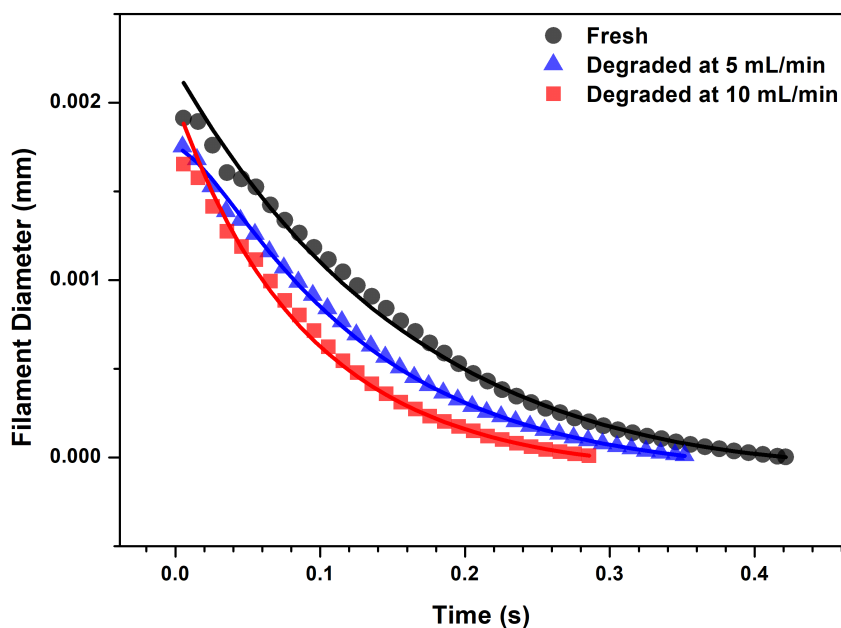


Figure 3.3: Evolution of the filament diameter of the fresh and degraded 4,000 ppm HPAM solutions at different flow rates through a 0.25 mm needle valve.

The relaxation time  $\lambda$  of the three solutions is obtained by fitting the exponential decay part of the diameter time-evolution according to eq. (2-2). The relaxation time of the fresh solution is  $\lambda = 0.042\text{s}$ , higher than the relaxation time of both degraded solutions:  $\lambda = 0.033\text{s}$  for the solution degraded at  $q = 5\text{mL}/\text{min}$  and  $\lambda = 0.024\text{s}$  for the solution degraded at  $q = 10\text{mL}/\text{min}$ . The lower relaxation time in extension is a clear indication that the polymer molecules were broken in the flow through the needle valve.

Figure 3.4 shows the apparent extensional viscosity of fresh and degraded HPAM solutions at flow rates of 5  $mL/min$  and 10  $mL/min$  as a function of Hencky strain. HPAM solution experiences strain-hardening in extensional flow due to polymer chain stretching (101, 196, 197). The apparent extensional viscosity rises with Hencky strain. Although degraded polymer solutions exhibit similar strain hardening behavior of the fresh solution, a decrease in the apparent extensional viscosity indicates degradation due to chain breakage in the flow through the needle valve (198, 199).

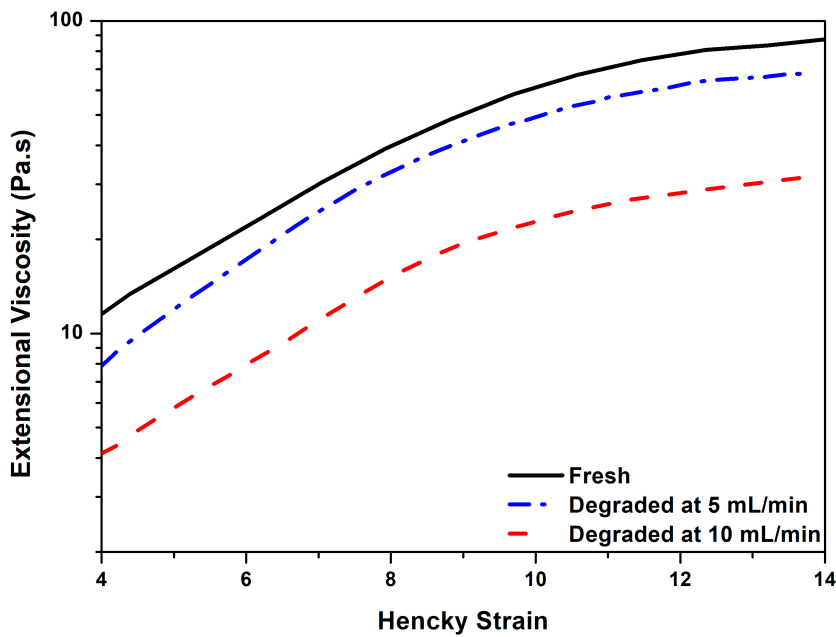


Figure 3.4: Apparent extensional viscosity of the fresh and degraded 4,000  $ppm$  HPAM solutions at different flow rates through a 0.25 mm needle valve.

The parameters that quantify the mechanical degradation in extension  $\Delta_{e\lambda}$  and  $\Delta_{e\eta}$  for the flow through the needle valve with a diameter orifice of 0.25mm are presented in Table 3.3. Clearly, the extend of mechanical degradation was stronger at the highest flow rate through the needle valve, i.e. higher deformation rate.

Flow rate ( $mL/min$ )	$\Delta_{e\lambda}$	$\Delta_{e\eta}$
5	0.23	0.21
10	0.63	0.42

Table 3.3: Mechanical degradation in extension of 4,000  $ppm$  HPAM solutions at different flow rates through the needle valve for a constriction diameter of 0.25mm.

### 3.3

#### The Effect of SiO<sub>2</sub> Nanoparticles on Mechanical Degradation of HPAM Solutions

The effect of the addition of SiO<sub>2</sub> nanoparticles in the 4,000 ppm HPAM solution on the mechanical degradation was analyzed by comparing the shear and extensional viscosity behavior of the fresh and degraded solutions, with and without the addition of the nanoparticles. The comparison was performed with the solutions degraded at 10mL/min and 0.25mm orifice diameter. At these flow conditions, the degree of polymer degradation is comparable to those encountered in polymer injection process as an enhanced oil recovery method (151).

Figure 3.5 presents the shear viscosity function of the fresh and degraded solutions, with and without nanoparticles, at nanoparticle concentration of 0.1%wt and 0.5%wt. The continuous lines represents the curve fit with the Williamson model. The solution without nanoparticles presented the reduction on the low-shear viscosity shown before. The mechanical degradation in shear was  $\Delta_s \approx 0.64$ . The addition of 0.1%wt of nanoparticles has a weak effect on the viscosity of the fresh solution. The low-shear viscosity of the NPs-HPAM fresh dispersion is only slightly higher than that of the fresh solution without nanoparticles. Remarkably, the shear viscosity of the degraded NPs-HPAM dispersion does not show strong reduction on the low-shear viscosity value. The mechanical degradation in shear was only  $\Delta_s \approx 0.12$ . At the range explored, the nanoparticle concentration has a weak effect on the rheological response. We proceeded with the analysis with the lowest nanoparticle concentration, e.g. 0.1%wt.

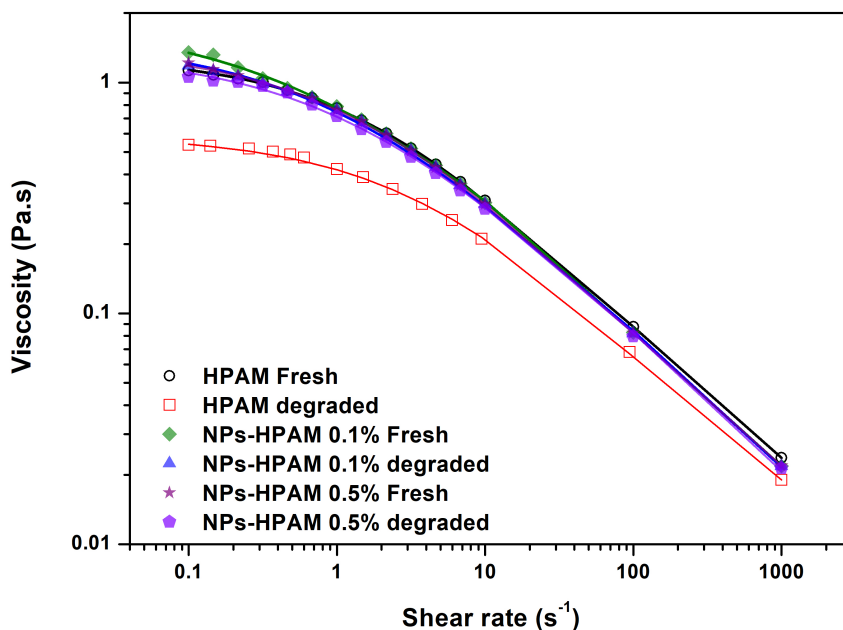


Figure 3.5: Steady-state shear viscosity of fresh and degraded HPAM solutions, with and without  $\text{SiO}_2$  nanoparticles. Solutions were degraded at  $10\text{mL}/\text{min}$  and  $0.25\text{mm}$  orifice diameter.

The inhibition of mechanical degradation is also evident in the extensional rheological properties of the solutions. The relaxation time of the fresh and degraded solutions, with and without nanoparticles are presented in Table 3.4. The relaxation time of the NPs-HPAM dispersion is very close to that of the fresh HPAM solution, indicating that the addition of nanoparticles inhibited the breakup of the polymer molecules in the flow through the needle valve.

Solution	Relaxation time $\lambda$ [s]
HPAM Fresh Solution	0.042
HPAM Degraded at 10 mL/min	0.024
NPs-HPAM Fresh Dispersion	0.040
NPs-HPAM Degraded at 10 mL/min	0.038

Table 3.4: Relaxation times of the fresh and degraded HPAM solutions, with and without nanoparticles. Samples were degraded at flow rate of  $10\text{ mL}/\text{min}$  and needle valve for a constriction diameter of  $0.25\text{ mm}$ .

Figure 3.6 shows the apparent extensional viscosity as a function of the Hencky strain for the fresh and degraded solutions, without and with nanoparticles. All the samples preserve the strain-hardening behavior, indicating their elastic response to extensional deformation (200). As in the shear viscosity

curves, the extensional viscosity curves of the fresh and degraded NPs-HPAM dispersion are very close to each other.

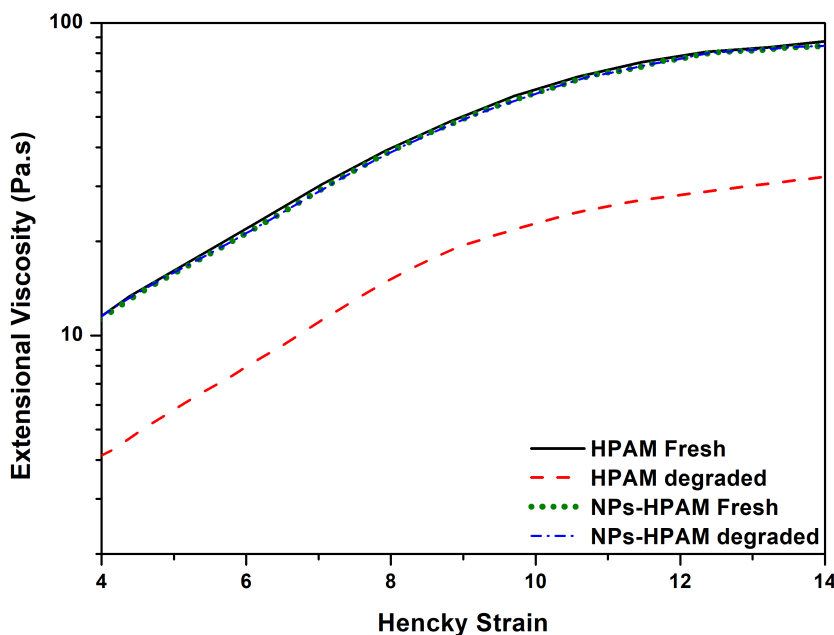


Figure 3.6: Apparent extensional viscosity of fresh and degraded HPAM solutions, with and without  $\text{SiO}_2$  nanoparticles. Solutions were degraded at  $10\text{ mL}/\text{min}$  and  $0.25\text{ mm}$  orifice diameter.

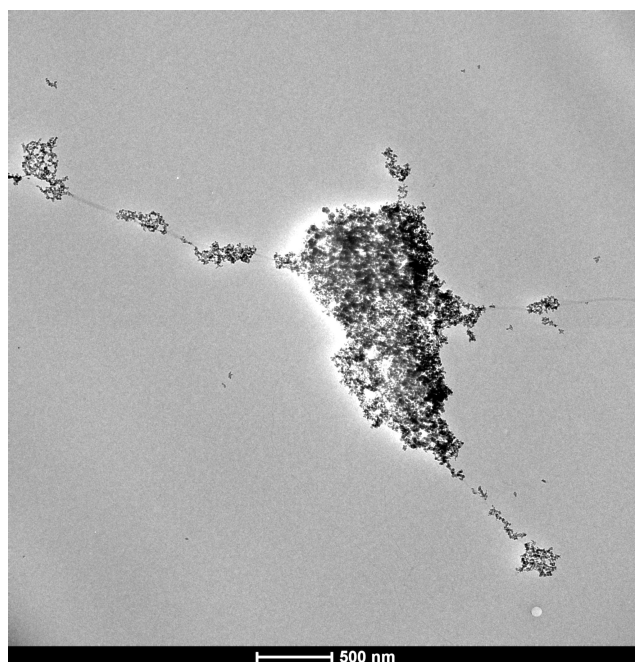
The incorporation of  $\text{SiO}_2$  nanoparticles effectively prevented the significant reduction in both shear and extensional viscosity that occurs in the solution without nanoparticles when the fluid is subjected to high deformation rate flows, leading to mechanical degradation. The mechanical degradation in shear and extension for the solutions with and without nanoparticles are presented in Table 3.5. The solutions without the addition of  $\text{SiO}_2$  nanoparticles present significant mechanical degradation, whereas the solutions with the addition of 0.1% wt nanoparticles show very weak mechanical degradation; the different degradation parameters are all very small.

Solution	$\Delta_s$	$\Delta_{e\eta}$	$\Delta_{e\lambda}$
HPAM Degraded at 10 mL/min	0.64	0.63	0.42
NPs-HPAM Degraded at 10 mL/min	0.12	0.00	0.05

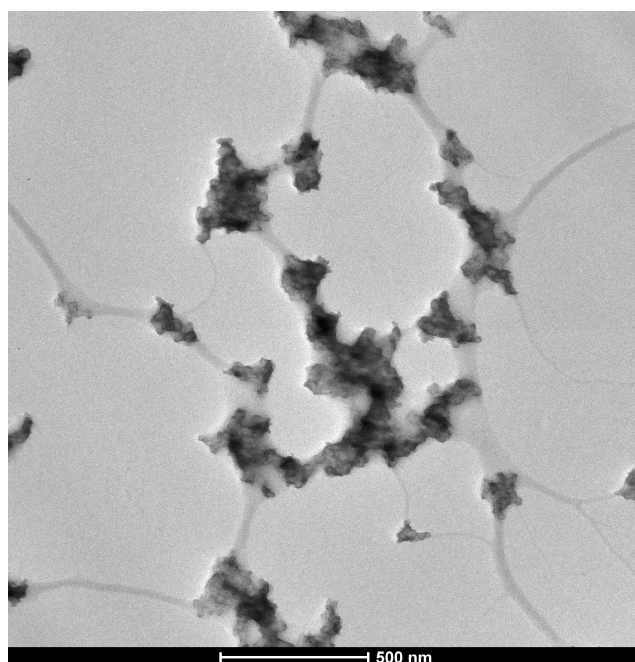
Table 3.5: Mechanical degradation in shear and extension for the solutions with and without nanoparticles. Samples were degraded at flow rate of  $10\text{ mL}/\text{min}$  and needle valve for a constriction diameter of  $0.25\text{ mm}$ .

The presence of  $\text{SiO}_2$  nanoparticles reinforce intermolecular associations and strengthen the network structure of HPAM, thus reducing its susceptibility

to mechanical degradation. This mechanism is clear in the TEM image of the degraded NPs-HPAM system, shown in Figure.3.7 (b). The nanoparticles are located in the joints of the polymer clusters, enhancing their strength.



(a) NPs-HPAM Fresh



(b) NPs-HPAM degraded

Figure 3.7: Transmission electron microscopy (TEM) images.

## 4

### **Flow for Fresh and Degraded Polymer Solutions and NPs-HPAM Dispersions through porous media micromodel**

This chapter presents and discusses results of oil displacement experiments in microfluidic devices used as a model of porous media. The study explores oil displacement strategies using both fresh and degraded polymer solutions. Microfluidic devices play a pivotal role in guiding our research, enabling a thorough examination of key parameters, including mechanical degradation, injection rates and the combined effects of SiO<sub>2</sub> nanoparticles.

By leveraging the unique capabilities of microfluidic devices, this research aims to provide a comprehensive understanding of how rheological parameters affect the performance of polymer solutions in displacing oil in porous media. The use of a microfluidic device enables the visualization of pore-scale phenomena, which helps the fundamental understanding of the physical processes that govern fluid displacement in the pore space.

#### **4.1**

##### **Mechanical degradation in the flow through a microfluidic porous media model**

In the Chapter 3, we delved into the mechanical degradation of polymer solutions during the flow through a valve. Before analyzing oil displacement in a porous media micromodel, we study the mechanical degradation of polymer solutions in the flow through a porous media micromodel. Simulating mechanical degradation during the flow through porous media valuable insights into polymer behavior across diverse scenarios, enhancing our understanding of real-world conditions.

We measured the shear viscosity and apparent extensional viscosity of the solution before and after the flow through the porous medium at different conditions to evaluate the impact of the flow in the rheological response. Executing degradation experiments on a micromodel, we controlled flow rates and residence times, gaining insights into molecule breaking mechanisms under various flow conditions.

### 4.1.1

#### Shear Viscosity and Mechanical Degradation of Polymer Solutions in a Microfluidic Porous Media

Microfluidic devices have emerged as effective tools for scrutinizing polymer rheology and mechanical degradation (201, 202, 203). Offering precise control over flow conditions, these devices create a platform for mimicking reservoir scenarios. We probed mechanical degradation of 4000 *ppm* HPAM solutions with low molecular weight, typical in flooding projects (204) by measuring its shear viscosity before and after flowing the solution through the micromodel. By simulating conditions akin to porous media, the microfluidic device enhanced understanding of flow behavior and degradation mechanisms under specific conditions.

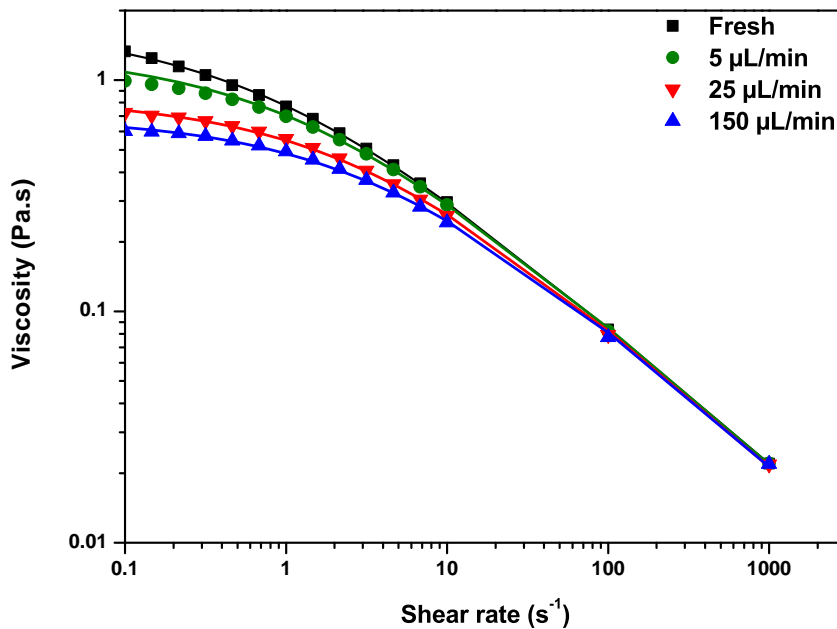


Figure 4.1: Shear viscosity curves of low molecular weight HPAM solutions at 4,000 *ppm*, fresh and degraded at different flow rates. Solid lines represent the Williamson model.

Figure 4.1 presents viscosity curves of a polymer solution before injection (fresh solutions) and samples collected from effluent of the flow through the micromodel at different flow rates. All flow curves exhibit a Newtonian plateau at low shear rates, transitioning to shear-thinning behavior at higher shear rates. The viscosity curves at low shear rate shift to lower values as they undergo varying degrees of mechanical degradation traversing the microfluidic device.

Flow rate [ $\mu L/min$ ]	$\Delta P$ [Psi]	$\eta_0$ [Pa.s]	$\Delta_s$ [%]
5	16	1.30 $\pm$ 0.02	19 $\pm$ 3
25	34	0.84 $\pm$ 0.01	48 $\pm$ 7
150	117	0.68 $\pm$ 0.01	57 $\pm$ 8

Table 4.1: Mechanical degradation in shear  $\Delta_s$  of 4,000 ppm HPAM solutions at different flow rates through the micromodel.

The mechanical degradation in shear  $\Delta_s$ , can be computed from the zero-shear viscosity parameter  $\eta_0$  obtained from fitting the data of the fresh and degraded solutions to the Williamson model. The results are presented in Table 4.1. This degradation is attributed to shearing and stretching of polymer chains, resulting in reduced solution viscosity (205).

Herrera et al.(206) highlighted the significant impact of flow rate on mechanical degradation in different restriction geometries. The highest flow rate explored of 150  $\mu L/min$  led to more considerable polymer degradation, with up to 57% degradation observed. These findings align with Nghe et al. (202), supporting the crucial role of flow rate in the mechanical degradation of polymer solutions during flow through in porous media.

### 4.1.2

#### Effect of mechanical degradation in the flow through a microfluidic porous media device on the apparent extensional viscosity of polymer solutions

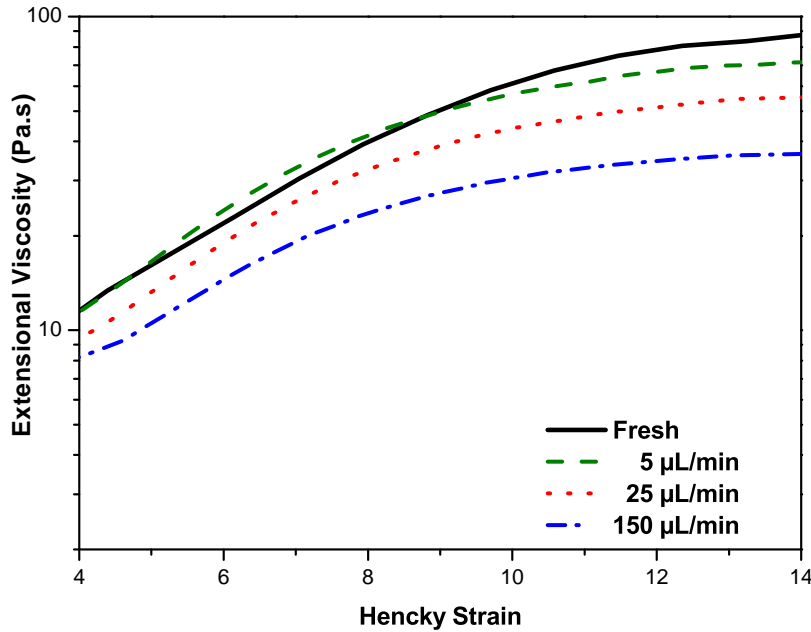


Figure 4.2: Apparent extensional viscosity curves of HPAM solutions at 4,000 ppm, fresh and degraded at different flow rates. The curves were fitted with Equation 2-6(186).

To complete our analysis, we measured the apparent extensional viscosity of the polymer solutions before and after degradation. This allowed us to determine the elastic behavior of the solution under extensional flow conditions in porous media. Examining how mechanical degradation impacts viscoelastic properties provides valuable insights into understanding changes in a solution’s ability to resist deformation and recover its original shape, crucial for applications where elasticity plays a significant role, such as flow in porous media.

Mechanical degradation significantly impacts the ability of polymer solutions to maintain their extensional properties (124). As observed in Figure 4.2, the viscosity of polymer solutions increases when they are stretched, a phenomenon known as strain-hardening behavior. However, we found that mechanical degradation decreased the strain-hardening behavior when comparing fresh and degraded polymers. The degraded HPAM polymer experiences chain breakage and reduced entanglement, resulting in a lower strain hardening capacity. In contrast, fresh HPAM has a more uniform structure of long polymer molecules that enables its chains to become more entangled and form a more

robust network when stretched. This leads to higher strain hardening, supporting the idea that the mechanical degradation of polymer solutions in a microfluidic device, as in the flow through a needle valve, not only affects their shear viscosity but also significantly impacts their extensional properties and viscoelastic behavior (149). High flow rates, as observed in our study, lead to reduced extensional viscosity of degraded HPAM solutions compared to fresh solutions, resulting in weaker deformation thickening behavior when compared to fresh HPAM solutions.

The relaxation time  $\lambda$  of the four solutions is obtained by fitting the exponential decay part of the diameter time-evolution according to Equation (2-8). The relaxation time of the fresh solution is  $\lambda = 0.045s$ , higher than the relaxation time the degraded solutions:  $\lambda = 0.042s$  for the solution degraded at  $q = 5\mu L/min$ ,  $\lambda = 0.033s$  for the solution degraded at  $q = 25\mu L/min$  and  $\lambda = 0.021s$  for the solution degraded at  $q = 150\mu L/min$ . The lower relaxation time in extension clearly indicates that the polymer molecules were broken in the flow through the microfluidic device.

The parameters that quantify the mechanical degradation in extension  $\Delta_{e\eta}$  and  $\Delta_{e\lambda}$  for the flow through the micromodel are presented in Table. 4.2. Clearly, the extent of mechanical degradation was stronger at the highest flow rate through the micromodel, i.e. higher deformation rate.

Flow rate ( $\mu L/min$ )	$\Delta_{e\eta}$	$\Delta_{e\lambda}$
5	0.18	0.05
25	0.37	0.24
150	0.58	0.51

Table 4.2: Mechanical degradation in extension of 4,000 ppm HPAM solutions at different flow rates through the microfluidic device.

Our study concludes that the mechanical degradation of polymer solutions in a microfluidic porous media device is similar to the degradation observed in the flow through a valve presented in Chapter 3. The comparison between the flow through a valve and a porous medium highlights the practicality and simplicity of valve experiments. The mechanical degradation behavior similarity emphasizes the relevance and reliability of microfluidic devices as tools for studying polymer behavior in porous media environments, and validates the use of valve flow experiments. The results indicate that both microfluidic devices and valve experiments can effectively reproduce reservoir conditions, providing valuable insights into polymer behavior under flowing conditions. This understanding is crucial for improving our knowledge of enhanced oil recovery processes. Additionally, the simplicity of valve experiments

allows for more efficient and accurate simulation of these conditions, leading to the development of more effective polymer flooding strategies tailored to enhanced oil recovery applications.

## 4.2

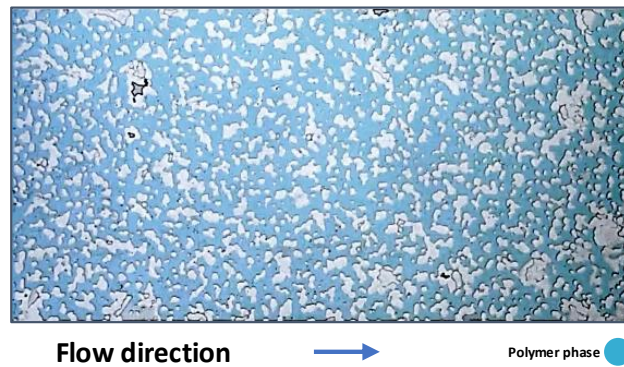
### Oil displacement by the injection of fresh polymer solutions

To investigate the effectiveness of fresh HPAM polymer solutions in oil displacement, we conducted experiments using a setup that allowed for polymer injection into a microfluidic device saturated with mineral oil. Our objective was to vary the injection rate and observe its impact on oil displacement while considering polymer properties. The insights gained from these experiments provide valuable information on using a fresh HPAM polymer as an effective agent for oil recovery.

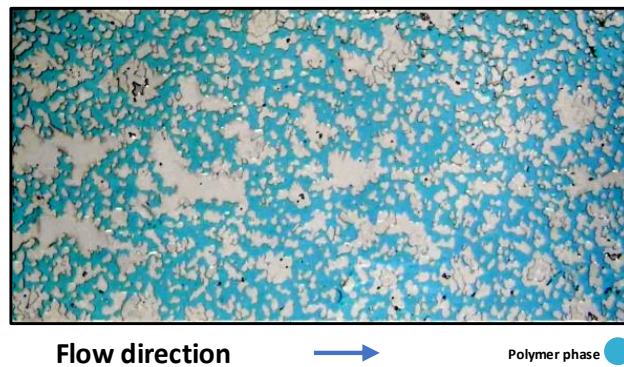
We injected five pore volumes at different flow rates:  $0.5 \mu\text{L}/\text{min}$  (Figure 4.3 A),  $0.1 \mu\text{L}/\text{min}$  (Figure 4.3 B), and  $0.03 \mu\text{L}/\text{min}$  (Figure 4.3 C), which corresponded to capillary numbers, defined as  $Ca = \mu V/\sigma$  of  $Ca=4 \times 10^{-3}$ ,  $Ca= 2 \times 10^{-3}$  and  $Ca=1 \times 10^{-3}$ . To calculate the capillary number, different viscosities are utilized for each flow rate, and their corresponding values are listed in the Table. 4.3. The analysis focused on the phase distribution in the pore space at the end of the injection process, where the blue phase represents the polymer solution, and the lighter phase represents the oil.

$Ca$	$\mu[cP]$
$4 \times 10^{-3}$	164.18
$2 \times 10^{-3}$	370.60
$1 \times 10^{-3}$	603.64

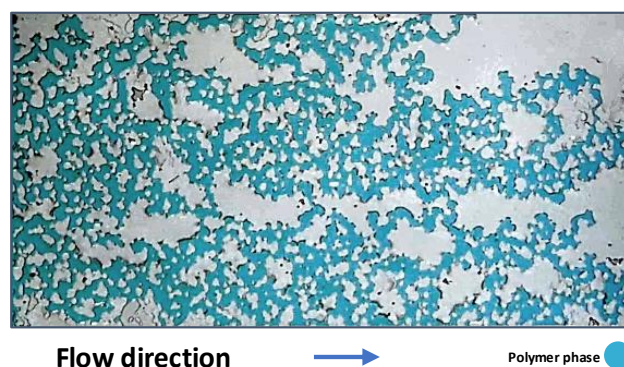
Table 4.3: Capillary number and viscosity of injected polymer solutions at different flow rates.



(a) 0.5  $\mu L/min$



(b) 0.1  $\mu L/min$



(c) 0.03  $\mu L/min$

Figure 4.3: Pore space occupation by the polymer (blue) and oil (transparent) at the end of the injection process at different flow rates.

The remaining oil saturation  $S_{or}$  at different flow rates is obtained by image processing, as explained before. The results, presented in Figure 4.4, indicate that injecting HPAM polymer solutions at higher flow rates, as measured by the capillary number, can improve oil recovery by increasing the displacement efficiency of the solution. These findings are consistent with previous studies (207, 208) and highlight the importance of considering injection rates when employing polymer flooding for enhanced oil recovery. By optimizing flow rates and capillary numbers, we can develop more efficient strategies for recovering oil from reservoirs.

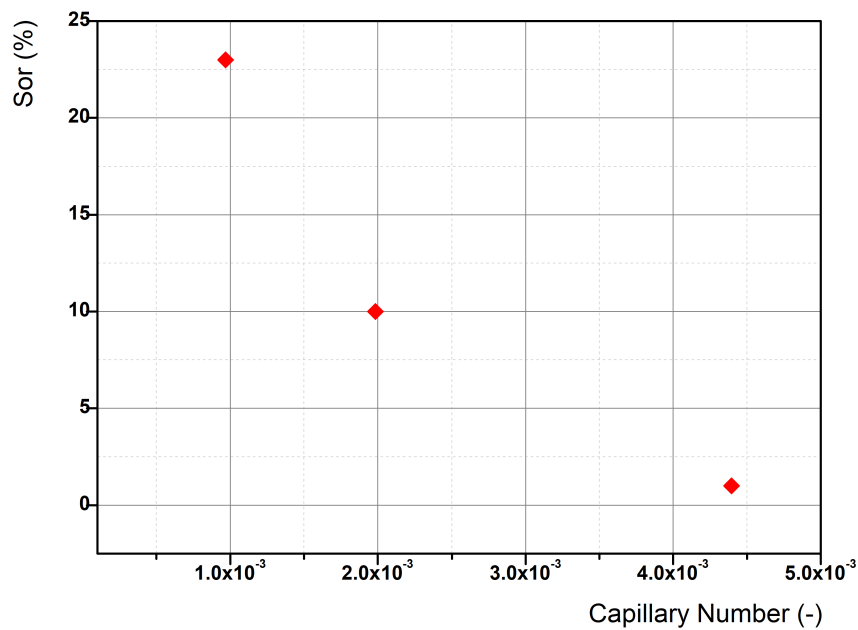


Figure 4.4: Residual oil saturation as a function of capillary number for fresh HPAM solutions.

Our findings revealed that the remaining oil saturation was  $S_{or} \approx 0.01$  at higher injection rates ( $0.5 \mu\text{L}/\text{min}$ ). This condition leads to a very high capillary number, not possible in EOR applications. In EOR applications, the aqueous phase is usually injected at a flow rate corresponding to a Darcy velocity of approximately 1 ft/day (209). For this reason, we utilized lower injection rates ( $0.1 \mu\text{L}/\text{min}$  and  $0.03 \mu\text{L}/\text{min}$ ), which led to a significant increase in the residual oil saturation to  $S_{or} \approx 0.10$  and  $S_{or} \approx 0.23$ , respectively. As discussed in the previous section, these values of flow rates are much lower than those that leads to mechanical degradation. The polymer solutions are not subjected to high enough deformation rates that could induce degradation of the polymer molecules(210).

The characteristics of the flow associated with oil displacement by an aqueous flow in porous media is governed by two key parameters: viscosity ratio ( $V$ ) and capillary number ( $Ca$ ). The viscosity ratio defined as  $V = \mu_o/\mu_w$  is the ratio of the viscosity of the displacing fluid to the displaced fluid, while the capillary number reflects the ratio of viscous force to capillary force(211). The viscosity of the polymer solution falls as the shear rate (flow rate) rises. At low flow rates, the polymer viscosity is higher than the oil viscosity, leading to a viscosity ratio lower than 1.

Flow rate ( $\mu L/min$ )	Capillary number	Viscosity Ratio
0.50	$4 \times 10^{-3}$	1.28
0.10	$2 \times 10^{-3}$	0.57
0.03	$1 \times 10^{-3}$	0.35

Table 4.4: Viscosity ratio and capillary number on residual oil recovery in microfluidic systems.

From the data presented in Table 4.4, it is evident that fluid injection at a high flow rate of  $0.5\mu L/min$  results in very low residual oil saturation. The high oil recovery rate at high injection flow rates is attributed to the eventual dominance of capillary forces over viscous forces.

A more balanced interaction between viscous and capillary forces is observed by reducing the injection flow rate by just 20% ( $0.1\mu L/min$ ). The displacement becomes more favorable as the capillary number decreases and the viscosity ratio is lower than 1.

Further reduction in flow rate to  $0.03\mu L/min$  shows a significant decrease in the viscosity ratio. This decrease leads to a more stable displacement. Despite the more stable displacement, the capillary number is low enough, which leads to higher residual oil saturation.

By analyzing the phase distribution and evaluating the flow rate, viscosity ratio, and capillary number, we observed that a fresh polymer solution with an injection rate of  $0.1\mu L/min$  ( $3ft/day$  at the reservoir scale) achieved the recovery percentages typically encountered in field-scale polymer flooding, as reported by other authors with concentrations similar to the one used in our research (212, 213, 214).

### 4.3

#### Oil displacement by injection of degraded HPAM solutions

A thorough study of the behavior of fresh and degraded HPAM polymer solutions is necessary to accurately compare their effectiveness in oil recovery. The study should include an analysis of the behavior of fresh polymer solu-

tions and an assessment of the impact of degraded HPAM solutions on oil displacement.

To evaluate the effectiveness of degraded HPAM solutions in EOR, we carried out flow injection tests using a micromodel saturated with mineral oil. The tests used a degraded solution that has passed through a valve with an orifice diameter of 0.25 mm at a flow rate of 10 mL/min.

Our findings indicate significant differences between the degraded and fresh HPAM polymer solutions. Specifically, the former displayed significantly lower shear viscosity than the latter. This is evident from the data presented in figure 4.5, which clearly demonstrates a marked difference in viscosity between the two types of solutions.

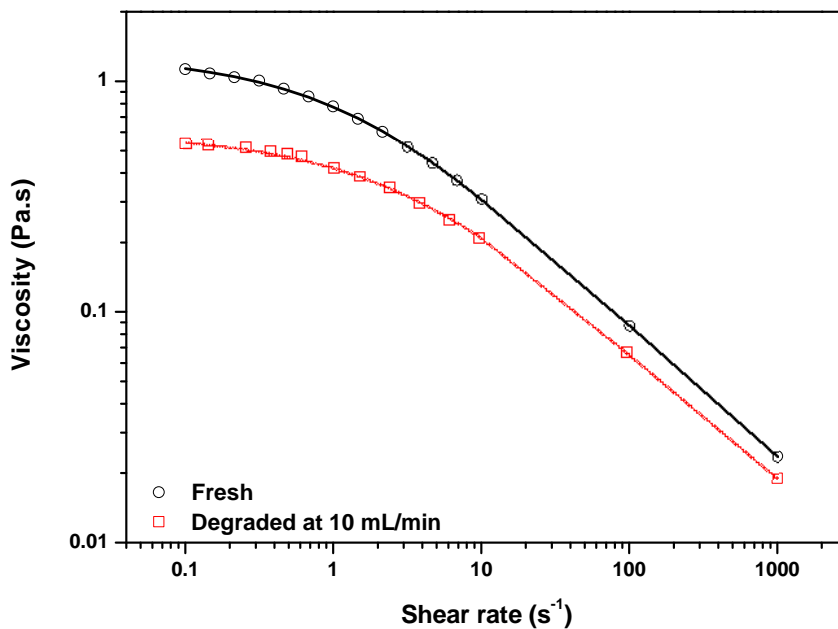


Figure 4.5: Steady-state shear viscosity of fresh and degraded HPAM solutions

The experimental system selected for the oil displacement study displayed the lowest extensional apparent viscosity. The results were obtained through careful measurements and observations, which are thoroughly documented in chapter 3. Upon closer examination, it was observed that the degradation of the HPAM polymer solution was the primary reason for this phenomenon. This finding is supported by figure 4.6, which provides conclusive evidence of the HPAM polymer solution's degradation. The figure clearly shows that the HPAM polymer solution experienced a significant decrease in the apparent extensional viscosity, which is a direct result of the degradation process. This

degradation was likely caused by the deformation of polymer chains during the flow of the solution through the valve.

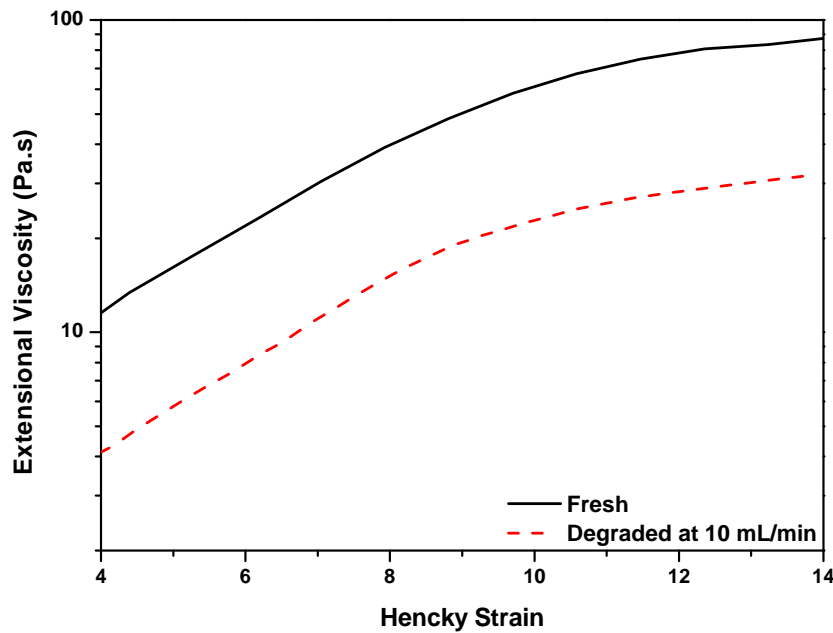


Figure 4.6: Apparent extensional viscosity of fresh and degraded HPAM solutions

In order to determine the apparent shear rate of the micromodel, we employed Equation 4-1, which was developed by Hirasaki et al. (215) and accounts for the complex rheological properties of non-Newtonian fluids as well as the porous nature of the medium. To analyze the rheological data of both fresh and degraded HPAM solutions, we utilized the Williamson model, which yielded exponent values of 0.62 and 0.60, respectively. The calculated shear rate of the micromodel was approximately  $7 \text{ s}^{-1}$ , a value that is widely recognized as a standard reference point for determining shear rates in reservoirs (198, 216, 150, 217).

$$\dot{\gamma}_{mp} = \left( \frac{3n + 1}{4n} \right)^{\frac{n}{n-1}} \left( \frac{12u}{\sqrt{150K\phi}} \right) \quad (4-1)$$

where:

$\dot{\gamma}_{mp}$  is the shear rate of the porous medium,

$u$  is the Darcy velocity,

$n$  is the exponent of the Power Law model,

$K$  is the permeability,

$\phi$  is the porosity.

The results of the study examining the use of HPAM polymer solutions in oil production indicate that fresh HPAM is more efficient in producing oil at a higher rate than degraded HPAM. The capillary number for injecting fresh and degraded solutions was  $Ca = 2 \times 10^{-3}$  and  $Ca = 1 \times 10^{-3}$ , respectively. Figure 4.7 (left) presents the curve of the injection. The HPAM led to about 80% oil recovery at one pore volume injected, while degraded HPAM only resulted in about 30% oil recovery at the same point. Furthermore, the graph reveals that the HPAM curve reached a steady state after two pore volumes were injected, whereas the degraded HPAM curve continued to rise slowly until it reached a steady state after three pore volumes were injected.

The images in Figure 4.7 (right) further support the superior oil displacement efficiency of fresh HPAM over degraded HPAM. Image (A) shows that HPAM occupied more pore space than degraded HPAM (B), which suggests a more efficient oil displacement. Moreover, the image demonstrates that fresh HPAM formed a more uniform and stable flow in the pores than degraded HPAM, contributing to its higher oil recovery. These results can be attributed to the rheological behavior of fresh HPAM, making it more suitable for displacing oil from the pores and driving it to the production well. In conclusion, the experiment determined that fresh HPAM is more effective and efficient in producing oil at a higher rate than degraded HPAM.

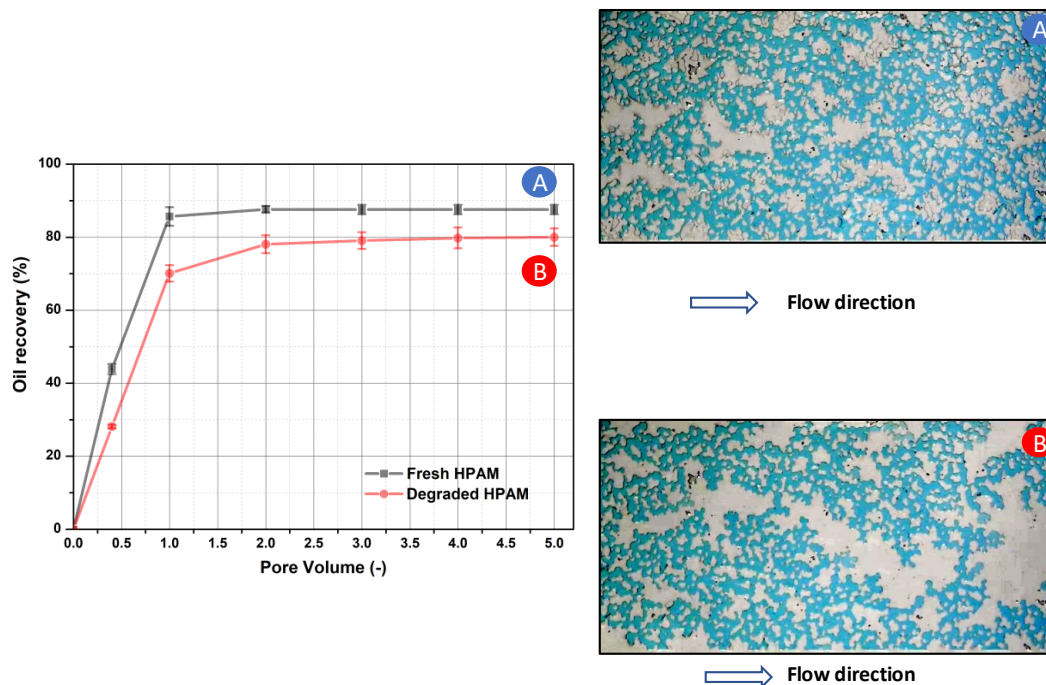


Figure 4.7: Evolution of the oil recovery obtained with both the fresh (A) and degraded HPAM solutions(B) (left). Pore occupation at five pore volumes injected (right). The pore occupation by the fluids is represented in blue.

#### 4.4 Oil displacement with NPs-HPAM dispersion

Our study aimed to test the effectiveness of degraded NPs-HPAM dispersions in oil displacement. We used a 4,000 ppm HPAM solution with 0.1% silica nanoparticles that experienced a degradation process by flowing it through a valve. Our observations, explained in more detail in chapter 3, showed that nanoparticles added to the HPAM polymer solution mitigate mechanical degradation. The rheological properties of the polymer solutions with nanoparticles were similar before and after passing through the needle valve. This indicated that silica nanoparticles can help maintain the solution's viscosity during degradation, which is a crucial factor in the oil recovery process.

Figures 4.8 and 4.9 obtained from our experiment demonstrate the positive impact of silica nanoparticles on the rheological properties of HPAM solutions during mechanical degradation.

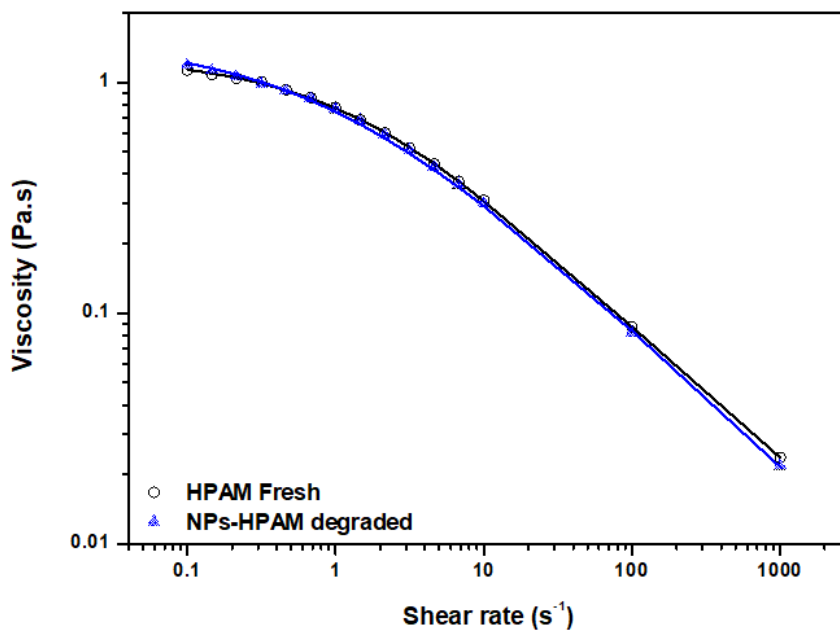


Figure 4.8: Steady-state shear viscosity of fresh and NPs-HPAM degraded solutions. The NPs-HPAM dispersion was degraded at  $10 mL/min$  and  $0.25 mm$  orifice diameter through a valve.

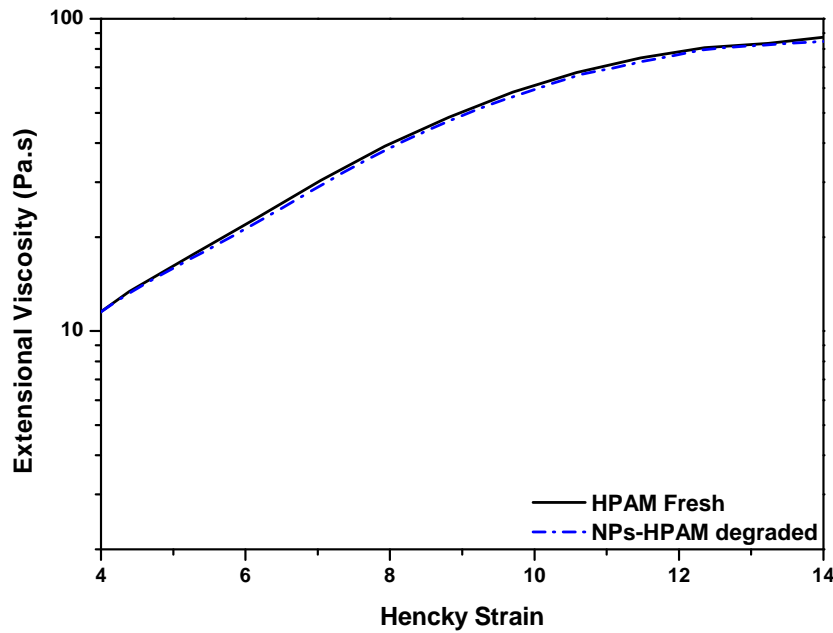


Figure 4.9: Apparent extensional viscosity of fresh and NPs-HPAM degraded solutions. The NPs-HPAM dispersion was degraded at  $10\text{mL}/\text{min}$  and  $0.25\text{mm}$  orifice diameter through a valve.

Recent research has shown that the incorporation of nanoparticles into polymer solutions can significantly enhance the recovery of oil (12, 218, 170). However, in order to obtain a better understanding of the underlying physical mechanisms and fluid distribution at the pore scale, the use of micromodels is crucial. These micromodels enable researchers to gain insights into the intricate details of fluid flow and displacement processes taking place within porous media at a microscopic level. Thus, the combination of nanoparticles and micromodels can be a powerful strategy for optimizing the EOR process (161, 219, 220, 221).

In our study, we conducted an experiment to examine the effectiveness of a solution of degraded NPs-HPAM in mobilizing oil from the porous media. We injected the solution through a glass micromodel that simulates the pore structure of a reservoir rock. The capillary number was  $Ca = 2 \times 10^{-3}$ , corresponding to a flow rate of  $0.1 \mu\text{L}/\text{min}$ .

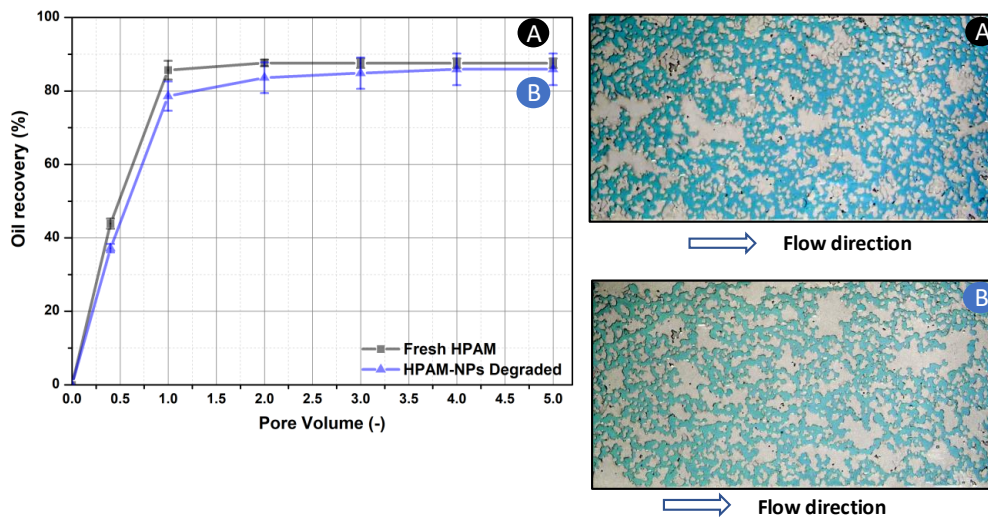


Figure 4.10: Comparison of oil displacement versus pore volume injected (left) and pore occupation at five pore volumes injected (right) using fresh HPAM (A) and NPs-HPAM degraded at  $10 \text{ mL/min}$  (B). The pore occupation by the fluids is represented in blue.

In the experiment, we observed that the recovery rate of degraded NPs-HPAM dispersion was initially slower than that of fresh HPAM at the start of the curve, as shown in Figure 4.10. This indicates that the degraded NPs-HPAM dispersion takes longer to mobilize oil from the micromodel. However, as we continued to inject more pore volumes, we noticed a gradual improvement in the recovery rate. Specifically, when we increased the pore volume injected to 2 PV, the recovery rate of degraded NPs-HPAM dispersion increased by up to 80% after 4 PV injections. These findings indicate that the use of silica nanoparticles in enhanced oil recovery has the potential to be a viable solution for mechanical degradation. It can achieve similar percentages of oil recovery compared to the fresh polymer solution.

Previous research has demonstrated the efficacy of nanofluid-enhanced polymer solutions in improving oil recovery. Kumar et al. (2022) (222) conducted a study that showed the addition of nanoparticles to polymers can enhance the rheological characteristics of polymeric nanofluid in adverse conditions, thereby enhancing its overall performance in oilfield applications. These findings align with our research, which supports the use of silica nanoparticles in polymer solutions to improve oil recovery in porous media.

The analysis presented in Figure 4.11 provides valuable insights into

the impact of incorporating silica nanoparticles into HPAM solutions for oil recovery. The oil recovery curve of the degraded NPs-HPAM dispersion shows a fast initial recovery rate and higher final recovery compared to the degraded HPAM polymer solution, indicating that the addition of nanoparticles helps improve oil mobilization from the micromodel. Furthermore, the gradual increase in recovery rate observed with increasing pore volumes suggests that the nanoparticles have a stabilizing effect on the polymer solution, preventing further degradation and enhancing its performance in displacing oil from porous media.

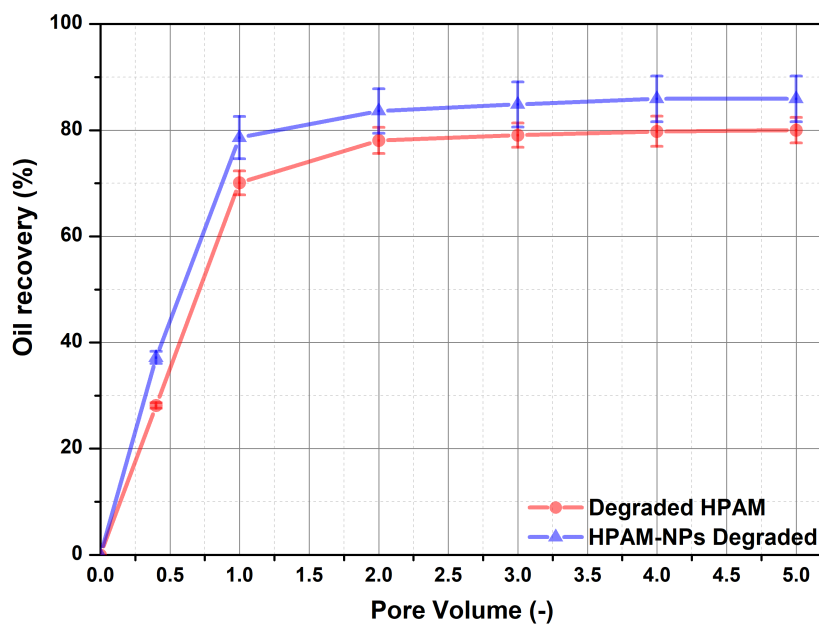


Figure 4.11: Performance of degraded HPAM solution and NPs-HPAM dispersion in the oil recovery process.

Our study found that incorporating silica nanoparticles into degraded HPAM solutions resulted in a 9-13% increase in oil recovery, which aligns with Yousefvand's research (2015) (161). This research indicated that NPs can effectively prevent the degradation of the elastic network structure of HPAM solutions under severe reservoir conditions. The combined application of NPs and HPAM has displayed a synergistic effect, making it a promising option for chemical enhanced oil recovery processes. Therefore, the results of the study show a clear indication of the significant benefits of utilizing silica nanoparticles to enhance the performance of degraded HPAM solutions in oil recovery processes.

The addition of silica nanoparticles to HPAM creates a stable, three-

dimensional network structure that can withstand extreme conditions such as mechanical degradation. This network structure increases the HPAM solution's capacity to resist shear forces and maintain its viscosity, which is crucial for efficiently displacing high-viscosity oil. Additionally, nanoparticles act as protective agents, preventing the breakdown of polymer molecules during polymer flooding (165, 223).

## 5

### Conclusion and future work

Mechanical degradation of HPAM solutions in the flow through a needle valve was characterized by shear and extensional rheology. The flow rate controlled the deformation rate of the flow through the valve and valve constriction. The degree of polymer molecule breakup was consistent with that encountered in the flow of polymer solutions through porous media micromodel. Mechanical degradation changes the flow behavior of polymer solution through porous media and reduces the effectiveness of polymer injection as an enhanced oil recovery method.

The results show that mechanical degradation leads to a decrease on the low-shear shear viscosity, relaxation time in extension and apparent extensional viscosity. For the 4,000 *ppm* HPAM solution, a concentration within the range used in polymer injection processes, the relative drop of the shear viscosity was as high as 64 %, and of the extensional viscosity was as high as 63 % . This behavior is associated with a reduction of the molecular weight distribution of the polymer solution caused by the breakup of the polymer molecules as they are deformed.

The results also clearly show that the addition of 0.1 % SiO<sub>2</sub> nanoparticles in the HPAM solutions mitigates the effect of the mechanical degradation. Both the shear and extensional rheological properties of polymer solutions with the addition of nanoparticles were very similar before and after flowing through the needle valve. Polymer solutions with the addition of nanoparticles have great potential to be used as an enhanced oil recovery method, as their rheological properties, and consequently their efficiency in oil displacement process, are not strongly affected by mechanical degradation that occurs in the flow of polymer solution through injection lines, valves and inside the reservoir.

Our research on fluid flow at the microscale has shown that the behavior and interactions of polymer solutions with porous media are greatly affected by mechanical degradation. We have also observed that SiO<sub>2</sub> nanoparticles in the polymer solution can act as stabilizers, preventing polymer degradation under high shear conditions in porous media. This results in improved effectiveness of the polymer solution in recovering trapped hydrocarbons. Our study highlights the potential of microfluidics as a tool to visualize and understand the complexities involved in oil recovery with polymers and nanoparticles. These findings can be used to develop more efficient strategies for enhanced oil recovery, contributing to the sustainable extraction of hydrocarbon resources.

Future studies must address the identified research gaps and opportunities to ensure the successful implementation of these systems in real-world EOR scenarios. This may involve conducting field trials and developing accurate scaling methods to bridge the gap between laboratory scale models and full-scale field operations. Additionally, exploring the effects of surface chemistry of nanoparticles on the rheological properties and oil displacement efficiency of nano-silica-polymer systems can lead to improved designs for EOR applications.

Given the challenges of using size exclusion chromatography with nanoparticle-laden polymer solutions, it is crucial to explore alternative methods for determining polymer chain size. Nanoparticles can interfere with chromatography, leading to inaccurate results. Intrinsic viscosity measurements offer a promising alternative, correlating the solution's viscosity to polymer molecular weight. This approach bypasses nanoparticle complications, providing reliable polymer characterization for enhanced oil recovery applications.

It is also important to consider the impact of nanoparticles on other crucial properties of two-phase flow in porous media, such as interfacial tension, interfacial rheology, and wettability, which could be included in future studies. It is essential to investigate the impact of nanoparticles on the stability of emulsions formed during oil recovery processes. Nanoparticles have the potential to enhance emulsion stability by creating a solid layer at the oil-water interface, thereby improving the emulsion's resistance to harsh reservoir conditions such as high temperatures and salinity. Understanding these interactions will provide valuable insights into optimizing nanoparticle use for enhanced oil recovery applications.

The implications of this research go beyond the laboratory scale, as the findings have the potential to impact the oil and gas industry significantly. It is clear that the study of polymer solutions, combined with nanoparticles, can revolutionize EOR techniques, increase the overall efficiency of oil recovery processes, and contribute to the sustainable management of hydrocarbon resources.

## 6

### Bibliography

- 1 THOMAS, A. **Essentials of polymer flooding technique**. [S.I.]: John Wiley & Sons, 2019. Cited 4 times in pages 9, 14, 15, and 16.
- 2 LINVILLE, B. Liquid fossil-fuel technology. quarterly technical progress report, october-december 1982. 1982. Cited 2 times in pages 9 and 14.
- 3 DRUETTA, P.; PICCHIONI, F. Influence of the polymer degradation on enhanced oil recovery processes. **Applied Mathematical Modelling**, Elsevier, v. 69, p. 142–163, 2019. Cited 4 times in pages 9, 14, 37, and 39.
- 4 AZAD, M. S.; TRIVEDI, J. J. Novel viscoelastic model for predicting the synthetic polymer's viscoelastic behavior in porous media using direct extensional rheological measurements. **Fuel**, Elsevier, v. 235, p. 218–226, 2019. Cited 3 times in pages 14, 32, and 33.
- 5 SCOTT, A. J.; ROMERO-ZERÓN, L.; PENLIDIS, A. Evaluation of polymeric materials for chemical enhanced oil recovery. **Processes**, MDPI, v. 8, n. 3, p. 361, 2020. Cited 2 times in pages 14 and 23.
- 6 AL-KINDI, S. et al. Partially hydrolyzed polyacrylamide: enhanced oil recovery applications, oil-field produced water pollution, and possible solutions. **Environmental Monitoring and Assessment**, Springer Science and Business Media Deutschland GmbH, v. 194, p. 1–19, 12 2022. ISSN 15732959. Disponible em: <<https://link.springer.com/article/10.1007/s10661-022-10569-9>>. Cited in page 14.
- 7 MUHAMMED, N. S. et al. Comparative study of green and synthetic polymers for enhanced oil recovery. **Polymers**, MDPI, v. 12, n. 10, p. 2429, 2020. Cited in page 14.
- 8 HASHMI, A. R. A. et al. Rheology and mechanical degradation of high-molecular-weight partially hydrolyzed polyacrylamide during flow through capillaries. **Journal of Petroleum Science and Engineering**, Elsevier, v. 105, p. 100–106, 5 2013. ISSN 0920-4105. Cited 6 times in pages 9, 14, 39, 40, 57, and 59.
- 9 SUN, D. et al. Adsorption behavior and shear degradation of ultrahigh-molecular-weight hydrolyzed polyacrylamide in a capillary flow. **Journal of Applied Polymer Science**, Wiley Online Library, v. 137, n. 2, p. 48270, 2020. Cited in page 14.
- 10 HENDRANINGRAT, L.; LI, S.; TORSÆTER, O. A coreflood investigation of nanofluid enhanced oil recovery. **Journal of Petroleum Science and Engineering**, Elsevier, v. 111, p. 128–138, 11 2013. ISSN 0920-4105. Cited 2 times in pages 14 and 41.

- 11 MAURYA, N. K.; MANDAL, A. Studies on behavior of suspension of silica nanoparticle in aqueous polyacrylamide solution for application in enhanced oil recovery. **Petroleum Science and Technology**, Taylor & Francis, v. 34, n. 5, p. 429–436, 2016. Cited 3 times in pages 14, 42, and 45.
- 12 CORREDOR, L. M. et al. Heavy oil recovery by surface modified silica nanoparticle/hpam nanofluids. **Fuel**, Elsevier, v. 252, p. 622–634, 2019. Cited 3 times in pages 14, 44, and 95.
- 13 YOUSEFVAND, H. A.; JAFARI, A. Stability and flooding analysis of nanosilica/nacl/hpam/sds solution for enhanced heavy oil recovery. **Journal of Petroleum Science and Engineering**, Elsevier, v. 162, p. 283–291, 2018. Cited in page 15.
- 14 CORREDOR, L. M. et al. Oil displacement efficiency of a silica/hpam nanohybrid. **Energy & Fuels**, ACS Publications, v. 35, n. 16, p. 13077–13085, 2021. Cited in page 15.
- 15 XU, L. et al. Hydrophobic effect further improves the rheological behaviors and oil recovery of polyacrylamide/nanosilica hybrids at high salinity. **Chemical Engineering Science**, Elsevier, v. 232, p. 116369, 2021. Cited in page 15.
- 16 REZAEI, A. et al. Using surface modified clay nanoparticles to improve rheological behavior of hydrolyzed polyacrylamid (hpam) solution for enhanced oil recovery with polymer flooding. **Journal of Molecular Liquids**, Elsevier, v. 222, p. 1148–1156, 2016. Cited 2 times in pages 15 and 45.
- 17 CORREDOR, L. M.; HUSEIN, M. M.; MAINI, B. B. Impact of pam-grafted nanoparticles on the performance of hydrolyzed polyacrylamide solutions for heavy oil recovery at different salinities. **Industrial & Engineering Chemistry Research**, ACS Publications, v. 58, n. 23, p. 9888–9899, 2019. Cited in page 15.
- 18 AGI, A. et al. Synthesis and application of rice husk silica nanoparticles for chemical enhanced oil recovery. **Journal of Materials Research and Technology**, Elsevier, v. 9, n. 6, p. 13054–13066, 2020. Cited 2 times in pages 15 and 44.
- 19 ZHENG, C. et al. Suspension of surface-modified nano-sio2 in partially hydrolyzed aqueous solution of polyacrylamide for enhanced oil recovery. **Colloids and Surfaces A: Physicochemical and Engineering Aspects**, Elsevier, v. 524, p. 169–177, 2017. Cited 2 times in pages 15 and 44.
- 20 KUMAR, S. et al. Simulation protocol for core flooding: relative permeability and capillary pressure analysis. p. OTC–24715, 2014. Cited in page 15.
- 21 SAADAT, M. et al. Development of a microfluidic method to study enhanced oil recovery by low salinity water flooding. **Acs Omega**, ACS Publications, v. 5, n. 28, p. 17521–17530, 2020. Cited in page 15.
- 22 KHARRAT, A. et al. Development of foam-like emulsion phases in porous media flow. **Journal of colloid and interface science**, Elsevier, v. 608, p. 1064–1073, 2022. Cited in page 15.

- 23 FANI, M. et al. Application of microfluidics in chemical enhanced oil recovery: A review. **Fuel**, Elsevier, v. 315, p. 123225, 2022. Cited 3 times in pages 10, 15, and 46.
- 24 RUEDA, E. et al. Experimental investigation of the effect of adding nanoparticles to polymer flooding in water-wet micromodels. **Nanomaterials**, MDPI, v. 10, n. 8, p. 1489, 2020. Cited 4 times in pages 10, 15, 48, and 49.
- 25 OMRAN, M.; AKARRI, S.; TORSÆTER, O. The effect of wettability and flow rate on oil displacement using polymer-coated silica nanoparticles: a microfluidic study. **Processes**, MDPI, v. 8, n. 8, p. 991, 2020. Cited in page 15.
- 26 MAGHZI, A. et al. An experimental investigation of silica nanoparticles effect on the rheological behavior of polyacrylamide solution to enhance heavy oil recovery. **Petroleum science and technology**, Taylor & Francis, v. 31, n. 5, p. 500–508, 2013. Cited 3 times in pages 15, 42, and 45.
- 27 BAGUL, A. Scco2-philic particles for enhanced oil recovery. 2015. Cited in page 15.
- 28 AGI, A. et al. Laboratory evaluation to field application of ultrasound: A state-of-the-art review on the effect of ultrasonication on enhanced oil recovery mechanisms. **Journal of Industrial and Engineering Chemistry**, Elsevier, v. 110, p. 100–119, 2022. Cited in page 16.
- 29 AGI, A. et al. Ultrasound-assisted nanofluid flooding to enhance heavy oil recovery in a simulated porous media. **Arabian Journal of Chemistry**, Elsevier, v. 15, n. 5, p. 103784, 2022. Cited in page 16.
- 30 THOMAS, S. Enhanced oil recovery-an overview. **Oil & Gas Science and Technology-Revue d'IFP Energies nouvelles**, v. 63, n. 1, p. 9–19, 2008. Cited 3 times in pages 9, 16, and 17.
- 31 GBADAMOSI, A. et al. Application of polymers for chemical enhanced oil recovery: a review. **Polymers**, MDPI, v. 14, n. 7, p. 1433, 2022. Cited in page 16.
- 32 DONG, X. et al. Eor potential in the post steam injection era: Current and future trends. p. D041S018R004, 2018. Cited in page 16.
- 33 ALAGORNI, A. H.; YAACOB, Z. B.; NOUR, A. H. An overview of oil production stages: enhanced oil recovery techniques and nitrogen injection. **International Journal of Environmental Science and Development**, IACSIT Press, v. 6, n. 9, p. 693, 2015. Cited in page 16.
- 34 GBADAMOSI, A. O. et al. An overview of chemical enhanced oil recovery: recent advances and prospects. **International Nano Letters**, Springer, v. 9, p. 171–202, 2019. Cited in page 16.
- 35 LAKE, L. W. Enhanced oil recovery. Old Tappan, NJ; Prentice Hall Inc., 1989. Cited in page 17.

- 36 WANG, D. Technical innovation greatly increase the recoverable reserve and ensure long-term high production of daqing oilfield. **Pet Geol Oilf Dev Daqing (PGOD)**, v. 38, p. 8–17, 2019. Cited in page 17.
- 37 CHANG, H. L. Polymer flooding technology yesterday, today, and tomorrow. **Journal of Petroleum Technology**, SPE, v. 30, n. 08, p. 1113–1128, 1978. Cited in page 17.
- 38 MANNING, R. K. **A technical survey of polymer flooding projects**. Tese (Doutorado), 1983. Cited in page 18.
- 39 NEEDHAM, R. B.; DOE, P. H. Polymer flooding review. **Journal of petroleum technology**, SPE, v. 39, n. 12, p. 1503–1507, 1987. Cited 2 times in pages 18 and 33.
- 40 DU, Y.; GUAN, L. Field-scale polymer flooding: lessons learnt and experiences gained during past 40 years. p. SPE–91787, 2004. Cited in page 18.
- 41 GAO, C. H. Scientific research and field applications of polymer flooding in heavy oil recovery. **Journal of Petroleum Exploration and Production Technology**, Springer, v. 1, p. 65–70, 2011. Cited in page 18.
- 42 MOGOLLÓN, J. L.; LOKHANDWALA, T. Rejuvenating viscous oil reservoirs by polymer injection: lessons learned in the field. p. SPE–165275, 2013. Cited in page 18.
- 43 SALEH, L. D.; WEI, M.; BAI, B. Data analysis and updated screening criteria for polymer flooding based on oilfield data. **SPE Reservoir Evaluation & Engineering**, OnePetro, v. 17, n. 01, p. 15–25, 2014. Cited in page 18.
- 44 RENOUF, G. A survey of polymer flooding in western canada. p. SPE–169062, 2014. Cited in page 19.
- 45 STANDNES, D. C.; SKJEVRAK, I. Literature review of implemented polymer field projects. **Journal of petroleum science and engineering**, Elsevier, v. 122, p. 761–775, 2014. Cited in page 19.
- 46 SHENG, J. J.; LEONHARDT, B.; AZRI, N. Status of polymer-flooding technology. **Journal of Canadian petroleum technology**, SPE, v. 54, n. 02, p. 116–126, 2015. Cited in page 19.
- 47 ZHANG, Y. et al. Survey and data analysis of the pilot and field polymer flooding projects in china. p. SPE–179616, 2016. Cited in page 19.
- 48 SONG, K. et al. Recent advances in polymer flooding in china. **Molecules**, MDPI, v. 27, n. 20, p. 6978, 2022. Cited in page 19.
- 49 GAO, S. et al. Associated polymer asp flooding scheme optimization design and field test after polymer flooding in daqing oilfield. p. D021S017R002, 2020. Cited in page 19.
- 50 GUO, H. et al. Recent advances in polymer flooding in china: lessons learned and continuing development. **SPE Journal**, SPE, v. 26, n. 04, p. 2038–2052, 2021. Cited 2 times in pages 19 and 41.

- 51 JENKINS, A. et al. Glossary of basic terms in polymer science (iupac recommendations 1996). **Pure and applied chemistry**, De Gruyter, v. 68, n. 12, p. 2287–2311, 1996. Cited in page 20.
- 52 ROGOŠIĆ, M.; MENCER, H.; GOMZI, Z. Polydispersity index and molecular weight distributions of polymers. **European polymer journal**, Elsevier, v. 32, n. 11, p. 1337–1344, 1996. Cited in page 20.
- 53 LEITE, F. et al. Estimation of molecular weight and polydispersity in conducting polymers using single-molecule force spectroscopy. In: IN: ENCONTRO DA SOCIEDADE BRASILEIRA DE PESQUISA EM MATERIAIS-SBPMAT, 7 . . . . [S.l.], 2008. Cited in page 20.
- 54 VACHA, M.; HABUCHI, S. Conformation and physics of polymer chains: a single-molecule perspective. **NPG Asia Materials**, Nature Publishing Group, v. 2, n. 4, p. 134–142, 2010. Cited in page 20.
- 55 GARCÍA, F.; SMULDERS, M. M. Dynamic covalent polymers. **Journal of Polymer Science Part A: Polymer Chemistry**, Wiley Online Library, v. 54, n. 22, p. 3551–3577, 2016. Cited in page 20.
- 56 BAHÚ, J. O. et al. Plant polysaccharides in engineered pharmaceutical gels. **Bioengineering**, MDPI, v. 9, n. 8, p. 376, 2022. Cited 2 times in pages 9 and 21.
- 57 GARCIA-OCHOA, F. et al. Xanthan gum: production, recovery, and properties. **Biotechnology advances**, Elsevier, v. 18, n. 7, p. 549–579, 2000. Cited in page 22.
- 58 BAKHSHI, M. et al. Effect of hydrophobic modification on the structure and rheology of aqueous and brine solutions of scleroglucan polymer. **Korean Journal of Chemical Engineering**, Springer, v. 34, p. 903–912, 2017. Cited in page 22.
- 59 AI, H. et al. Improved welan gum production by *alcaligenes* sp. atcc31555 from pretreated cane molasses. **Carbohydrate Polymers**, Elsevier, v. 129, p. 35–43, 2015. Cited in page 22.
- 60 GUPTA, P. K. et al. An update on overview of cellulose, its structure and applications. **Cellulose**, IntechOpen London, UK, v. 201, n. 9, p. 84727, 2019. Cited in page 22.
- 61 RELLEGADLA, S.; PRAJAPAT, G.; AGRAWAL, A. Polymers for enhanced oil recovery: fundamentals and selection criteria. **Applied microbiology and biotechnology**, Springer, v. 101, p. 4387–4402, 2017. Cited in page 22.
- 62 TANG, G.; MORROW, N. R. Salinity, temperature, oil composition, and oil recovery by waterflooding. **SPE Reservoir Engineering**, OnePetro, v. 12, n. 04, p. 269–276, 1997. Cited in page 22.
- 63 ABRAHAM, S.; RAJAMANICKAM, D.; SRINIVASAN, B. Research article preparation, characterization and cross-linking of chitosan by microwave assisted synthesis. **Sci. Int**, v. 6, p. 18–30, 2018. Cited in page 22.

- 64 LI, X.; ZHANG, F.; LIU, G. Review on polymer flooding technology. v. 675, n. 1, p. 012199, 2021. Cited in page 22.
- 65 MAHAJAN, S. et al. Polymers for enhanced oil recovery: Fundamentals and selection criteria revisited. **Applied Microbiology and Biotechnology**, Springer, p. 1–18, 2021. Cited 2 times in pages 12 and 22.
- 66 SORBIE, K. Polymer-improved oil recovery. 1991. Cited 2 times in pages 23 and 54.
- 67 SHENG, J. J. **Enhanced oil recovery field case studies**. [S.l.]: Gulf Professional Publishing, 2013. Cited in page 23.
- 68 ROCK, A. et al. On the role of polymer viscoelasticity in enhanced oil recovery: Extensive laboratory data and review. **Polymers**, MDPI, v. 12, n. 10, p. 2276, 2020. Cited 4 times in pages 9, 23, 35, and 36.
- 69 VIKEN, A. L.; SKAUGE, T.; SPILDO, K. Rheological properties of a hydrophobically modified anionic polymer: effect of varying salinity and amount of hydrophobic moieties. **Journal of Applied polymer science**, Wiley Online Library, v. 133, n. 23, 2016. Cited in page 23.
- 70 CHOI, B.; JEONG, M. S.; LEE, K. S. Temperature-dependent viscosity model of hpam polymer through high-temperature reservoirs. **Polymer degradation and stability**, Elsevier, v. 110, p. 225–231, 2014. Cited in page 23.
- 71 XUE, S. et al. Improving oil recovery of the heterogeneous low permeability reservoirs by combination of polymer hydrolysis polyacrylamide and two highly biosurfactant-producing bacteria. **Sustainability**, MDPI, v. 14, n. 1, p. 423, 2021. Cited in page 23.
- 72 LEE, S. et al. Development of a comprehensive rheological property database for eor polymers. p. SPE–124798, 2009. Cited in page 23.
- 73 SOSA-FERNANDEZ, P. et al. Electrodialysis-based desalination and reuse of sea and brackish polymer-flooding produced water. **Desalination**, Elsevier, v. 447, p. 120–132, 2018. Cited 4 times in pages 9, 10, 23, and 54.
- 74 SCHROEDER, C. M. Single polymer dynamics for molecular rheology. **Journal of Rheology**, The Society of Rheology, v. 62, n. 1, p. 371–403, 2018. Cited in page 24.
- 75 TERAOKA, I. **Polymer solutions**. [S.l.: s.n.], 2002. Cited in page 24.
- 76 REGALADO, E. J.; SELB, J.; CANDAU, F. Viscoelastic behavior of semidilute solutions of multisticker polymer chains. **Macromolecules**, ACS Publications, v. 32, n. 25, p. 8580–8588, 1999. Cited in page 24.
- 77 HACHEM, E.-K.; BELGHAZDIS, M.; BENDOUCHE, A. Adsorption of the polymer on a clay matrix: Theoretical study. **International Journal of Integrated Engineering**, v. 14, n. 3, p. 21–32, 2022. Cited 2 times in pages 9 and 24.

- 78 MEZGER, T. **The rheology handbook: for users of rotational and oscillatory rheometers**. [S.l.]: European Coatings, 2020. Cited 3 times in pages 24, 25, and 26.
- 79 WANG, D. et al. Study of the mechanism of polymer solution with viscoelastic behavior increasing microscopic oil displacement efficiency and the forming of steady" oil thread" flow channels. p. SPE-68723, 2001. Cited 3 times in pages 9, 25, and 35.
- 80 GEORGE, H. F.; QURESHI, F. Newton's law of viscosity, newtonian and non-newtonian fluids. **Encyclopedia of tribology**, Springer Boston, MA, p. 2416–2420, 2013. Cited 3 times in pages 9, 25, and 26.
- 81 SOCHI, T. Flow of non-newtonian fluids in porous media. **Journal of Polymer Science Part B: Polymer Physics**, Wiley Online Library, v. 48, n. 23, p. 2437–2767, 2010. Cited in page 25.
- 82 GRIGORESCU, G.; KULICKE, W.-M. Prediction of viscoelastic properties and shear stability of polymers in solution. **Viscoelasticity, Atomistic Models, Statistical Chemistry**, Springer, p. 1–40, 2000. Cited in page 26.
- 83 SOCHI, T. Non-newtonian flow in porous media. **Polymer**, Elsevier, v. 51, n. 22, p. 5007–5023, 2010. Cited in page 26.
- 84 METIU, H.; FREED, K. F. Bulk viscosity of polymer solutions. **The Journal of Chemical Physics**, American Institute of Physics, v. 67, n. 7, p. 3303–3315, 1977. Cited 2 times in pages 9 and 27.
- 85 OTSUBO, Y. Rheology control of suspensions by soluble polymers. **Langmuir**, ACS Publications, v. 11, n. 6, p. 1893–1898, 1995. Cited in page 27.
- 86 HE, X.-r. et al. Macromolecular motions and hydrodynamic radius variation in dilute solutions under shear action. **Polymer International**, Wiley Online Library, v. 64, n. 6, p. 766–772, 2015. Cited in page 27.
- 87 AL-HAMAIRI, A.; ALAMERI, W. Development of a novel model to predict hpm viscosity with the effects of concentration, salinity and divalent content. **Journal of Petroleum Exploration and Production Technology**, Springer, v. 10, p. 1949–1963, 2020. Cited 2 times in pages 27 and 37.
- 88 OSTWALD, W. de waele-ostwald equation. **Kolloid Zeitschrift**, v. 47, n. 2, p. 176–187, 1929. Cited in page 28.
- 89 YASUDA, K.; ARMSTRONG, R.; COHEN, R. Shear flow properties of concentrated solutions of linear and star branched polystyrenes. **Rheologica Acta**, Springer, v. 20, n. 2, p. 163–178, 1981. Cited in page 28.
- 90 HERSCHEL, W. H.; BULKLEY, R. Konsistenzmessungen von gummi-benzollösungen. **Kolloid-Zeitschrift**, Springer, v. 39, p. 291–300, 1926. Cited in page 28.
- 91 REINER, M. The Deborah number. **Physics today**, AIP Publishing, v. 17, n. 1, p. 62–62, 1964. Cited in page 28.

- 92 FERRY, J. D. **Viscoelastic properties of polymers**. [S.I.]: John Wiley & Sons, 1980. Cited in page 28.
- 93 MACOSKO, C. W. Rheology principles. **Measurements and Applications**, VCH Publishes, 1994. Cited 2 times in pages 28 and 30.
- 94 XING, X. et al. An improved time-series model considering rheological parameters for surface deformation monitoring of soft clay subgrade. **Sensors**, MDPI, v. 19, n. 14, p. 3073, 2019. Cited 2 times in pages 9 and 29.
- 95 PETRIE, C. J. Extensional viscosity: A critical discussion. **Journal of Non-Newtonian Fluid Mechanics**, Elsevier, v. 137, n. 1-3, p. 15–23, 2006. Cited in page 29.
- 96 MCKINLEY, G. H.; SRIDHAR, T. Filament-stretching rheometry of complex fluids. **Annual Review of Fluid Mechanics**, Annual Reviews 4139 El Camino Way, PO Box 10139, Palo Alto, CA 94303-0139, USA, v. 34, n. 1, p. 375–415, 2002. Cited in page 30.
- 97 HASSAGER, O.; WANG, Y.; HUANG, Q. Extensional rheometry of model liquids: Simulations of filament stretching. **Physics of Fluids**, AIP Publishing, v. 33, n. 12, 2021. Cited in page 30.
- 98 HUANG, Q. When polymer chains are highly aligned: a perspective on extensional rheology. **Macromolecules**, ACS Publications, v. 55, n. 3, p. 715–727, 2022. Cited in page 30.
- 99 CREUS, G. J. **Viscoelasticity—basic theory and applications to concrete structures**. [S.I.]: Springer Science & Business Media, 2012. v. 16. Cited in page 32.
- 100 AZAD, M. S. et al. Capillary breakup extensional rheometry of associative and hydrolyzed polyacrylamide polymers for oil recovery applications. **J. Appl. Polym. Sci**, Wiley Periodicals, Inc, v. 135, p. 46253, 2018. Cited 3 times in pages 32, 33, and 76.
- 101 AZAD, M. S.; TRIVEDI, J. J. Quantification of the viscoelastic effects during polymer flooding: a critical review. **SPE Journal**, SPE, v. 24, n. 06, p. 2731–2757, 2019. Cited 3 times in pages 32, 33, and 77.
- 102 AZAD, M. S.; TRIVEDI, J. J. Extensional effects during viscoelastic polymer flooding: understanding unresolved challenges. **SPE Journal**, SPE, v. 25, n. 04, p. 1827–1841, 2020. Cited in page 32.
- 103 ZEYNALLI, M. et al. A comprehensive review of viscoelastic polymer flooding in sandstone and carbonate rocks. **Scientific Reports**, Nature Publishing Group UK London, v. 13, n. 1, p. 17679, 2023. Cited in page 32.
- 104 IRFAN, M.; STEPHEN, K. D.; LENN, C. P. An experimental study to investigate novel physical mechanisms that enhance viscoelastic polymer flooding and further increase desaturation of residual oil saturation. **Upstream Oil and Gas Technology**, Elsevier, v. 6, p. 100026, 2021. Cited in page 33.

- 105 NASCIMENTO, F. P. et al. Low salinity water–polymer flooding in carbonate oil reservoirs: A critical review. **Macromolecular Reaction Engineering**, Wiley Online Library, p. 2300007, 2023. Cited 2 times in pages 9 and 34.
- 106 HU, R. et al. Research progress of viscoelastic surfactants for enhanced oil recovery. **Energy Exploration & Exploitation**, SAGE Publications Sage UK: London, England, v. 39, n. 4, p. 1324–1348, 2021. Cited in page 34.
- 107 ZHANG, C. et al. Influence of viscous and capillary forces on immiscible fluid displacement: Pore-scale experimental study in a water-wet micromodel demonstrating viscous and capillary fingering. **Energy & Fuels**, ACS Publications, v. 25, n. 8, p. 3493–3505, 2011. Cited in page 34.
- 108 LUO, J. et al. Polymer solution properties and displacement mechanisms. **Enhanced oil recovery-polymer flooding**, Petroleum Industry Press Beijing, p. 1–72, 2006. Cited in page 35.
- 109 YIN, H.; WANG, D.; ZHONG, H. Study on flow behaviors of viscoelastic polymer solution in micropore with dead end. p. SPE–101950, 2006. Cited in page 35.
- 110 XIA, H. et al. Mechanism of the effect of micro-forces on residual oil in chemical flooding. p. SPE–114335, 2008. Cited in page 35.
- 111 WANG, D. et al. Viscous-elastic polymer can increase microscale displacement efficiency in cores. p. SPE–63227, 2000. Cited in page 35.
- 112 JIANG, H. et al. The effect of elasticity on displacement efficiency in the lab and results of high concentration polymer flooding in the field. p. SPE–115315, 2008. Cited in page 35.
- 113 XIA, H. et al. Elasticity of hpam solutions increases displacement efficiency under mixed wettability conditions. p. SPE–88456, 2004. Cited in page 35.
- 114 XIA, H. et al. Effect of polymer solution viscoelasticity on residual oil. **Petroleum science and technology**, Taylor & Francis, v. 26, n. 4, p. 398–412, 2008. Cited in page 35.
- 115 WEI, B.; ROMERO-ZERÓN, L.; RODRIGUE, D. Oil displacement mechanisms of viscoelastic polymers in enhanced oil recovery (eor): a review. **Journal of Petroleum Exploration and Production Technology**, Springer, v. 4, p. 113–121, 2014. Cited in page 35.
- 116 HUH, C.; POPE, G. A. Residual oil saturation from polymer floods: laboratory measurements and theoretical interpretation. p. SPE–113417, 2008. Cited in page 35.
- 117 LOPES, L. F.; SILVEIRA, B.; MORENO, R. Rheological evaluation of hpam fluids for eor applications. **International Journal of Engineering & Technology**, v. 14, n. 3, p. 35–41, 2014. Cited in page 36.
- 118 ALTUNINA, L. et al. Oil-displacing surfactant composition with controlled viscosity for enhanced oil recovery from heavy oil deposits. **Georesources**, v. 18, n. 4, p. 1, 2016. Cited in page 36.

- 119 DAVARPANAH, A. A feasible visual investigation for associative foam polymer injectivity performances in the oil recovery enhancement. **European Polymer Journal**, Elsevier, v. 105, p. 405–411, 2018. Cited in page 36.
- 120 HINCAPIE, R. et al. Oil mobilization by viscoelastic flow instabilities effects during polymer eor: A pore-scale visualization approach. p. D011S002R002, 2017. Cited in page 36.
- 121 LANGANKE, N. et al. Flow of viscoelastic polymer solutions in porous media: Influence of molecular weight and dispersity. 2023. Cited in page 36.
- 122 AIT-KADI, A.; CARREAU, P.; CHAUVETEAU, G. Rheological properties of partially hydrolyzed polyacrylamide solutions. **Journal of Rheology**, The Society of Rheology, v. 31, n. 7, p. 537–561, 1987. Cited in page 37.
- 123 STAVLAND, A. et al. Polymer flooding–flow properties in porous media versus rheological parameters. 2010. Cited in page 37.
- 124 DUPAS, A. et al. Impact of polymer mechanical degradation on shear and extensional viscosities: towards better injectivity forecasts in polymer flooding operations. p. SPE–164083, 2013. Cited 2 times in pages 37 and 85.
- 125 EKANEM, E. M. et al. Signature of elastic turbulence of viscoelastic fluid flow in a single pore throat. **Physical Review E**, APS, v. 101, n. 4, p. 042605, 2020. Cited 2 times in pages 9 and 37.
- 126 CHAUVETEAU, G. Rodlike polymer solution flow through fine pores: influence of pore size on rheological behavior. **Journal of Rheology**, The Society of Rheology, v. 26, n. 2, p. 111–142, 1982. Cited in page 37.
- 127 BOGER, D. Viscoelastic flows through contractions. **Annual review of fluid mechanics**, Annual Reviews 4139 El Camino Way, PO Box 10139, Palo Alto, CA 94303-0139, USA, v. 19, n. 1, p. 157–182, 1987. Cited 2 times in pages 37 and 39.
- 128 DUPUIS, D. et al. Shear thickening and time-dependent phenomena: The case of polyacrylamide solutions. **Journal of non-newtonian fluid mechanics**, Elsevier, v. 54, p. 11–32, 1994. Cited in page 37.
- 129 SERIGHT, R. S.; SEHEULT, M.; TALASHEK, T. Injectivity characteristics of eor polymers. **SPE Reservoir Evaluation & Engineering**, SPE, v. 12, n. 05, p. 783–792, 2009. Cited in page 37.
- 130 WU, S. Shear and elongational rheology of partially hydrolyzed polyacrylamide used for enhanced oil recovery. **Applied Rheology**, Sciendo, v. 23, n. 5, p. 53800, 2013. Cited in page 38.
- 131 WEI, B.; LI, H.; KONG, L. Flow characteristics of partially hydrolyzed polyacrylamides during converging into a capillary. **Journal of Macromolecular Science, Part B**, Taylor & Francis, v. 55, n. 5, p. 483–493, 2016. Cited 2 times in pages 38 and 42.

- 132 JOUENNE, S.; HEURTEUX, G. Correlation of Mobility Reduction of HPAM Solutions at High Velocity in Porous Medium with Ex-Situ Measurements of Elasticity. **SPE Journal**, v. 25, n. 01, p. 465–480, 02 2020. ISSN 1086-055X. Disponível em: <<https://doi.org/10.2118/198899-PA>>. Cited in page 38.
- 133 HONG, S.; SOONG, D.; SHEN, M. Viscoelastic properties of entangled polymers: The transient network model. **Journal of Applied Physics**, American Institute of Physics, v. 48, n. 10, p. 4019–4025, 1977. Cited in page 38.
- 134 TANAKA, F.; EDWARDS, S. Viscoelastic properties of physically crosslinked networks. 1. transient network theory. **Macromolecules**, ACS Publications, v. 25, n. 5, p. 1516–1523, 1992. Cited in page 38.
- 135 KAWALE, D. **Elastic Instabilities in Polymer-Solution Flow Through Porous Media**. Tese (Doutorado) — Delft University of Technology, 2017. Cited in page 38.
- 136 GENNES, P. D. Coil-stretch transition of dilute flexible polymers under ultrahigh velocity gradients. **The Journal of Chemical Physics**, American Institute of Physics, v. 60, n. 12, p. 5030–5042, 1974. Cited in page 38.
- 137 ODELL, J.; MÜLLER, A.; KELLER, A. Non-newtonian behaviour of hydrolysed polyacrylamide in strong elongational flows: a transient network approach. **Polymer**, Elsevier, v. 29, n. 7, p. 1179–1190, 1988. Cited in page 38.
- 138 WANG, S. Q. Transient network theory for shear-thickening fluids and physically crosslinked networks. **Macromolecules**, ACS Publications, v. 25, n. 25, p. 7003–7010, 1992. Cited in page 38.
- 139 BRISCOE, B.; LUCKHAM, P.; ZHU, S. Pressure influences upon shear thickening of poly (acrylamide) solutions. **Rheologica acta**, Springer, v. 38, n. 3, p. 224–234, 1999. Cited in page 38.
- 140 SKAUGE, A. et al. Polymer flow in porous media: Relevance to enhanced oil recovery. **Colloids and Interfaces**, MDPI, v. 2, n. 3, p. 27, 2018. Cited in page 38.
- 141 ALIABADIAN, E. et al. Rheology of fumed silica nanoparticles/partially hydrolyzed polyacrylamide aqueous solutions under small and large amplitude oscillatory shear deformations. **Journal of rheology**, AIP Publishing, v. 62, n. 5, p. 1197–1216, 2018. Cited in page 38.
- 142 BROWNE, C. A.; DATTA, S. S. Elastic turbulence generates anomalous flow resistance in porous media. **Science advances**, American Association for the Advancement of Science, v. 7, n. 45, p. eabj2619, 2021. Cited in page 38.
- 143 ZHANG, Z.; LI, J.; ZHOU, J. Microscopic roles of “viscoelasticity” in hpma polymer flooding for eor. **Transport in porous media**, Springer, v. 86, p. 199–214, 2011. Cited in page 39.
- 144 ZAMANI, N. et al. Pore scale modelling of polymer flow. p. cp–342, 2013. Cited in page 39.

- 145 AL-SHAKRY, B. et al. Polymer injectivity: influence of permeability in the flow of eor polymers in porous media. p. D032S013R004, 2019. Cited in page 39.
- 146 SORBIE, K. S. **Polymer-improved oil recovery**. [S.l.]: Springer Science & Business Media, 2013. Cited 2 times in pages 39 and 54.
- 147 ZAITOUN, A. et al. Shear stability of eor polymers. **Spe Journal**, SPE, v. 17, n. 02, p. 335–339, 2012. Cited in page 39.
- 148 DUPAS, A. et al. Seuil de dégradation mécanique de solutions de polymères utilisés en récupération assistée des hydrocarbures. **Oil and Gas Science and Technology**, v. 67, p. 931–940, 2012. ISSN 12944475. Cited in page 39.
- 149 AL-SHAKRY, B. et al. Impact of mechanical degradation on polymer injectivity in porous media. **Polymers**, MDPI, v. 10, n. 7, p. 742, 2018. Cited 2 times in pages 40 and 86.
- 150 JOUENNE, S.; CHAKIBI, H.; LEVITT, D. Polymer stability after successive mechanical-degradation events. **SPE journal**, SPE, v. 23, n. 01, p. 18–33, 2018. Cited 2 times in pages 40 and 92.
- 151 WANG, D. et al. Sweep improvement options for the daqing oil field. **All Days**, OnePetro, 4 2006. Disponível em: <<https://onepetro.org/SPEIOR/proceedings/06IOR/All-06IOR/Tulsa,%20Oklahoma,%20USA/141080>>. Cited 2 times in pages 40 and 78.
- 152 MARTIN, F. Mechanical degradation of polyacrylamide solutions in core plugs from several carbonate reservoirs. **SPE Formation Evaluation**, SPE, v. 1, n. 02, p. 139–150, 1986. Cited in page 41.
- 153 SERIGHT, R. S. How much polymer should be injected during a polymer flood? review of previous and current practices. v. 2017, n. 1, p. 1–37, 2017. Cited in page 41.
- 154 ASGHARI, K.; NAKUTNYY, P. Experimental results of polymer flooding of heavy oil reservoirs. p. PETSOC–2008, 2008. Cited in page 41.
- 155 SERIGHT, R. S. Potential for polymer flooding reservoirs with viscous oils. **SPE Reservoir Evaluation & Engineering**, SPE, v. 13, n. 04, p. 730–740, 2010. Cited in page 41.
- 156 GRAESSLEY, W. W. The entanglement concept in polymer rheology. **The entanglement concept in polymer rheology**, Springer, p. 1–179, 2005. Cited in page 41.
- 157 GBADAMOSI, A. O. et al. Recent advances and prospects in polymeric nanofluids application for enhanced oil recovery. **Journal of Industrial and Engineering Chemistry**, Elsevier, v. 66, p. 1–19, 2018. Cited in page 41.
- 158 HU, L. et al. The in situ “grafting from” approach for the synthesis of polymer brushes on upconversion nanoparticles via nir-mediated raft polymerization. **Polymer Chemistry**, Royal Society of Chemistry, v. 12, n. 4, p. 545–553, 2021. Cited 3 times in pages 9, 41, and 42.

- 159 PAVITHRA, K. et al. Polymer-dispersant-stabilized ag nanofluids for heat transfer applications. **Journal of Thermal Analysis and Calorimetry**, Springer, v. 146, p. 601–610, 2021. Cited 2 times in pages 9 and 41.
- 160 MAGHZI, A. et al. The impact of silica nanoparticles on the performance of polymer solution in presence of salts in polymer flooding for heavy oil recovery. **Fuel**, Elsevier, v. 123, p. 123–132, 2014. Cited in page 42.
- 161 YOUSEFVAND, H.; JAFARI, A. Enhanced oil recovery using polymer/-nanosilica. **Procedia Materials Science**, Elsevier, v. 11, p. 565–570, 2015. Cited 3 times in pages 42, 95, and 97.
- 162 KANG, W. et al. Mechanism of silica nanoparticles' better-thickening effect on amphiphilic polymers in high salinity condition. **Journal of Molecular Liquids**, Elsevier, v. 277, p. 254–260, 2019. Cited in page 42.
- 163 METIN, C. O.; BARAN, J. R.; NGUYEN, Q. P. Adsorption of surface functionalized silica nanoparticles onto mineral surfaces and decane/water interface. **Journal of Nanoparticle Research**, Springer, v. 14, p. 1–16, 2012. Cited in page 42.
- 164 CHEN, W.-h. et al. Stability, rheology and displacement performance of nano-sio<sub>2</sub>/hpam/nacl dispersion systems. **Journal of Fuel Chemistry and Technology**, Elsevier, v. 48, n. 5, p. 568–576, 2020. Cited in page 43.
- 165 HU, Z. et al. Rheological properties of partially hydrolyzed polyacrylamide seeded by nanoparticles. **Industrial & Engineering Chemistry Research**, ACS Publications, v. 56, n. 12, p. 3456–3463, 2017. Cited 2 times in pages 43 and 98.
- 166 CHERAGHIAN, G. Application of nano-fumed silica in heavy oil recovery. **Petroleum Science and Technology**, Taylor & Francis, v. 34, n. 1, p. 12–18, 2016. Cited in page 44.
- 167 ALIABADIAN, E. et al. Prevention of network destruction of partially hydrolyzed polyacrylamide (hpam): Effects of salt, temperature, and fumed silica nanoparticles. **Physics of Fluids**, AIP Publishing, v. 31, n. 1, 2019. Cited in page 44.
- 168 KUMAR, S. et al. Enhancing the performance of hpam polymer flooding using nano cuo/nanoclay blend. **Processes**, MDPI, v. 8, n. 8, p. 907, 2020. Cited in page 44.
- 169 LIU, J. et al. Preparation and properties of nano-silica hybrid hydrophobic associated polyacrylamide for polymer flooding. **Journal of Petroleum Science and Engineering**, Elsevier, v. 208, p. 109434, 2022. Cited in page 45.
- 170 SANTAMARIA, O. et al. Phenomenological study of the micro-and macroscopic mechanisms during polymer flooding with sio<sub>2</sub> nanoparticles. **Journal of Petroleum Science and Engineering**, Elsevier, v. 198, p. 108135, 2021. Cited 2 times in pages 45 and 95.

- 171 NILSSON, M. A. et al. Effect of fluid rheology on enhanced oil recovery in a microfluidic sandstone device. **Journal of non-newtonian fluid mechanics**, Elsevier, v. 202, p. 112–119, 2013. Cited in page 46.
- 172 LI, P.; DENG, H.; MOLINS, S. The effect of pore-scale two-phase flow on mineral reaction rates. **Frontiers in Water**, Frontiers, v. 3, p. 734518, 2022. Cited 2 times in pages 10 and 47.
- 173 AMORIM, C. de et al. Visualization and quantification of mobility reduction in porous media flow associated with pore blocking by emulsion drops. **Industrial & Engineering Chemistry Research**, ACS Publications, 2023. Cited 2 times in pages 10 and 48.
- 174 KUMAR, G.; MANI, E.; SANGWAI, J. S. Microfluidic investigation of surfactant-assisted functional silica nanofluids in low-salinity seawater for enhanced oil recovery using reservoir-on-a-chip. **Energy & Fuels**, ACS Publications, 2023. Cited 2 times in pages 49 and 65.
- 175 SANCHEZ, A. **Colloidal gels of fumed silica: Microstructure, surface interactions and temperature effects**. [S.l.]: North Carolina State University, 2006. Cited in page 55.
- 176 HUTIN, A.; CARVALHO, M. S. Effect of contamination from direct sonication on characterization of nanofluid stability. **Powder Technology**, p. 117–157, 2022. ISSN 0032-5910. Cited 2 times in pages 12 and 55.
- 177 DEPARTMENT, A. P. I. P. **Recommended Practices for Evaluation of Polymers Used in enhanced oil recovery operations**. [S.l.]: American Petroleum Institute, 1990. v. 63. Cited in page 56.
- 178 HUTIN, A.; CARVALHO, M. S. Effect of contamination from direct sonication on characterization of nanofluid stability. **Powder Technology**, Elsevier, v. 399, p. 117157, 2 2022. ISSN 0032-5910. Cited in page 56.
- 179 ALMEIDA, L. S. da S. **Mechanical Degradation of Polymer Solutions in Extensional Laminar Flow**. Tese (Doutorado) — PUC-Rio, 2021. Cited in page 59.
- 180 NEHDI, M.; RAHMAN, M.-A. Estimating rheological properties of cement pastes using various rheological models for different test geometry, gap and surface friction. **Cement and Concrete Research**, v. 34, n. 11, p. 1993–2007, 2004. ISSN 0008-8846. Disponível em: <<https://www.sciencedirect.com/science/article/pii/S000888460400105X>>. Cited in page 59.
- 181 BRAITHWAITE, G.; MCKINLEY, G. **Capillary Breakup Extensional Rheometer CaBER® Addendum to Operators Manual, User's Guide and Theory Reference Version: 1.4-05 GB DRAFT**. [s.n.], 2000. Disponível em: <<http://www.campoly.com>>. Cited 2 times in pages 60 and 62.
- 182 HARLEN, O. Simulation of the filament stretching rheometer. Presentation at the Isaac Newton Institute during Dynamics of Complex Fluids (DCF) program. 1996. Cited in page 61.

- 183 YAO, M.; MCKINLEY, G. H. Numerical simulation of extensional deformations of viscoelastic liquid bridges in filament stretching devices. **Journal of Non-Newtonian Fluid Mechanics**, Elsevier, v. 74, n. 1-3, p. 47–88, 1998. Cited in page 61.
- 184 RODD, L. E. et al. Capillary break-up rheometry of low-viscosity elastic fluids. **Applied Rheology**, Scienco, v. 15, n. 1, p. 12–27, 2005. Cited 2 times in pages 61 and 62.
- 185 OLSSON, F.; YSTRÖM, J. Some properties of the upper convected maxwell model for viscoelastic fluid flow. **Journal of non-newtonian fluid mechanics**, Elsevier, v. 48, n. 1-2, p. 125–145, 1993. Cited in page 63.
- 186 OLIVEIRA, M. S.; YEH, R.; MCKINLEY, G. H. Iterated stretching, extensional rheology and formation of beads-on-a-string structures in polymer solutions. **Journal of non-Newtonian fluid mechanics**, Elsevier, v. 137, n. 1-3, p. 137–148, 2006. Cited 3 times in pages 11, 63, and 85.
- 187 MAQUEIRA, L. et al. Quantification of sulfonated polyacrylamide copolymers in produced water by size exclusion chromatography and uv detection. **Rio Oil & Gas Expo and Conference**, 2022. Disponível em: <<http://dx.doi.org/10.48072/2525-7579.rog.2022.049>>. Cited in page 64.
- 188 MONCAYO, E. A. et al. Sticky bacteria: Combined effect of galactose and high ferric iron concentration on extracellular polymeric substances production and the attachment of acidithiobacillus ferrooxidans on a polymetallic sulfide ore surface. **Frontiers in Microbiology**, Frontiers, v. 13, p. 951402, 2022. Cited in page 64.
- 189 ENHANCED Oil Recovery Chips - Microfluidic Chips - Micronit. Micronit, 2024. Accessed: 2024-02-08. Disponível em: <<https://store.micronit.com/microfluidic-chips/enhanced-oil-recovery-chips.html>>. Cited 2 times in pages 10 and 66.
- 190 BROEKE, J.; PÉREZ, J. M. M.; PASCAU, J. **Image processing with ImageJ**. [S.l.]: Packt Publishing Ltd, 2015. Cited in page 69.
- 191 MORRIS, C.; JACKSON, K. Mechanical Degradation Of Polyacrylamide Solutions In Porous Media. All Days, 04 1978. SPE-7064-MS. Disponível em: <<https://doi.org/10.2118/7064-MS>>. Cited in page 75.
- 192 SID, A. N. E. H. et al. Optimization of partially hydrolyzed polyacrylamide (hpam) utilized in water-based mud while drilling. **Processes**, v. 11, n. 4, 2023. ISSN 2227-9717. Disponível em: <<https://www.mdpi.com/2227-9717/11/4/1133>>. Cited in page 75.
- 193 WU, H. et al. Effect of entanglement on rheological and ultimate properties of inorganic hpam gels. **Journal of Molecular Liquids**, v. 351, p. 118669, 2022. ISSN 0167-7322. Disponível em: <<https://www.sciencedirect.com/science/article/pii/S0167732222002069>>. Cited in page 75.

- 194 STRANDMAN, S. et al. Polyacrylamides revisited: flocculation of kaolin suspensions and mature fine tailings. **The Canadian Journal of Chemical Engineering**, v. 96, n. 1, p. 20–26, 2018. Disponível em: <<https://onlinelibrary.wiley.com/doi/abs/10.1002/cjce.22940>>. Cited in page 75.
- 195 XU, L. et al. Extensional rheology of hydrophobically associating polyacrylamide solution used in chemical flooding: Effects of temperature, nacl and surfactant. **Chemical Engineering Science**, Elsevier, v. 273, p. 118644, 2023. Cited in page 76.
- 196 ZHANG, Z. Y.; LI, J.; ZHOU, J. Microscopic roles of “viscoelasticity” in hpm polymer flooding for eor. **Transport in Porous Media**, v. 86, p. 199–214, 2011. Cited in page 77.
- 197 PATEL, V. et al. Characterization of co-and post-hydrolyzed polyacrylamide molecular weight and radius distribution under saline environment. **Journal of Applied Polymer Science**, Wiley Online Library, v. 138, n. 26, p. 50616, 2021. Cited in page 77.
- 198 AL-SHAKRY, B. et al. Impact of mechanical degradation on polymer injectivity in porous media. **Polymers**, v. 10, n. 7, 2018. ISSN 2073-4360. Disponível em: <<https://www.mdpi.com/2073-4360/10/7/742>>. Cited 2 times in pages 77 and 92.
- 199 ZHU, H. et al. The impact of extensional viscosity on oil displacement efficiency in polymer flooding. **Colloids and Surfaces A: Physicochemical and Engineering Aspects**, Elsevier, v. 414, p. 498–503, 2012. Cited in page 77.
- 200 WALTER, A. V. et al. Effect of salt valency and concentration on shear and extensional rheology of aqueous polyelectrolyte solutions for enhanced oil recovery. **Rheologica Acta**, Springer, v. 58, p. 145–157, 2019. Cited in page 79.
- 201 HU, X. et al. The use of microfluidics in rheology. **Macromolecular Materials and Engineering**, Wiley Online Library, v. 296, n. 3-4, p. 308–320, 2011. Cited in page 83.
- 202 NGHE, P.; TABELING, P.; AJDARI, A. Flow-induced polymer degradation probed by a high throughput microfluidic set-up. **Journal of Non-Newtonian Fluid Mechanics**, Elsevier, v. 165, n. 7-8, p. 313–322, 2010. Cited 2 times in pages 83 and 84.
- 203 OBER, T. J. et al. Microfluidic extensional rheometry using a hyperbolic contraction geometry. **Rheologica Acta**, Springer, v. 52, n. 6, p. 529–546, 2013. Cited in page 83.
- 204 WANG, D. et al. Sweep improvement options for the daqing oil field. p. SPE-99441, 2006. Cited in page 83.
- 205 MAERKER, J. Shear degradation of partially hydrolyzed polyacrylamide solutions. **Society of Petroleum Engineers Journal**, SPE, v. 15, n. 04, p. 311–322, 1975. Cited in page 84.

- 206 HERRERA, J.-J. et al. Cfd simulation of hpam eor solutions mechanical degradation by restrictions in turbulent flow. **CT&F-Ciencia, Tecnología y Futuro**, Instituto Colombiano del Petróleo (ICP)-ECOPETROL SA, v. 10, n. 2, p. 115–129, 2020. Cited in page 84.
- 207 GUO, H. et al. Proper use of capillary number in chemical flooding. **Journal of Chemistry**, Hindawi, v. 2017, 2017. Cited in page 89.
- 208 LIMA, N. M.; AVENDAÑO, J.; CARVALHO, M. S. Effect of viscoelasticity on oil displacement in a microfluidic porous medium. **Journal of the Brazilian Society of Mechanical Sciences and Engineering**, Springer, v. 44, n. 4, p. 144, 2022. Cited in page 89.
- 209 HASHMI, A. A. et al. Rheology and mechanical degradation of high-molecular-weight partially hydrolyzed polyacrylamide during flow through capillaries. **Journal of Petroleum Science and Engineering**, Elsevier, v. 105, p. 100–106, 2013. Cited in page 89.
- 210 HERBAS, J. G. et al. Comprehensive micromodel study to evaluate polymer eor in unconsolidated sand reservoirs. p. SPE–172669, 2015. Cited in page 89.
- 211 KUŁYNYCZ, V.; PIKŁOWSKA, A.; KULYNYCH, O. Overview of the nanoparticles application for reservoir engineering and enhanced oil recovery (eor) methods. **AGH Drilling, Oil, Gas**, v. 35, n. 1, 2018. Cited in page 90.
- 212 ERINCIK, M. Z. **New discovery to reduce residual oil saturation by polymer flooding**. Tese (Doutorado), 2017. Cited in page 90.
- 213 HU, J.; LI, A.; MEMON, A. Experimental investigation of polymer enhanced oil recovery under different injection modes. **ACS omega**, ACS Publications, v. 5, n. 48, p. 31069–31075, 2020. Cited in page 90.
- 214 SU, Y. C.; WU, W. X. Study on characteristics and oil displacement characteristics of high concentration polymer system. **Advanced Materials Research**, Trans Tech Publ, v. 391, p. 255–259, 2012. Cited in page 90.
- 215 HIRASAKI, G.; POPE, G. Analysis of factors influencing mobility and adsorption in the flow of polymer solution through porous media. **Society of Petroleum Engineers Journal**, SPE, v. 14, n. 04, p. 337–346, 1974. Cited in page 92.
- 216 LIU, R. et al. Star-like hydrophobically associative polyacrylamide for enhanced oil recovery: Comprehensive properties in harsh reservoir conditions. **Journal of the Taiwan Institute of chemical engineers**, Elsevier, v. 80, p. 639–649, 2017. Cited in page 92.
- 217 ALFAZAZI, U. et al. Experimental investigation of polymer injectivity and retention under harsh carbonate reservoir conditions. **Journal of Petroleum Science and Engineering**, Elsevier, v. 192, p. 107262, 2020. Cited in page 92.
- 218 ZHANG, R. et al. Rheology of diluted and semi-diluted partially hydrolyzed polyacrylamide solutions under shear: Experimental studies. **Petroleum**, Elsevier, v. 3, n. 2, p. 258–265, 2017. Cited in page 95.

219 CHERAGHIAN, G. An experimental study of surfactant polymer for enhanced heavy oil recovery using a glass micromodel by adding nanoclay. **Petroleum Science and Technology**, Taylor & Francis, v. 33, n. 13-14, p. 1410–1417, 2015. Cited in page 95.

220 BEHZADI, A.; MOHAMMADI, A. Environmentally responsive surface-modified silica nanoparticles for enhanced oil recovery. **Journal of Nanoparticle Research**, Springer, v. 18, p. 1–19, 2016. Cited in page 95.

221 ROSTAMI, P. et al. The effect of nanoparticles on wettability alteration for enhanced oil recovery: micromodel experimental studies and cfd simulation. **Petroleum Science**, Springer, v. 16, p. 859–873, 2019. Cited in page 95.

222 KUMAR, D. et al. Experimental investigation of go-hpam and sio<sub>2</sub>-hpam composite for ceor: Rheology, interfacial tension reduction, and wettability alteration. **Colloids and Surfaces A: Physicochemical and Engineering Aspects**, Elsevier, v. 637, p. 128189, 2022. Cited in page 96.

223 CORREDOR-ROJAS, L. M. et al. Rheological behavior of surface modified silica nanoparticles dispersed in partially hydrolyzed polyacrylamide and xanthan gum solutions: Experimental measurements, mechanistic understanding, and model development. **Energy & Fuels**, ACS Publications, v. 32, n. 10, p. 10628–10638, 2018. Cited in page 98.